11-17-2016

Advancements in Thermal Integrity Profiling Data Analysis

Kevin Russell Johnson
University of South Florida, krjohns8@mail.usf.edu

Advancements in Thermal Integrity Profiling Data Analysis

by

Kevin R. Johnson

A dissertation submitted in partial fulfillment
of the requirements for the degree of
Doctor of Philosophy
Department of Civil and Environmental Engineering
College of Engineering
University of South Florida

Major Professor: Austin Gray Mullins, Ph.D.
Michael Stokes, Ph.D.
Abla Zayed, Ph.D.
Frank Pyrtle, III, Ph.D.
Sarah Kruse, Ph.D.

Date of Approval:
October 28, 2016

Keywords: effective radius, temperature prediction modeling,
hyperbolic corrections, T-R relationship, drilled shaft

DEDICATION

To my father who inspired me to pursue engineering and has motivated me throughout.

ACKNOWLEDGEMENTS

I would first and foremost like to thank Dr. Gray Mullins for his mentorship and guidance throughout this study and beyond. I would also like to acknowledge the Florida Department of Transportation for funding portions of this study, as well as Pile Dynamics, Inc. and Foundation & Geotechnical Engineering, LLC for their technical support and contributions to the furtherance of Thermal Integrity Profiling. I would also like to thank the entire Structural Research group at the University of South Florida. Finally, I want to thank my parents, entire family, and loving fiancée Tori for their support and encouragement in achieving my goals.

TABLE OF CONTENTS

LIST OF TABLES

LIST OF FIGURES

ABSTRACT

Thermal Integrity Profiling (TIP) is a relatively new non-destructive test method for evaluating the post-construction quality of drilled shafts. Therein anomalies in a shaft are indicated by variations in its thermal profile when measured during the curing stages of the concrete. A considerable benefit with this method is in the ability to detect anomalies both inside and outside the reinforcement cage, as well as provide a measure of lateral cage alignment. Similarly remarkable, early developments showed that the shape of a temperature profile (with depth) matched closely with the shape of the shaft, thus allowing for a straightforward interpretation of data. As with any test method, however, the quality of the results depends largely on the level of analysis and the way in which test data is interpreted, which was the focus of this study. This dissertation presents the findings from both field data and computer models to address and improve TIP analysis methods, specifically focusing on: (1) the analysis of non-uniform temperature distributions caused by external boundary conditions, (2) proper selection of temperature-radius relationships, and (3) understanding the effects of time on analysis.

Numerical modeling was performed to identify trends in the temperature distributions in drilled shafts during concrete hydration. Specifically, computer generated model data was used to identify the patterns of the non-linear temperature distributions that occur at the ends of a shaft caused by the added heat loss boundary in the longitudinal direction. Similar patterns are observed at locations in a shaft where drastic changes in external boundary conditions exist (e.g. shafts that transition from soil to water or air). Numerical modeling data was also generated to examine the

relationship between measured temperatures and shaft size/shape which is a fundamental concept of traditional TIP analysis.

A case study involving a shaft from which 24hrs of internal temperature data was investigated and compared to results from a computer generated model made to mimic the field conditions of the shaft. Analysis of field collected and model predicted data was performed to examine the treatment of non-linear temperature distributions at the ends of the shaft and where a mid-shaft change in boundary was encountered. Additionally, the analysis was repeated for data over a wide range of concrete ages to examine the effects of time on the results of analysis.

Finally, data from over 200 field tested shafts was collected and analyzed to perform a statistical evaluation of the parameters used for interpretation of the non-linear distributions at the top and bottom of each shaft. This investigation incorporated an iterative algorithm which determined the parameters required to provide a best-fit solution for the top and bottom of each shaft. A collective statistical evaluation of the resulting parameters was then used to better define the proper methods for analyzing end effects.

Findings revealed that the effects of non-uniform temperature distributions in drilled shaft thermal profiles can be offset with a curve-fitting algorithm defined by a hyperbolic tangent function that closely matches the observed thermal distribution. Numerical models and statistical evaluations provided a rationale for proper selection of the function defining parameters. Additionally, numerical modeling showed that the true temperature-to-radius relationship in drilled shafts is non-linear, but in most cases a linear approximation is well suited. Finally, analysis of both model and field data showed that concrete age has virtually no effect on the final results of thermal profile analysis, as long as temperature measurements are taken within the dominate stages of concrete hydration.

CHAPTER 1: INTRODUCTION

The vast majority of bridges in the U.S. are founded on concrete deep foundations, the most common forms of which are driven piles and drilled shafts. While both foundation types are well suited for resisting large loads, drilled shafts have the advantage of being able to do so with a much smaller footprint in many applications. This often makes them the foundation of choice not only for bridges, but for many tall buildings, lighting and signage structures, and some retaining walls. In the family of concrete deep foundations, drilled shafts are generally classified as those that are constructed by means of a drilled excavation which is stabilized prior to the placement of reinforcement and concrete (Brown 2010). They typically range in sizes of 3 to 12 feet in diameter and can extend as deep as 300 feet into the ground (Brown 2010). Steel reinforcement is provided by a rebar cage, typically 6 inches in from the sidewalls. Although drilled shaft foundations are reputed for their strength, reliability, and economy, their construction requires careful attention to quality control and quality assurance. Due to the blind nature of the underground concreting process, defects in drilled shafts are common. This is particularly true among excavations extending below the water table which are stabilized with drilling fluids (Mullins 2010). Intrusion of soil from the excavation side walls, encapsulation of slurry, or improper flow of concrete through congested reinforcement cages can occur during construction, often without any indication to the contractor. As a result, the as-built shaft may contain areas of degraded concrete quality, exposed rebar, reduced cross section, or combinations thereof. Defects such as these reduce both the structural and geotechnical capacity of the shaft, and allow pathways for corrosion, rendering

the shaft unfit for service in many cases. Figure 1.1 shows the severity of defects which can form in drilled shafts.

Figure 1.1 Shaft with severe necking (left), and shafts from a soldier pile wall with numerous defects (right). (Mullins & Winters, 2012)

Even with careful attention to quality control during construction, quality assurance after construction is necessary to validate the integrity of the as-built shaft. Unlike above ground structures however, visual inspection of drilled shafts is rarely available. Excavation and core sampling methods can provide some visual confirmation but they are expensive, time consuming, and can further compromise the integrity of a shaft. These methods are only employed when strong suspicion warrants them. Similarly, load testing is expensive and can cause structural damage to shafts. (Anderson, 2011)

1.1 Quality Assurance of Drilled Shafts

This two-fold problem - a high probability of defects with a low ability to detect them - lends itself to an array of creative inspection techniques. Non-destructive testing methods developed over the last 40 years have greatly improved the quality assurance process for drilled shafts by allowing contractors to verify structural integrity without the need for excessive coring

or load testing. Methods such as Sonic Echo and Impulse Response are able to detect anomalies from entirely above ground. They involve generating a small compressive disturbance at the top of the shaft which travels downward through the shaft's length and is reflected back to the top where it is measured. Methods like this are the least intrusive but are limited in their ability to define the nature and severity of detected anomalies, especially at increasing depths. They also suffer from a phenomenon known as the "shadow effect" wherein wave disturbances from a shallow anomaly will prevent the detection of any deeper anomalies. More effective means of inspection involve down-hole measurements and are commonly referred to as integrity profiling methods. Most states have adopted the use of at least one or more of these methods and have requirements in place for all drilled shaft to be constructed with access tubes that can accommodate them. Table 1.1 summarizes the most popular methods of drilled shaft integrity profiling. (Brown, 2010)

Table 1.1 Down-hole methods for drilled shaft quality assurance.

Testing Method	Measurement	Indicator	Coverage
Cross-hole Sonic Logging (CSL)	Wave speed reduction	Density	Majority of area within reinforcement cage
Gamma Gamma Logging (GGL)	Gamma particle count	Density	3-5 inch radial zone around access tubes
Thermal Integrity Profiling (TIP)	Temperature	Cement hydration	Entire cross-section

Developed in the late 1990's, Thermal Integrity Profiling (TIP) is the youngest of these methods, but is a rapidly increasing form of post-construction quality assurance for drilled shafts. Where this method excels is in its ability to detect anomalies across the entire cross section of a shaft, both inside and outside the reinforcement cage. Multiple studies have proven the

effectiveness of TIP for shaft evaluation, and several states have adopted its use. As with any test method, however, the quality of the results depends largely on the level of analysis and the way in which test data is interpreted, which is the focus of this study. (Anderson, 2011)

1.2 Thermal Integrity Profiling (TIP)

The chemical processes that take place during cement hydration are highly exothermic, meaning that energy is released in the form of heat as the reactions occur. In massive concrete elements, such as drilled shafts, a significant amount of energy is released during the curing process over a period of days. In fact, a single concrete truck containing 9 cubic yards of concrete can contain the equivalent energy of 400-500lbs of TNT. The difference, of course, is the time over which the energy is released. Table 1.2 provides a list of energy quantities comparable to that of a single drilled shaft.

Table 1.2 Comparison of energy in a drilled shaft.

1 drilled shaft, 6 ft. diameter x 80 ft. deep	12,800 MJ
30 Mark 82 aerial bombs	13,200 MJ
2 cross-country trips in a Hummer	11,500 MJ
2 bolts of lightning	10,000 MJ
5 months average household usage	13,400 MJ
A lifetime supply of Red Bull (1 per day for 75 yrs)	13,200 MJ

The amount of heat released during concrete hydration is dictated by cement content, and the resulting temperature distribution is largely a function of shaft geometry. Cement content and shaft size are also the key contributors to strength and durability, thus all of these factors tie together and, combined, define shaft serviceability (Mullins & Winters, 2012). TIP takes advantage of this thermal energy, measuring the elevated temperatures within a shaft caused by the heat produced during concrete hydration. Therein anomalies in a shaft are indicated by variations in the observed thermal profile.

Temperature measurements can be achieved in either of two ways – via probe with infrared sensors which is lowered down access tubes, or by thermal wires which are attached to the reinforcement cage and cast with the shaft. Figure 1.2 shows the testing equipment and the access tubes where measurements are taken using the probe method. A thermal probe, equipped with 4 infrared sensors, is lowered down each access tube (dry) at a rate of about 3 – 5 inches/sec. While temperature is measured by the sensors, depth is recorded by the encoder assembly. The optimal time for testing is during the peak of concrete hydration, which can range from 12 to 72 hours after concrete placement, depending on shaft size. Figure 1.3 shows use of the wire method, wherein several thermistors are strung together on one foot intervals and fastened to the reinforcement cage prior to concreting. With this method, data may be continually recorded over several days, but the instrumentation must be disposable as it is cast permanently in the concrete. (ASTM D7949)

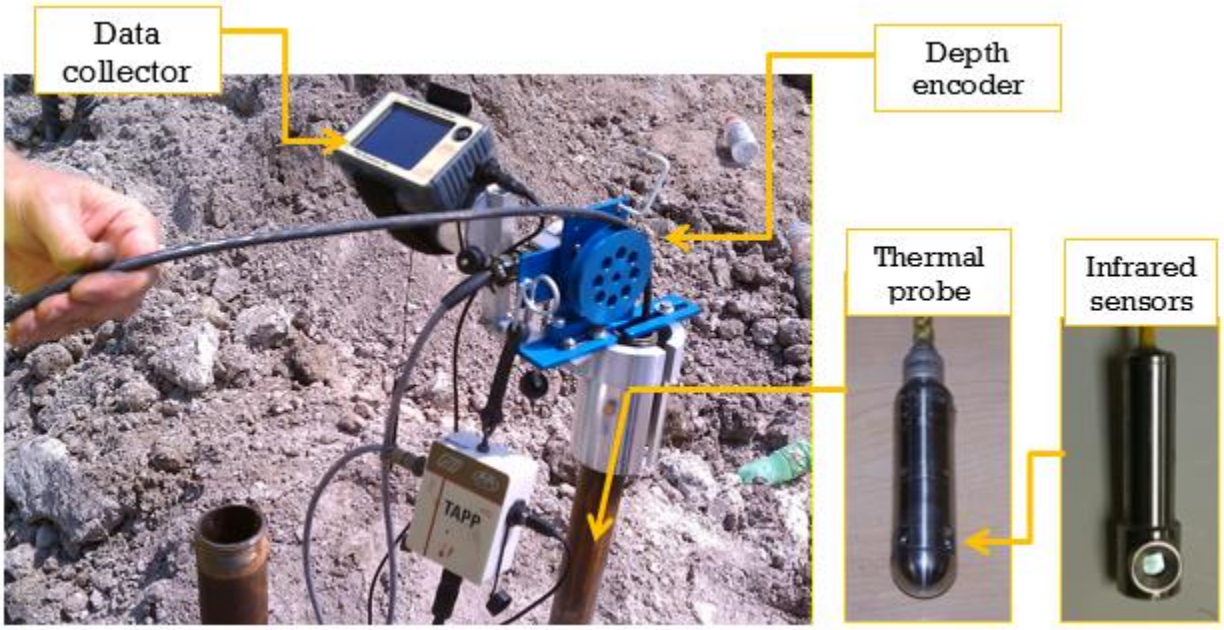

Figure 1.2 TIP setup – probe method.

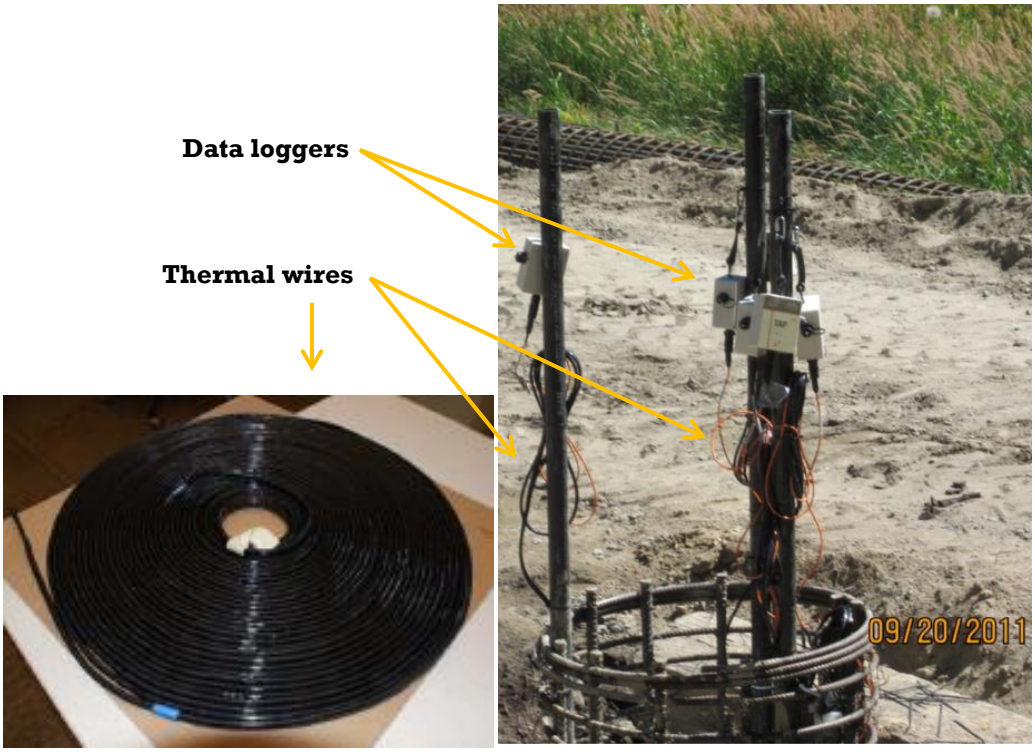

Figure 1.3 TIP setup – wire method.

Despite the procedural standards set forth by ASTM D7949 for testing, ASTM does not provide a standardized method for analysis of collected data. Therefore interpretation of TIP results is still highly subjective among end users. While the TIP analysis methods most commonly used in practice today have allowed for successful evaluation of shaft integrity, the approaches rely on empirically developed values and lack robust scientific rationale in certain aspects of interpretation. The focus of this dissertation is to provide an objective and standardized procedure for analyzing thermal integrity data.

1.3 Organization

This dissertation presents the findings from both field data and computer models to address and improve the applicability of TIP analysis methods, specifically focusing on: (1) the analysis of non-uniform temperature distributions caused by external boundary conditions, (2) proper selection of temperature-radius relationships, and (3) understanding the effects of time on analysis.

Chapter 2 proposes curve-fitting algorithms whereby non-uniform temperature distributions can be addressed, thereby allowing these portions of data to be analyzed using traditional methods. Chapter 3 presents a case study in which data was collected continuously up to 24hrs after concreting. Comparing the data to computer generated model data, the trends were examined as they relate to time of testing (i.e. concrete age). Chapter 4 presents a statistical evaluation of over 200 field tested shafts where all curve fitting parameters were varied through a wide range of values until a best-fit solution was obtained. Finally, Chapter 5 summarizes the findings and provides recommendations for proper analysis and interpretation of thermal integrity data.

CHAPTER 2: TEMPERATURE PREDICTION MODELING[1]

Thermal integrity profiling (TIP) is an increasingly popular form of post-construction quality assurance for drilled shafts. Therein anomalies in a shaft are indicated by variations in its thermal profile. As with any test method, the quality of the results depends largely on the level of analysis and the way in which test data is interpreted. With thermal integrity profiling, data interpretation techniques can fall into two schools of thought: (1) use of construction logs and concrete yield plots as a means to calibrate thermal data to shaft dimensions or (2) use of temperature prediction software to compare measured to model predicted thermal profiles. In theory, a signal matching approach using modeled shafts could reveal the shaft geometry that would produce the measured thermal profiles. However, the accuracy of models is largely dependent on input parameters such as shaft dimensions, boundary conditions, and concrete hydration behavior. Although the margins of error associated with these parameters can easily accumulate, useful trends and relationships about the temperature distributions within drilled shafts and surrounding environments can be identified. This chapter examines computer generated trends and demonstrates ways in which they can be merged with existing TIP analysis techniques to produce a heightened level of data interpretation.

2.1 Introduction

With the advent of thermal methods for post-construction quality assurance of drilled shafts, contractors have the ability to detect anomalies throughout the entire cross section of a shaft

[1] Portions of this chapter were published in the ASCE Geo-Congress 2014 Technical Papers. Permission is included in Appendix C.

and assess its general shape, concrete quality, cage alignment, and concrete cover. Thermal integrity profiling (TIP) reveals the temperature distributions that result from cement hydration which can in turn be used to infer the distribution of concrete underground. While direct observation of thermal profiles alone can be useful in obtaining qualitative information about a shaft, a quantifiable assessment of shaft integrity must come from more detailed analysis. Traditional analysis techniques make use of construction logs and concrete yield plots to calibrate temperature measurements which can then be converted to effective radius, a quantity that can represents the presence or lack of quality concrete. More advanced methods of analysis involve the use of temperature prediction software to compare modeled thermal profiles to those measured by TIP. These methods are more rigorous and limited to the accuracy of estimated input parameters. Recent investigation into the trends and relationships revealed by models however has led to more enhanced methods of traditional analysis, including methods for correcting for end effects and developing a temperature-radius relationship that is both accurate and conservative against false positives.

2.2 Background

In mass concrete elements, such as drilled shafts, a significant amount of energy is released during the curing process over a period of days. TIP takes advantage of this and detects anomalies based on variations in a shaft's thermal profile during the curing stages (Anderson, 2011). Figure 2.1 illustrates the way in which heat is dissipated from the shaft to its surroundings and the temperature distributions that result from it. For a perfectly cylindrical shaft, the vertical distribution of temperature is nearly uniform over the majority of its length. The exception is near the ends where there is a distinct region of decreasing temperature. This temperature "roll-off" at the top and bottom is due to the added mode of heat loss in the longitudinal direction. The radial

distribution of temperature is bell-shaped, with peak temperatures occurring at the center of the shaft and decreasing radially towards the surrounding soil. With a typical configuration of access tubes (one tube per 0.3m of diameter, evenly spaced around the reinforcing cage, per ASTM D7949), data collected from thermal integrity testing provides a continuous temperature profile vertically and discrete measurements laterally (red dots in Figure 2.1). The vertical profile reveals any bulges, necks, or inclusions that may be present, while comparison among tube temperatures indicates lateral cage alignment. (Mullins & Winters 2012)

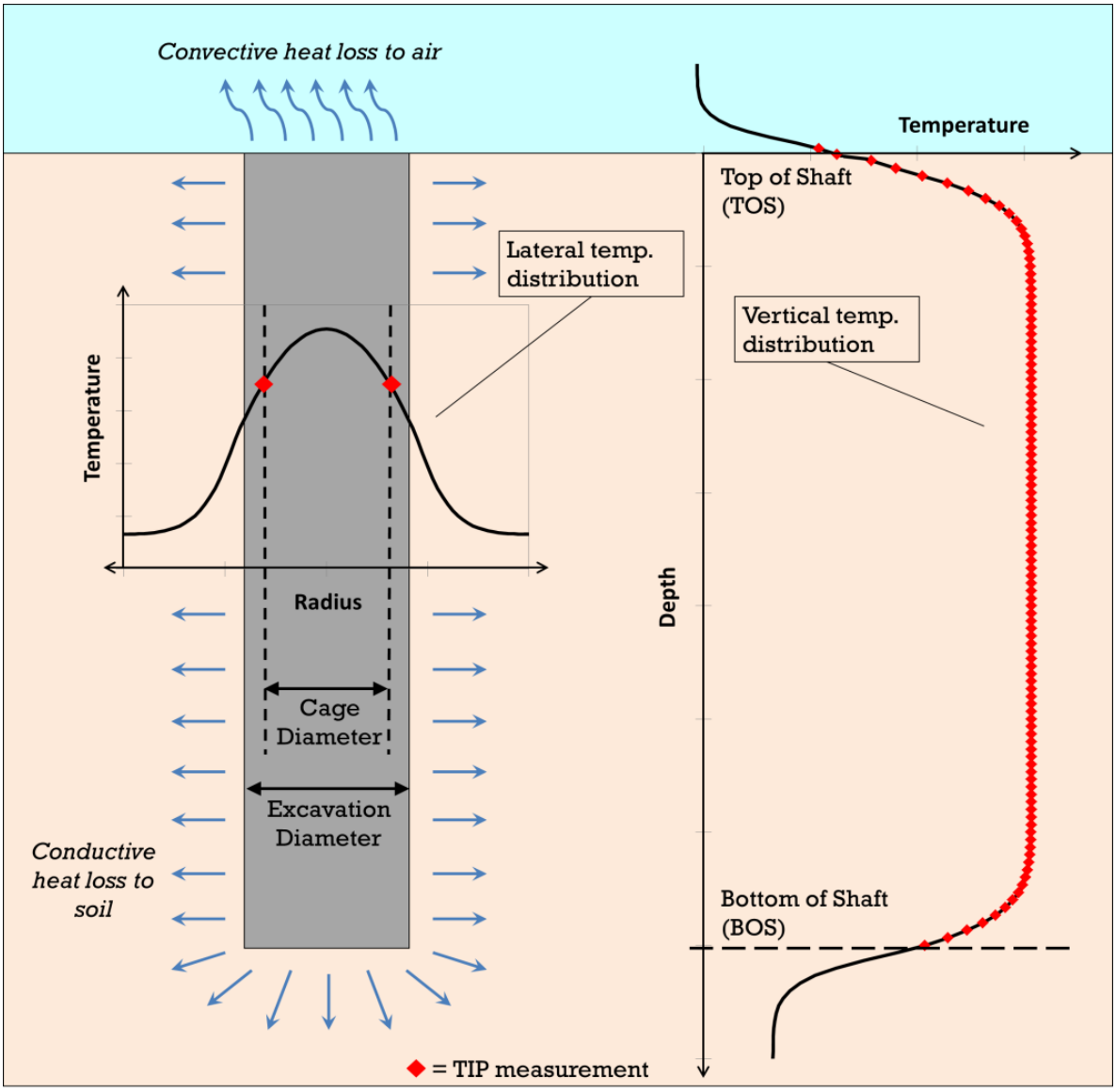

Figure 2.1 Temperature distributions in an idealized shaft.

Direct observation of measured temperature profiles can provide immediate qualitative information about a shaft, such as general shape, relative cage alignment, and the types of anomalies that may be present. However, in order to quantify this information with actual dimensions, more rigorous methods of analysis are required. Mullins & Winters (2011) suggests the following breakdown of analysis techniques:

- Level 1: Direct observation of the temperature profiles
- Level 2: Superimposed construction logs and concrete yield data
- Level 3: Three dimensional thermal modeling
- Level 4: Signal matching numerical models to field data

In most drilled shaft constructions, it is customary to record and plot the volume of concrete placed with each truck along with the change in height to top of concrete resulting from each placement. These logs, known as yield plots, can be compared with theoretical yield plots based on the design diameter of the shaft, and any variation therein can be used to deduce the actual effective average diameter (or radius) of the shaft over the measured height change. This information can then be used to provide a series of calibration points for measured thermal data (Mullins & Winters, 2011). Figure 2.2 shows a case study where both the concrete yield plot data and thermal profile are plotted together.

This type of calibration essentially eliminates the need to make the assumptions about thermal properties that are required for modeling analysis. By plotting the effective radius against measured temperature, a best-fit linear regression can be used to form a temperature-radius relationship, as shown in Figure 2.3. The assumption of linearity is valid for temperatures measurements taken in the regions near the edge of the shaft, as the temperature distribution there

is strongly linear. In either direction away from this region however, a linear relationship will tend under-predict anomaly size. (Mullins & Winters, 2011)

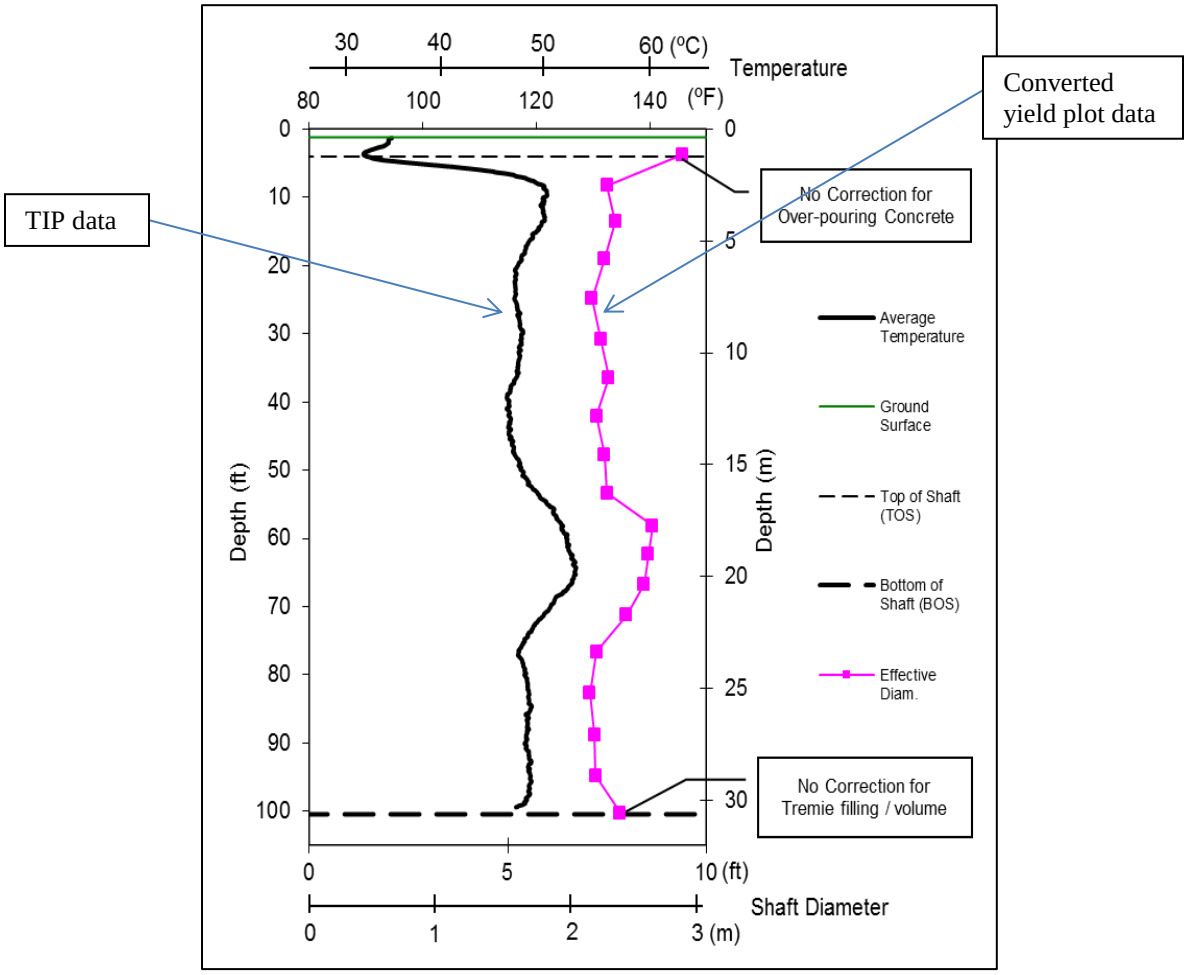

Figure 2.2 Yield plot data compared with thermal data. (Adapted from Mullins, 2010)

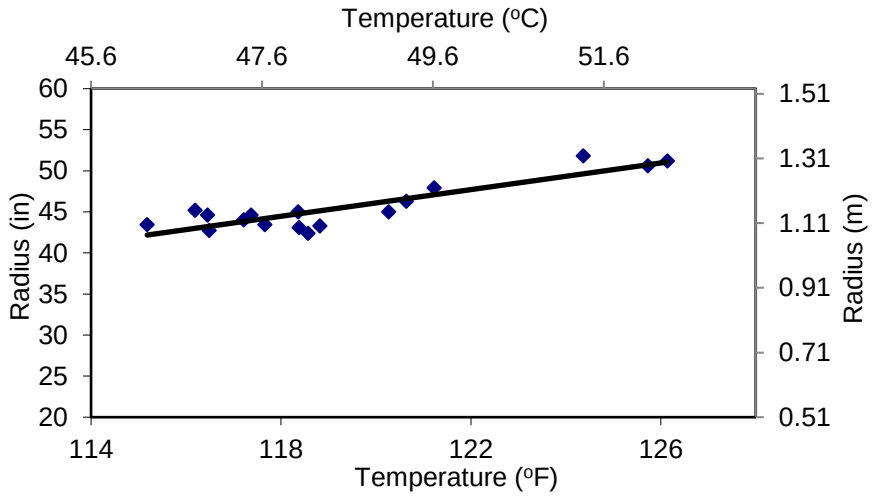

Figure 2.3 Multi-point regressed T-R relationship. (Mullins, G., Winters, D., 2011, p. 40)

2.3 Thermal Modeling for Drilled Shafts

For analysis of TIP data using computer models, temperature prediction software is used to solve the finite-difference form of the general heat equation (Eq. 2.1) based on input shaft dimensions, thermal properties, and boundary conditions.

$$\frac{\partial}{\partial x}\left(k\frac{\partial T}{\partial x}\right)+\frac{\partial}{\partial y}\left(k\frac{\partial T}{\partial y}\right)+\frac{\partial}{\partial z}\left(k\frac{\partial T}{\partial z}\right)+q=\rho C_p\frac{\partial T}{\partial t} \quad \{2.1\}$$

where,

$T = temperature$

$k = thermal\ conductivity$

$\rho = density$

$C_p = specific\ heat$

$q = rate\ of\ heat\ generation$

The thermal properties of concrete vary through the curing stages and are typically expressed as a function of the degree of hydration. The hydration of Portland cement is the result of many different chemical reactions that take place, all of which release heat in the process (i.e. exothermic), though be it at separate times and magnitudes. Since the evolution of heat is a direct indication of completed reactions, it serves as a defining measure for the progression of hydration. Therein, at any given time, the rate of hydration is defined by the instantaneous rate of heat generation, q (Eq. 2.2), and the degree of hydration, α, is defined as the fraction of cumulative heat evolved, $H(t)$, to the ultimate amount of heat available, H_u (Eq. 2.3) (Schindler & Folliard, 2005). The variation in time and rate of the multiple types of reactions results in a hydration process that is not constant, but rather occurs in phases. In general, there are five distinguishable stages of hydration: *(1) initial hydration, (2) dormant period, (3) acceleration, (4) deceleration, and (5)*

steady state (Mindess et al., 2003). This behavior results in rate of heat generation and degree of hydration curves that follow the general pattern of those shown in Figure 2.4.

$$q = rate\ of\ heat\ generation = \frac{d}{dt}H(t) \quad \{2.2\}$$

$$\alpha = degree\ of\ hydration = \frac{H(t)}{H_u} \quad \{2.3\}$$

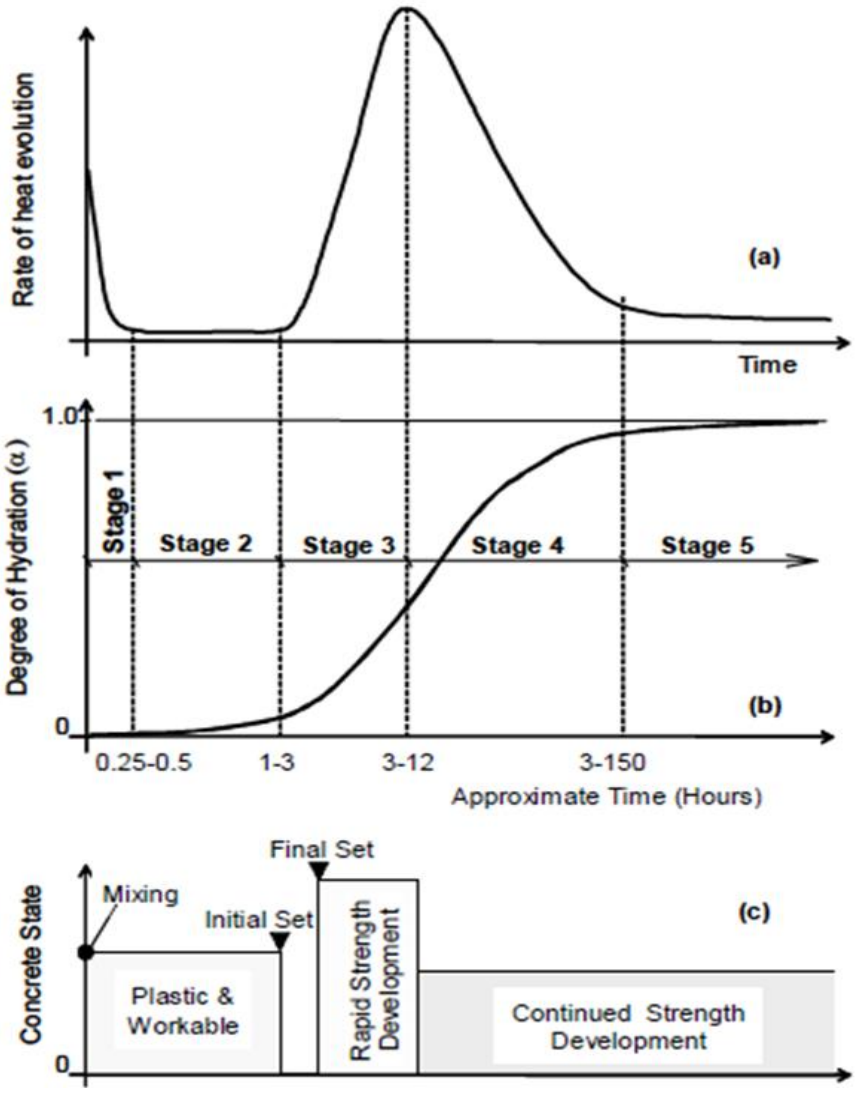

Figure 2.4 Hydration behavior of concrete. (Schindler et al., 2002)

The most widely accepted method for modeling this hydration behavior involves the concept of equivalent age, t_e, which invokes the Arrhenius theory for rate processes to account for

the temperature dependency of reactions (Eq. 2.4), combined with an exponential formulation which approximates the S-shaped degree of hydration curve (Eq. 2.5). (Schindler & Folliard, 2005)

$$t_e = Equivalent\ Age = \sum_0^t e^{-\frac{E_a}{R}\left(\frac{1}{T}-\frac{1}{T_r}\right)} \cdot \Delta t \qquad \{2.4\}$$

$$\alpha = \alpha_u \cdot \exp\left[-\left(\frac{\tau}{t_e}\right)^{\beta}\right] \qquad \{2.5\}$$

In Equation 2.4, R is the natural gas constant (*8.314 J/mol/K*) and E_a is the activation energy, a property which represents the temperature sensitivity of the hydration process. T is the temperature (^oK) of concrete at time t. In Equation 2.5, α_u, β, and τ are parameters that describe the shape of the hydration curve, corresponding to the ultimate degree of hydration, the rate of the acceleration phase, and the start of the acceleration phase, respectively, as shown in Figures 2.5 – 2.7 (Folliard et al., 2008). These shape parameters, as well as properties E_a and H_u, are unique to every concrete batch and are best determined experimentally on an individual basis. They can be found through a combination of isothermal and adiabatic or semi-adiabatic calorimetry testing, wherein T_r is the reference temperature (^oK) at which testing is conducted.

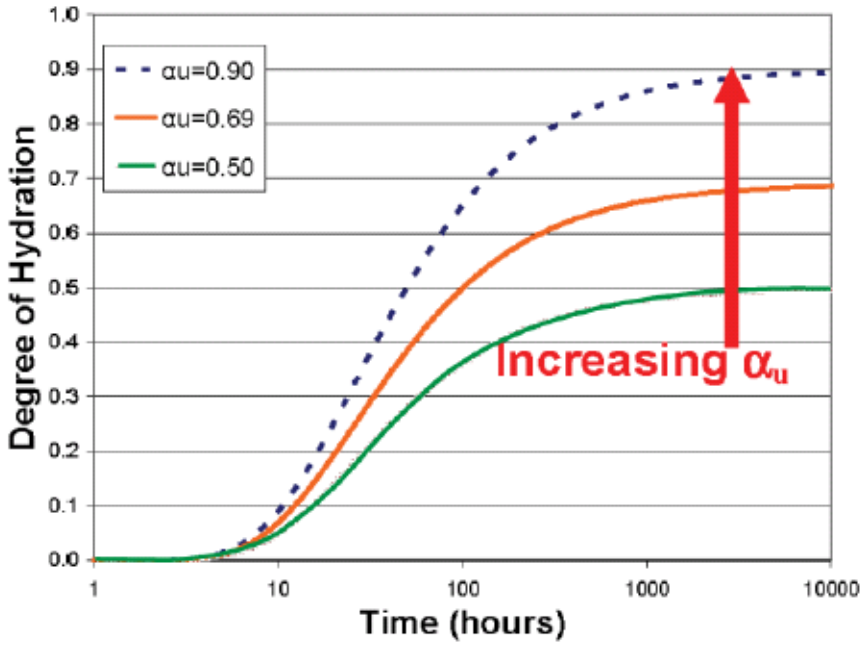

Figure 2.5 Effect of shape parameter α_u on hydration curve. (Folliard et al., 2008)

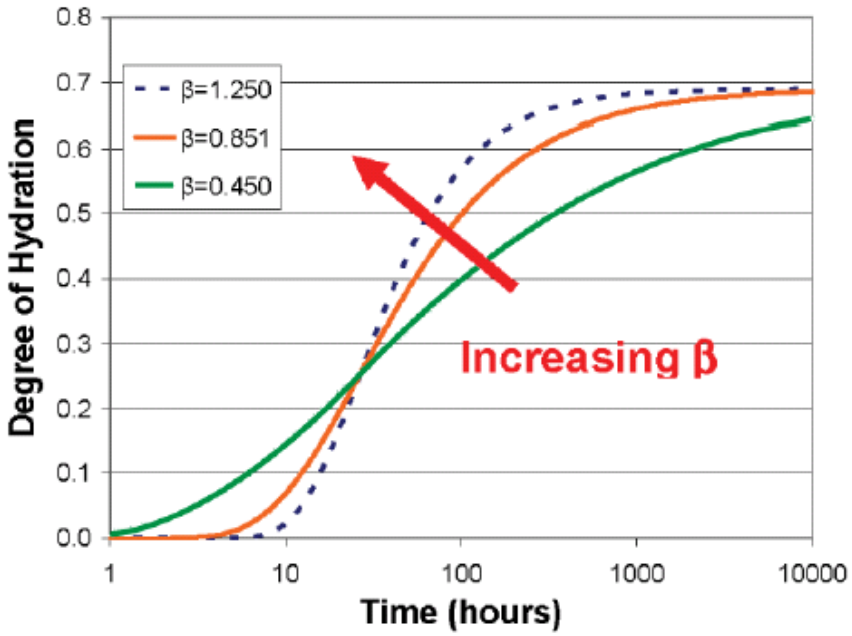

Figure 2.6 Effect of shape parameter β on hydration curve. (Folliard et al., 2008)

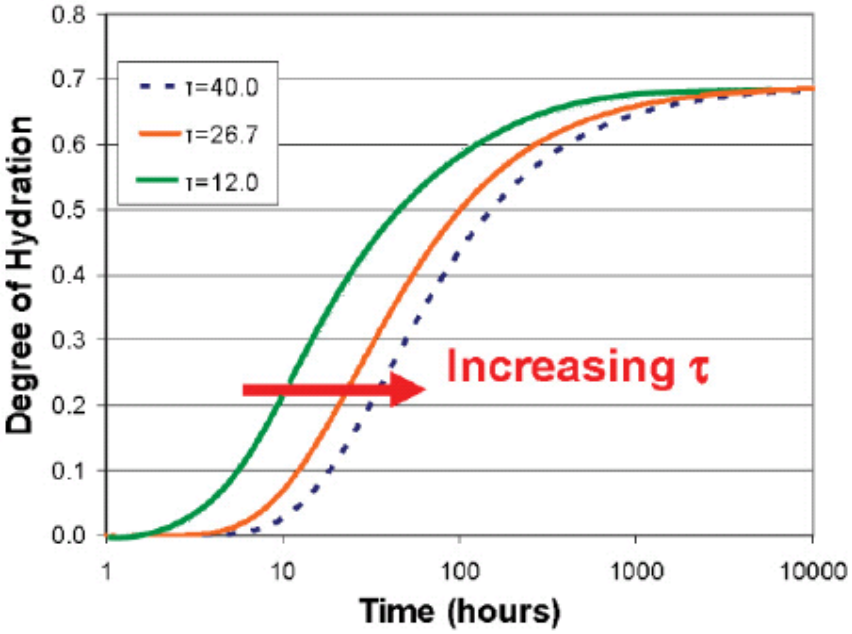

Figure 2.7 Effect of shape parameter τ on hydration curve. (Folliard et al., 2008)

Although exact determination of a concrete's hydration behavior requires laboratory testing, empirical correlations developed through past research can be used to accurately estimate hydration parameters based on cement and concrete compositions. Bogue (1947) first correlated

the total heat of hydration of Portland cement to its major compounds, producing the relationship shown in Equation 2.6.

$$H_{cem} = 500 \cdot p_{C_3S} + 260 \cdot p_{C_2S} + 866 \cdot p_{C_3A} + 420 \cdot p_{C_4AF} + 624 \cdot p_{SO_3} + 1186 \cdot p_{FreeCaO} + 850 \cdot p_{MgO} \quad \{2.6\}$$

Several studies since then have extended this concept to correlate the additional hydration parameters used in the exponential α model and to include a broader range of variables such as supplementary cementitious materials, chemical admixtures, and cement fineness. Some of the most notable and recent work to examine such relationships includes studies from Schindler & Folliard (2005), Ge (2006), and Poole (2007), the latter of which is currently the most comprehensive. The constitutive empirical correlations that make up this model are provided in Appendix A. This set of equations is specific to cement compositions as determined by Bogue calculations (Poole, 2007). While other relationships exist for correlation with cement compositions as determined by x-ray diffraction analysis, which is considered a more accurate method (Taylor, 1997), the Bogue relationships are used here as these are the values most commonly found on cement mill certificates.

With a working model for hydration behavior of concrete, thermal properties that are hydration dependent can be determined as they vary with time. Since the rate of heat generation, q, is an inherent part of the model definition, it can be found by substituting Equations 2.3, 2.4, and 2.5 into Equation 2.2 and differentiating. The resulting expression is given in Equation 2.7.

$$q = H_u W_c \left(\frac{\tau}{t_e}\right)^{\beta} \left(\frac{\beta}{t_e}\right) \alpha \frac{E_a}{R} \left(\frac{1}{T_r} - \frac{1}{T_c}\right) \quad \{2.7\}$$

For estimating thermal conductivity, k, and specific heat, C_p, Schindler & Folliard (2002) suggest using the empirical models shown in Equations 2.8 and 2.9 in conjunction with values found in Appendix B (Tables B.1 and B.2).

$$k = k_{uc}(1.33 - 0.33\alpha) \quad \{2.8\}$$

where,

$$k_{uc} = Thermal\ conductivity\ of\ mature\ concrete$$

$$C_p = \frac{1}{\rho}\left(W_c \alpha C_{ref} + W_c(1-\alpha)C_c + W_a C_a + W_w C_w\right) \quad \{2.9\}$$

where,

$$C_{ref} = 8.4T + 339, where\ T\ is\ temperature\ in\ °K$$

$$C_{c,a,w} = Specific\ heat\ of\ cement, aggregate, \&\ water$$

$$W_{c,a,w} = Weight\ of\ cement, aggregate, \&\ water$$

In thermal modeling of drilled shafts, equally important as the thermal properties of concrete are the thermal properties of surrounding materials. For deep foundations, this is primarily soil or rock and the dominant mode of heat transfer is conduction, thus the same thermal properties k, C_p, & ρ apply. These properties can vary widely with soil type, moisture content, and porosity. Table B.3 in Appendix B gives typical values for various soil and rock types.

In the case of deep foundation construction, Standard Penetration Testing (SPT) data and borehole information are often available, and can provide further insight into the thermal properties of subsurface materials. In-situ soil density, ρ, is a commonly needed property by geotechnical designers and can be estimated directly from uncorrected SPT blow count (N) values using the empirical correlations shown in Appendix B (Figure B.4). Thermal conductivity is not typically considered a result of SPT analysis, but research has shown that it is largely dependent on soil type, density, and saturation state. Pauly (2010) investigated these relationships by culminating results from past studies involving the thermal behavior of soil and correlating them to the information provided by boring log data. To this end, an algorithm was developed to estimate values of density and thermal conductivity of soils based on the depth, soil type, blow count, and

water table elevation as determined from SPT boring logs. The overall range of correlations investigated and regressed by Pauly (2010) are presented as functions of thermal conductivity vs. dry density for variable moisture contents, for both coarse grained (sandy) and fine grained (clayey) soils, are presented in Figure 2.8. The individual regressions are provided in Appendix B (Figures B.2 – B.15).

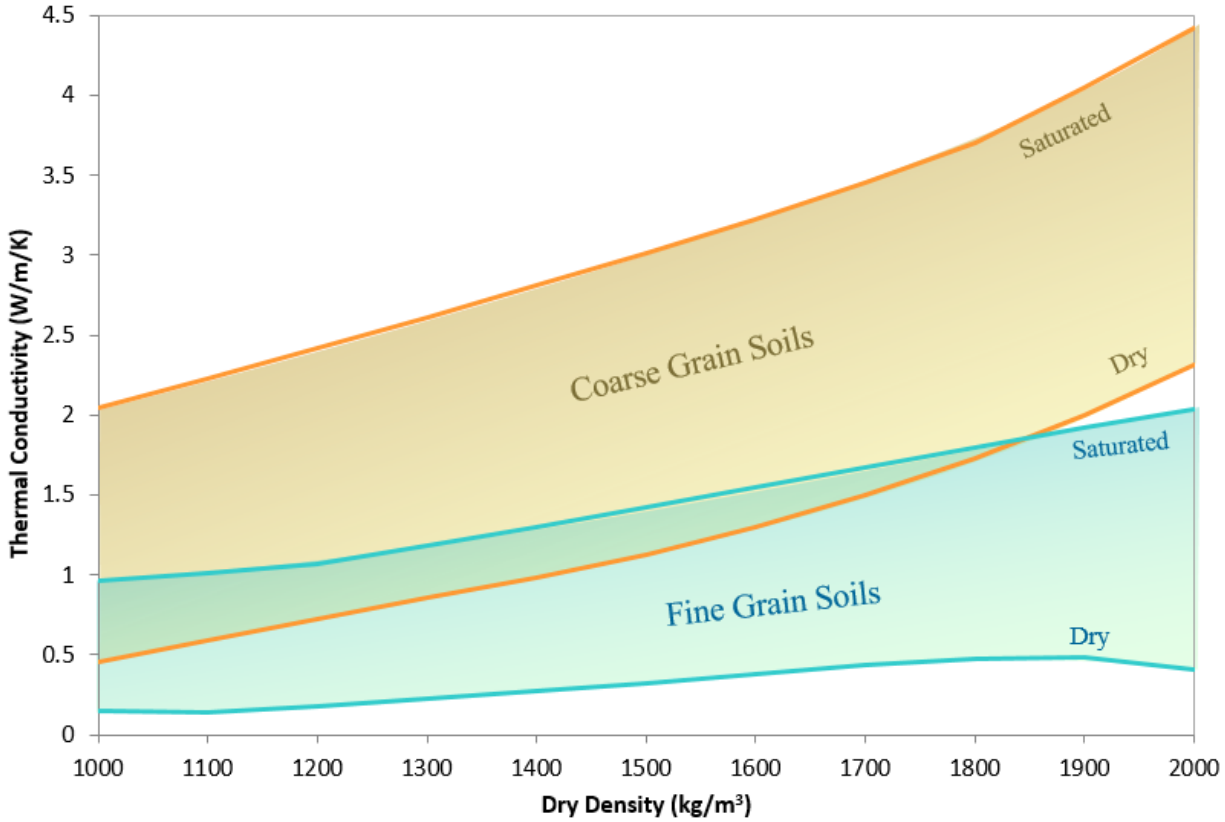

Figure 2.8 Thermal conductivity vs. dry density based on soil type and moisture content.

2.4 End Effects

The signature temperature roll-offs at the top and bottom of every thermal profile have long been problematic for traditional analysis techniques. In the process of developing a temperature-radius relationship, inclusion of the temperatures in these regions in the regression results a falsely steep slope. Conversely, a regression developed with exclusion of these regions results in a relationship that is applicable to the rest of the shaft but leaves the ends to remain unanalyzed.

Through modeling however, a better understanding of the nature of these temperature distributions is gained and a method in which they can be accounted for and included in analysis is proposed herein.

Figure 2.9 shows the end regions of a model temperature profile for a 1.8m (6ft) diameter shaft at 24hrs with surrounding soil temperature set at 22.8°C (73°F). Examining the bottom, several key characteristics can be noted about the shape of the curve. The temperature decrease starts at around 1.5m (5ft) above bottom of shaft (BOS) and continues with an upward concavity which lessens as it approaches the interface between concrete and soil. At the interface is an inflection point where the curve continues to decrease, but with a downward concavity, until it starts asymptotically approaching the surrounding soil temperature. Examination of the same curve for different times, shaft sizes, and soil temperatures reveals the way in which some of these characteristics change but the general shape of the curves remains the same.

By fitting a mathematical function to these curves and identifying the variables that define the shape of that function, the need to perform an excessive number of computer simulations can be eliminated. The best fit for this type of curve is given by a hyperbolic tangent (*tanh*) function. By applying the proper scales and offsets, the basic *tanh* function can be transformed to fit the end region temperature distribution curves. The function and transformations are presented in Equation 2.10.

$$T_{fit} = -\left(\frac{T_{max}-T_{min}}{2}\right)\tanh\left(\frac{z-z_0}{\alpha}\right) + \left(\frac{T_{max}+T_{min}}{2}\right) \qquad \{2.10\}$$

where for the top,

$$T_{max} = Nominal\ shaft\ temperature\ below\ roll-off$$

$$T_{min} = Equivalent\ air\ temperature$$

$$z_0 = Top\ of\ Shaft\ (TOS)\ depth$$

$$\alpha = slope\ factor$$

and for the bottom,

$$T_{max} = Nominal\ shaft\ temperature\ above\ roll-off$$

$$T_{min} = Soil\ temperature$$

$$z_0 = Bottom\ of\ Shaft\ (BOS)\ depth$$

$$\alpha = slope\ factor$$

In analysis of TIP data, the measured top and bottom roll-offs are individually fit with hyperbolic tangent curves by adjusting the transformation variables to values that produce the best fit curve and are within a range of values appropriate for the given shaft. The nominal shaft temperature for each end is obtained from the nearest region of relatively uniform temperature measurements within the shaft. This can generally be found at a distance into the shaft that is roughly equal to the shaft diameter. Soil temperature can be obtained by using the yearly average temperature of the geographical location. As most shafts extend deeper than 3m (10ft), soil temperature at the toe is unaffected by seasonal temperature changes and can mostly be considered constant for a given city or location (Figure 2.10).

Equivalent air temperature is a pseudo – temperature that accounts for the additional cooling by convection and is therefore usually significantly lower than actual air temperature. Its value should be set such that the inflection point of the curve is in the range of actual air temperature. TOS and BOS depths should be near reported values, but should be adjusted as needed to fit the curve, up to a foot in either direction. Finally, slope factors should be adjusted until the best fit is achieved. These values generally range between 0.5 and 5 and increase with time. Once the best fit curves are determined, corrected temperatures can be found according to Equation 2.11.

$$T_{cor} = \frac{T_{measured} - T_{min}}{T_{fit} - T_{min}} (T_{max} - T_{min}) + T_{min} \quad \{2.11\}$$

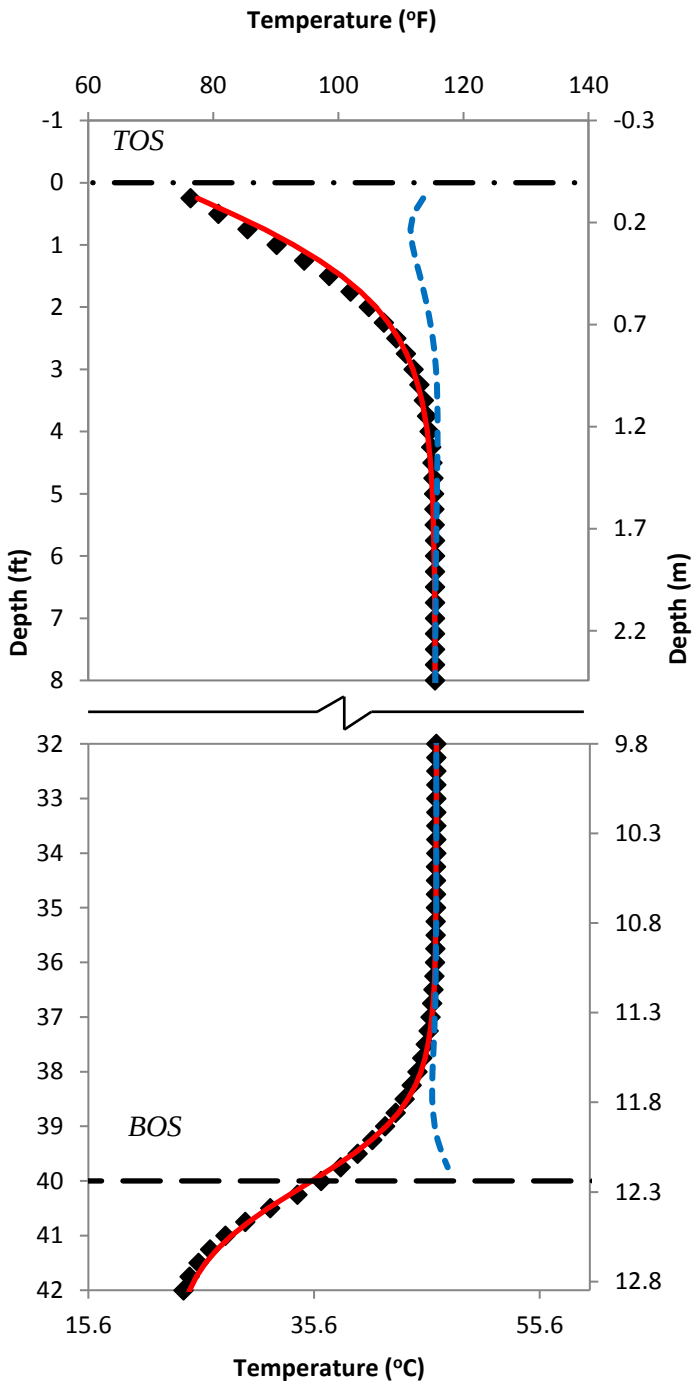

TOS

$T_{max} = 46.4℃ (115.5°F)$
$T_{min} = -2.2℃ (28°F)$
$z_0 = 0m\ (0ft)$
$\alpha = -1.9$

BOS

$T_{max} = 46.4℃ (115.5°F)$
$T_{min} = 22.8℃ (73°F)$
$z_0 = 12.2m\ (40.1ft)$
$\alpha = 1.5$

Figure 2.9 Model temperature distributions for the top and bottom of a 6ft shaft at 24 hours (black), with best fit hyperbolic tangent curves (red), and corrected temperatures (blue).

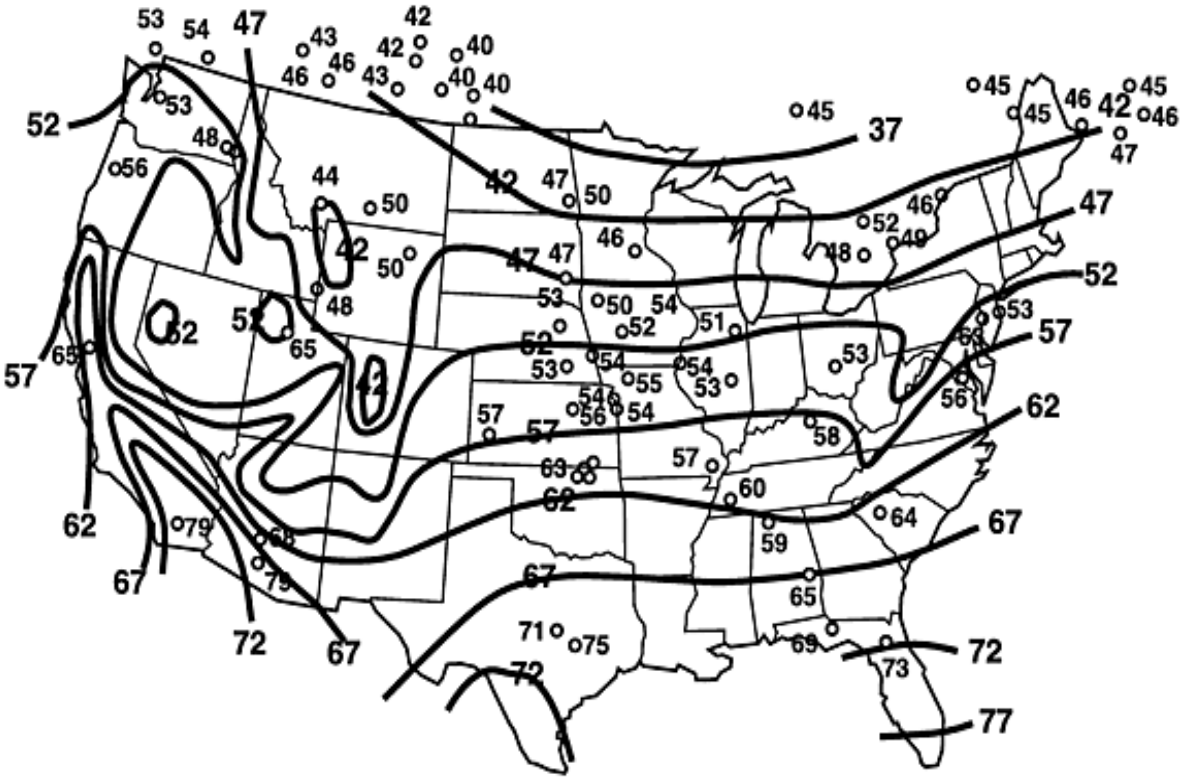

Figure 2.10 Ground temperatures in the United States. (Pauly, 2010)

2.5 Temperature-Radius Relationship

Once corrected temperatures have been established for the top and bottom regions, a temperature-radius (T-R) relationship can be developed that applies to all regions. For shafts that are nearly uniform or those that require relatively few trucks for pouring, the concrete yield plot may not contain a wide enough range of data points to generate a T-R relationship by linear regression, as in Figure 2.3. Instead, when plotted against temperature, the yield plot points will be tightly clustered, revealing no useful trends. In such cases, the total volume and length of the shaft can be averaged to determine an average radius for the shaft, and TIP data can be averaged over the entire length to give an average temperature of the entire shaft. This provides a single point to which a T-R relationship can be calibrated, but lacks the information needed to determine the slope of the curve.

Determining the proper way to develop a useful T-R relationship begins with an understanding of the way that the radial temperature distribution changes as shaft size changes. Figure 2.10 shows a series of radial temperature distributions resulting from modeled shafts with diameters ranging from 0.3 to 4.6m (1 – 15ft). As with the longitudinal end effect curves, several key characteristics of these bell shaped curves are worth examining. At the left end of the curves (shaft center), peak temperatures increase with the first few increasing shaft sizes but are virtually the same for all shafts larger than a certain size. This is due to the fact that, in large shafts, the center is so far removed from the heat loss boundary that temperatures are able to approach those of adiabatic conditions, making it close to what would be experienced in an infinitely large shaft or one with perfectly insulated boundaries. Likewise, the right side of the curves approach what would be expected of an infinitesimally small shaft, which is a measured temperature equal to that of the surrounding soil. All temperature distributions eventually reach soil temperature at a radial distance which is approximately proportional to shaft size. Lastly, examining the shape of each curve, it can be seen that an inflection point occurs at the interface between concrete and soil.

For a given measurement location, a vertical slice through these curves produces the theoretical temperature-radius relationship. Plotting the temperature from each curve at a given radial distance against the respective shaft size corresponding to each curve reveals this unique relationship. Considering a shaft of 36in radius with a cage of 30in radius, the vertical slice shown in Figure 2.11 produces the T-R relationship shown in Figure 2.12. This relationship is non-linear with upper and lower asymptotes approaching concrete adiabatic temperature and ambient soil temperature, respectively.

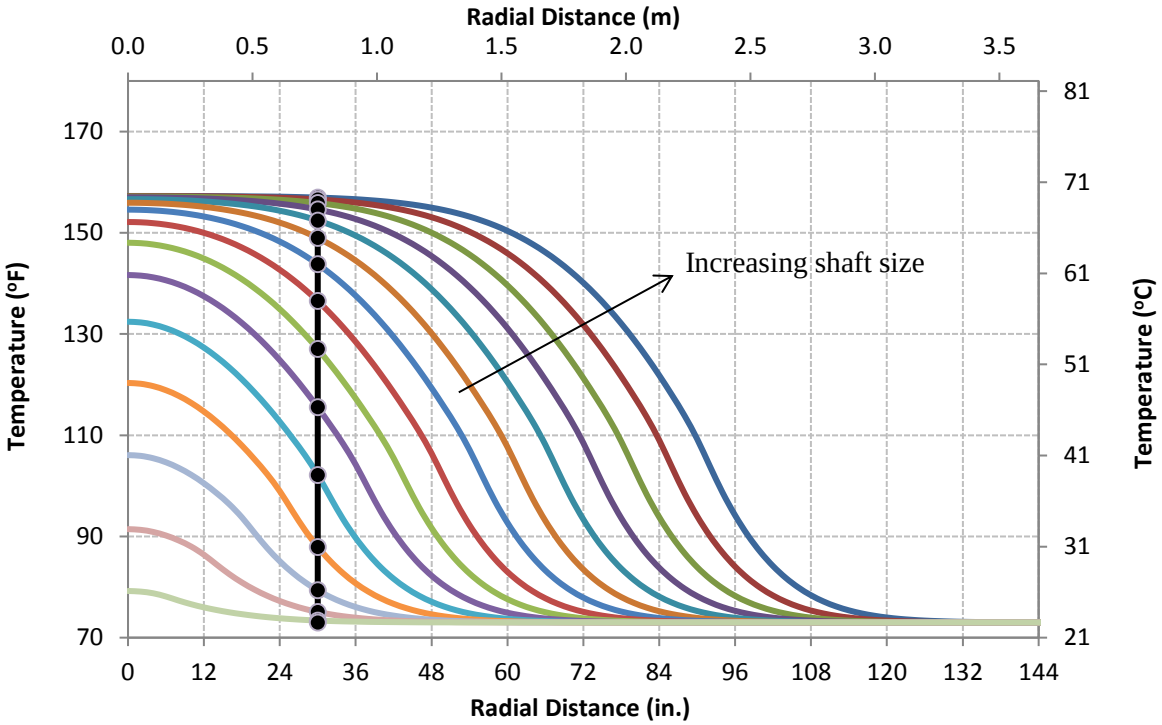

Figure 2.11 Radial temperature distributions for varying shaft sizes (0.3 - 4.6m diameter, 0.3m increments) at 24hrs.

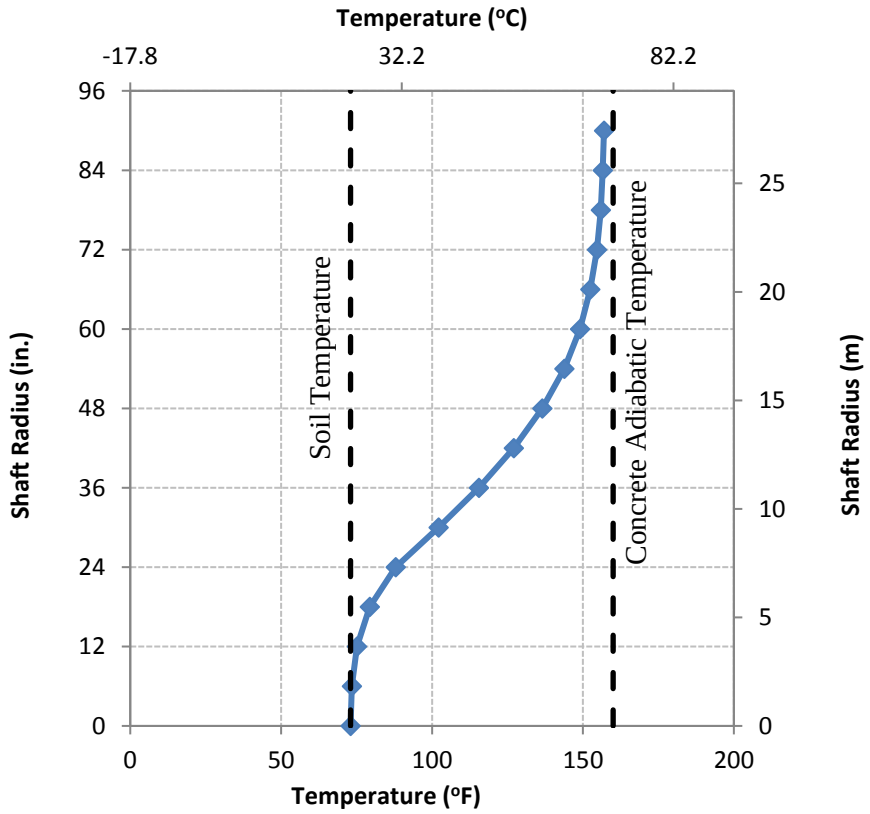

Figure 2.12 Theoretical T-R curve for measurements taken at a 0.762m (30in) radius and 24hrs.

In most cases, when measurements are taken at cage location, the average T-R point (average temperature, average radius) will fall towards the center of the curve, near the inflection point. This region is also the most linear portion of the curve, allowing for a linear regression to represent a close approximation for a T-R relationship in most cases.

Figure 2.12 represents a T-R curve for measurements taken at a reinforcement cage with 0.762m (30in) radius, which would be typical of a shaft that is expected to have an average radius of about 36 inches. Plotting this point on the curve, it can be seen that the best fit slope for a linear T-R relationship would be one that corresponds to line having a negative y-intercept and an x-intercept somewhere between zero and soil temperature.

However, for different times, soil temperatures, and other parameters, these values would be different. In fact, any shift of the T-R curve left or right, would cause the linear approximation to produce false negatives. A leftward shift of the true curve would cause necking anomalies to be interpreted as more severe than they really are. Likewise, a rightward shift of the true curve would cause bulges to appear bigger than they really are. If the slope of the true curve decreases, then anomalies in either direction are over-predicted.

To combat this, a linear relationship that is both accurate and conservative should be used. This can be achieved by drawing a line that passes through the calibrated point (*average temperature, average radius*) and the origin (*0, 0*). It can be shown through modeling that a linear curve generated this way is conservative for all times and all soil temperatures above 30^{o}F, anything below which is an inconceivable soil temperature for any region of the world with drilled shaft construction.

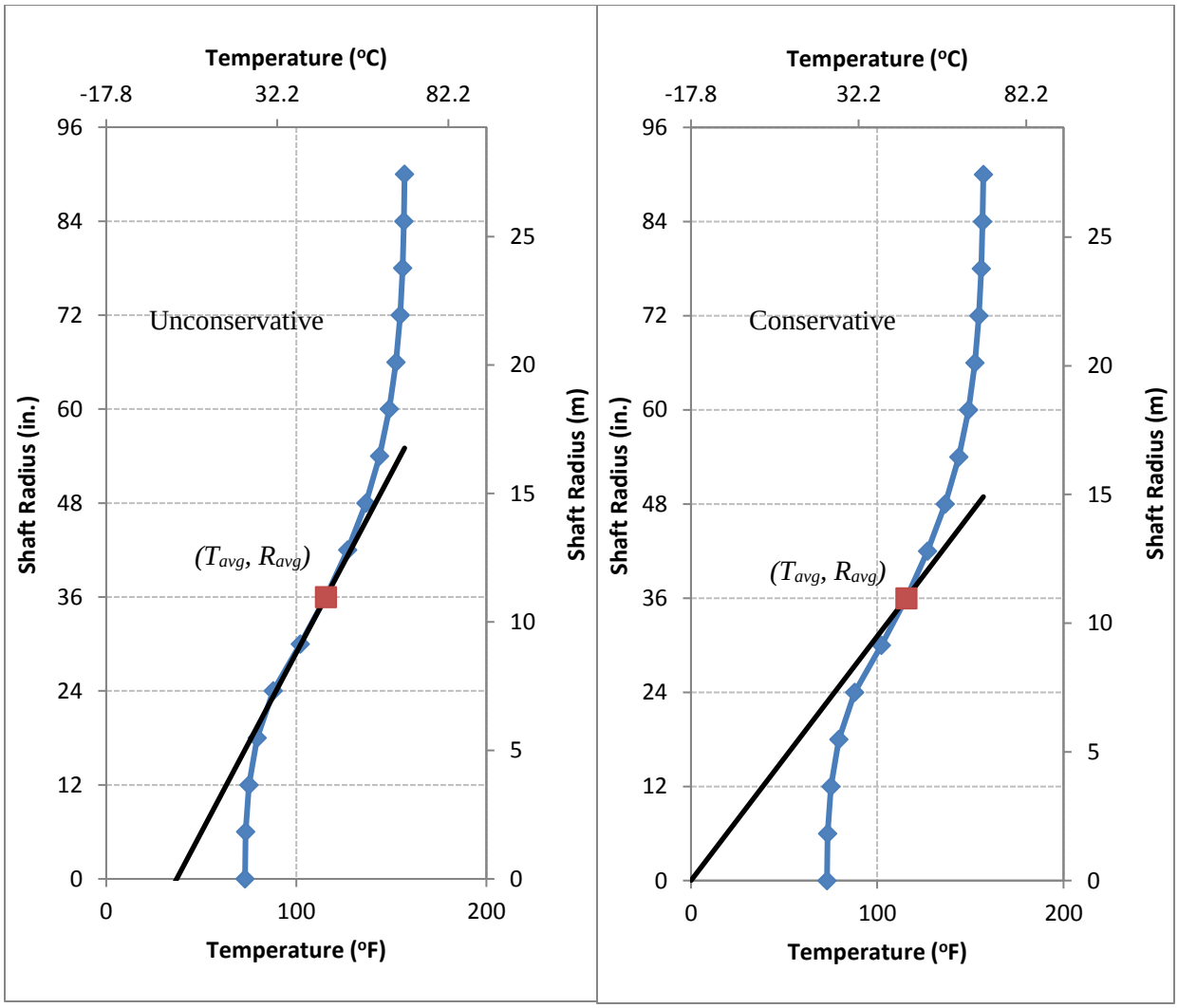

Figure 2.13 Theoretical T-R curve with a linear T-R curve that is accurate but not conservative (left), and a linear T-R curve that is accurate and conservative (right).

2.6 Case Study

For the widening of the Lee Roy Selmon Expressway in Tampa, FL in 2012 -2013, over 200 drilled shafts were poured. Due to the non-redundant design, 100% of the shafts were tested using TIP and analyzed using the methods presented here. Figures 2.13 – 2.15 are an excerpt of the analysis performed on a 4 ft. diameter shaft. Application of the methods for correcting end effects and using a single point T-R relationship are illustrated herein.

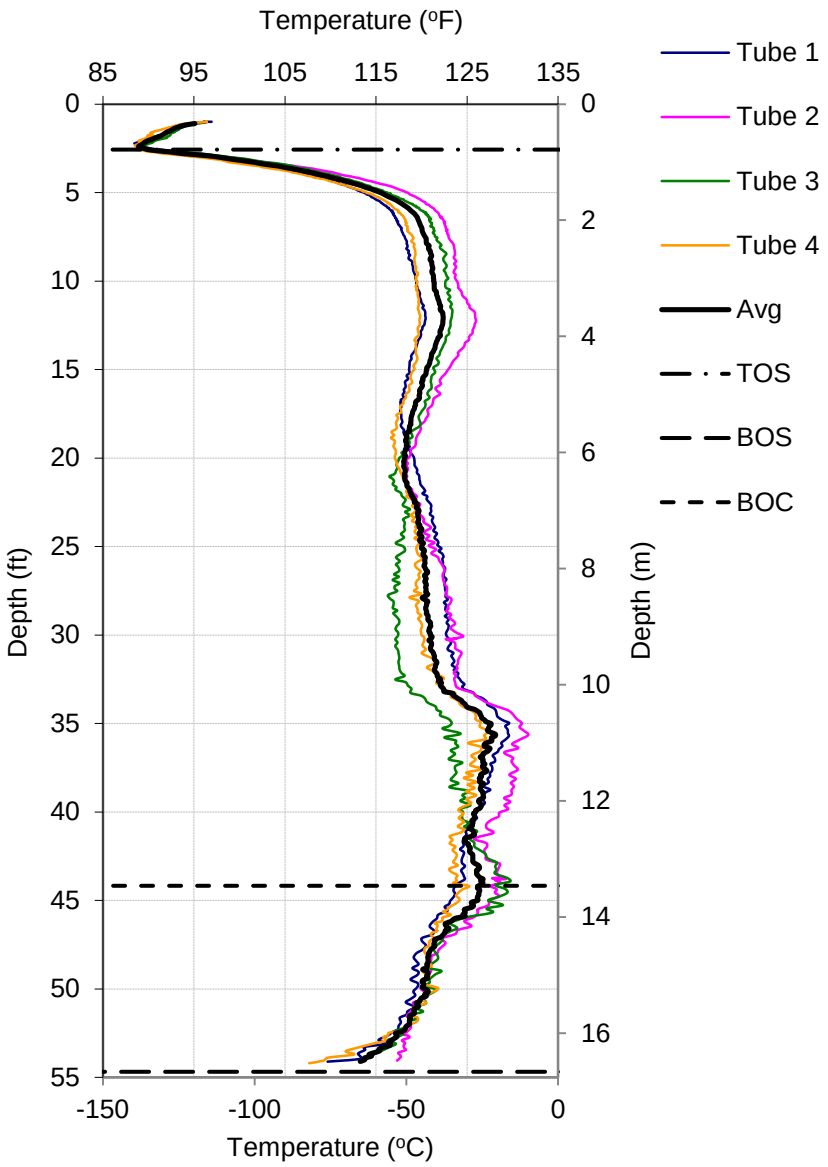

Figure 2.14 Raw TIP data for tested shaft.

Figure 2.14 shows the temperature corrections for the ends of the shaft. Since the modeled curve (red) is in good agreement with the measured data (black), the corrected temperature profile (blue) indicates no anomalies in these regions. Note that setting T_{min} = 3.9°C (39°F) for the top curve results in a top of shaft temperature of 32°C (90°F), well within reason for Florida in August. T_{min} for the bottom of shaft is taken as the annual average temperature for Tampa, FL.

	T.O.S.
Depth:	0.59 m (1.95 ft)
α	2.30
T_{min}:	3.89°C (39°F)
T_{max}:	49.4°C (121°F)

	B.O.S.
Depth:	17.15 m (56.28 ft)
α	2.50
T_{min}:	22.8°C (73°F)
T_{max}:	49.4°C (121°F)

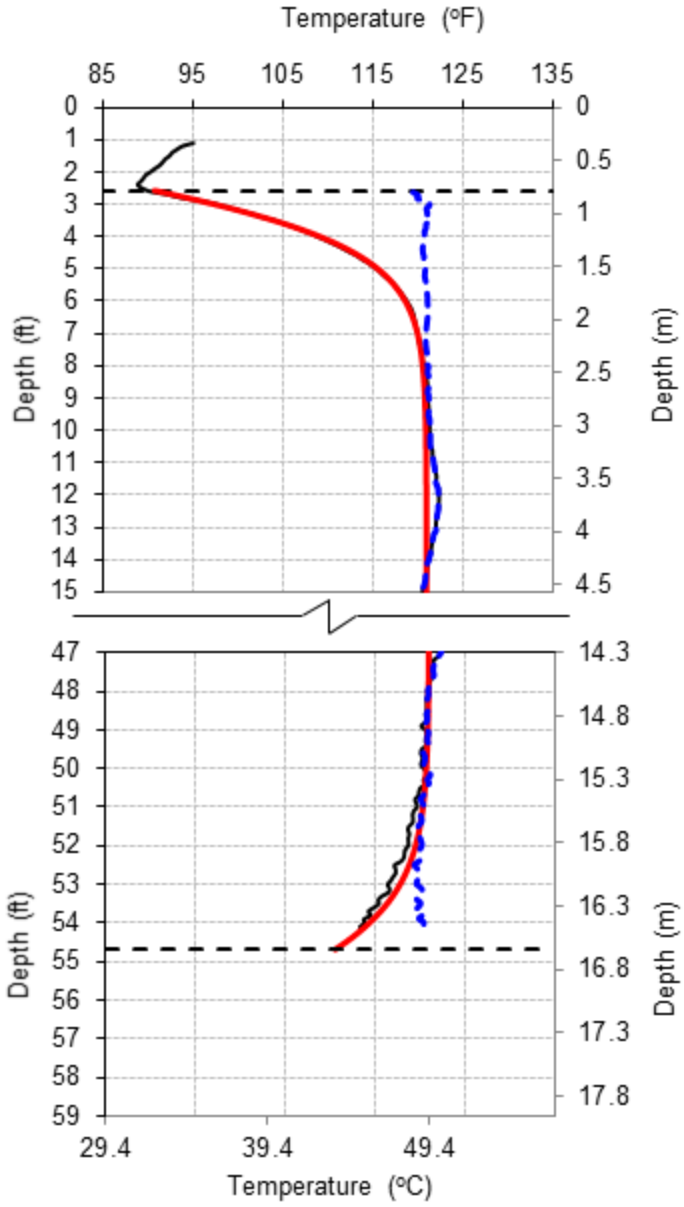

Figure 2.15 Curve fit and temperature corrections for top and bottom of tested shaft.

After correcting the end temperatures, the average corrected temperature for the entire shaft is calculated as 49.96°C (121.92°F). From the construction log, the concrete volume placed (CVP), length of shaft, and volume of steel are used to calculate an average shaft radius of 0.628m (24.72in). These values are used to determine the T-R relationship which is then used to compute the effective radius for each tube at every depth, as shown in Figure 2.15. The difference between

effective radius and cage radius provides an estimate of concrete cover, and the difference in radius among opposing tubes (e.g. 1 & 3, 2 & 4) indicates cage alignment.

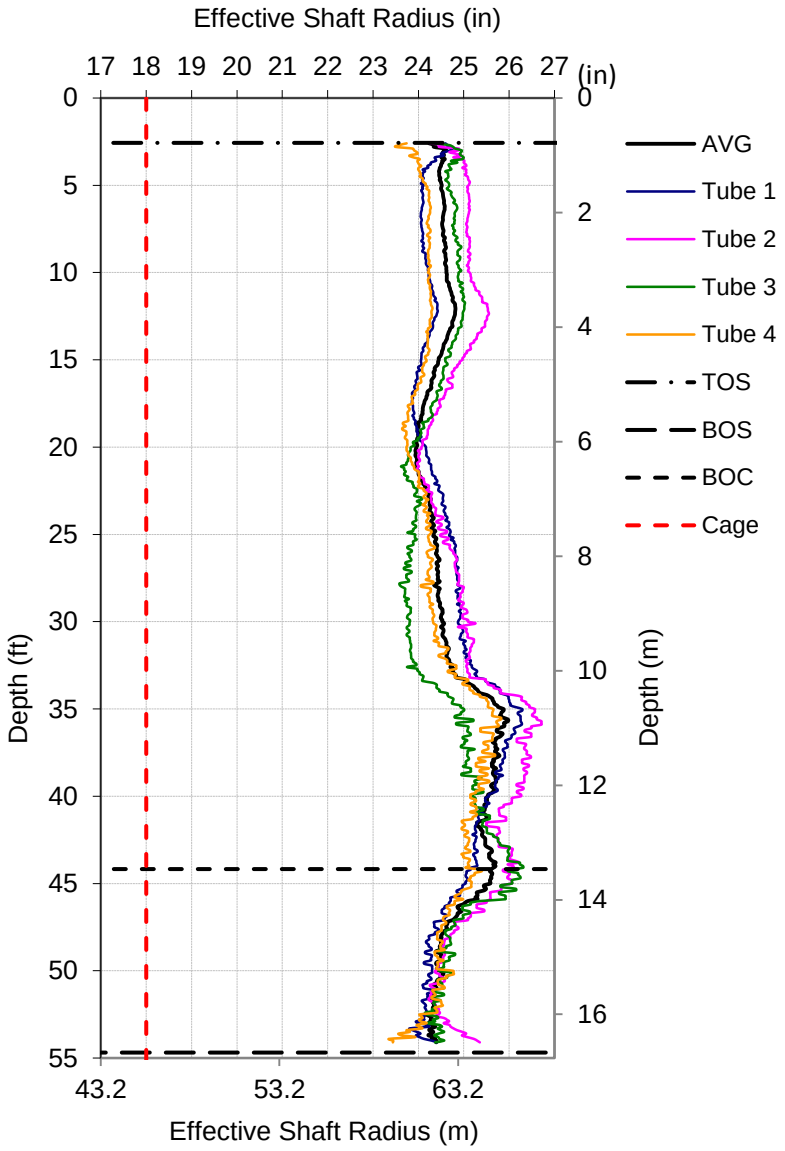

Figure 2.16 Effective shaft radius for tested shaft.

2.7 Chapter Summary

The information gained from computer generated thermal models provides valuable information about temperature distributions in drilled shafts that can be used to better understand TIP measurements and enhance the methods used to analyze them. Insight provided by models has

led to methods for converting temperature to effective radius that are both accurate and conservative, as well as a method for analyzing the end regions of shafts, which do not follow a typical temperature-radius relationship. The techniques presented here have been successfully applied in hundreds of TIP analyses to date and have proved to provide a heightened level of shaft assessment based on temperature profiles.

CHAPTER 3: ANALYZING THERMAL INTEGRITY PROFILES[2]

Thermal Integrity Profiling (TIP) is the most recent non-destructive test method to gain widespread popularity in post-construction evaluation of drilled shafts. The allure lies in its ability to detect anomalies across the entire cross section of a shaft as well as provide a measure of lateral cage alignment. Similarly remarkable, early developments showed that the shape of a temperature profile (with depth) matched closely with the shape of the shaft, thus allowing for a fairly straightforward interpretation of data. Immediately apparent however, was that the relationship between shape and temperature was with two major exceptions: (1) near the ends of the shaft where heat can escape both radially and longitudinally and (2) where drastic changes in the surroundings are encountered (e.g. soil to water, soil to air). Today, methods for analyzing these portions of data exist, but can often involve tedious levels of parameter iterations and trial-and-error thermal modeling. This is particularly true when the effects of time are not well understood. A comparison of model and field results is presented to provide further insight into these types of temperature distributions and to address the difficulties associated with their analysis. This chapter shows how thermal modeling can be used to track the effects of time on analysis, and concludes with a case study that demonstrates the findings.

3.1 Introduction

Thermal Integrity Profiling (TIP) is an in-situ, non-destructive method for evaluating the post-construction quality of cast-in-place deep foundations. Due to the blind nature of the

[2] Portions of this chapter were published in DFI Journal, Vol. 10, No. 1. Permission is included in Appendix C.

underground concreting process, as well as the lack of visual inspection thereafter, quality assurance in drilled shaft construction relies heavily on the means of other physical measurements to infer the quality and distribution of concrete. Common methods include Cross-hole Sonic Logging (CSL), which measures the time for acoustic waves to travel between access tubes, and Gamma-Gamma Logging (GGL), which measures the attenuation of gamma radiation in the material immediately surrounding access tubes. Both are effective in detecting anomalies, but have limited zones of detection due to the positioning of source and receiver probes.

Developed in the late 1990's, TIP is the most recent of non-destructive test methods to gain popularity in drilled shaft evaluation. Its uniqueness from other methods, like CSL and GGL, lies in its ability to detect anomalies across 100% of the cross section of a shaft as well as provide a measure of lateral cage alignment. However, as with any test method, the quality of results depends largely on the level of analysis and the way in which test data is interpreted.

3.2 Background

Concrete hydration is a highly exothermic process, and in large concrete elements, such as drilled shafts, a significant amount of energy is released, causing elevated temperatures in both the shaft and surrounding soil, typically for several days. The amount of temperature increase at any given point depends on the volume of hydrating concrete in proximity as well as the cementitious content of that concrete, both of which help to define shaft serviceability. TIP takes advantage of this and detects anomalies based on variations in the thermal profile of a shaft during the curing stages. Temperature measurements can be achieved in either of two ways – via thermal probe which is lowered down access tubes, or thermal wires which are attached to the reinforcement cage and cast within the shaft. (Anderson, 2011)

Figure 2.1 illustrates the way in which heat is dissipated from a shaft to its surroundings, and the temperature distributions that result from it. For a perfectly cylindrical shaft, the vertical distribution of temperature is uniform throughout the majority of its length. The exception is near the ends where there is a distinct region of decreasing temperature. This temperature "roll-off" at the top and bottom is due to the added mode of heat loss in the longitudinal direction. The radial temperature distribution is bell-shaped, with peak temperatures occurring at the center of the shaft and decreasing radially towards the surrounding soil. With a typical configuration of access tubes (one tube per 0.3m of diameter, evenly spaced around the reinforcing cage, per ASTM D7949), data collected from thermal integrity testing provides a continuous temperature profile vertically and discrete measurements laterally (indicated by red dots in Figure 2.1). The vertical profile reveals any bulges, necks, or inclusions that may be present, while comparison among tube temperatures indicates lateral cage alignment. (Mullins & Winters, 2012)

Direct observation of measured temperature profiles can provide immediate qualitative information about a shaft, such as general shape, relative cage alignment, and the types of anomalies that may be present. An increase or decrease in all tube temperatures indicates a bulge or neck in the shaft, respectively; whereas an equal but opposite variation of opposing tube temperatures indicates cage eccentricity. Circular shaped temperature roll-offs that extend about one diameter from the top and bottom of the shaft indicate normal end conditions. Figure 3.1 illustrates these types of observations.

While direct observation of profiles is useful in identifying anomalies, a measurable assessment of shaft integrity is obtained by converting temperatures to values of effective shaft radius. Because measured temperatures are affected by both shaft size and cementitious content, it can be conceived that the temperature resulting from an anticipated shaft radius consisting of

intact, quality concrete could also result from a larger radius consisting of compromised concrete. In this sense, the term effective radius implies the radius of intact, quality concrete that would produce the measured temperature.

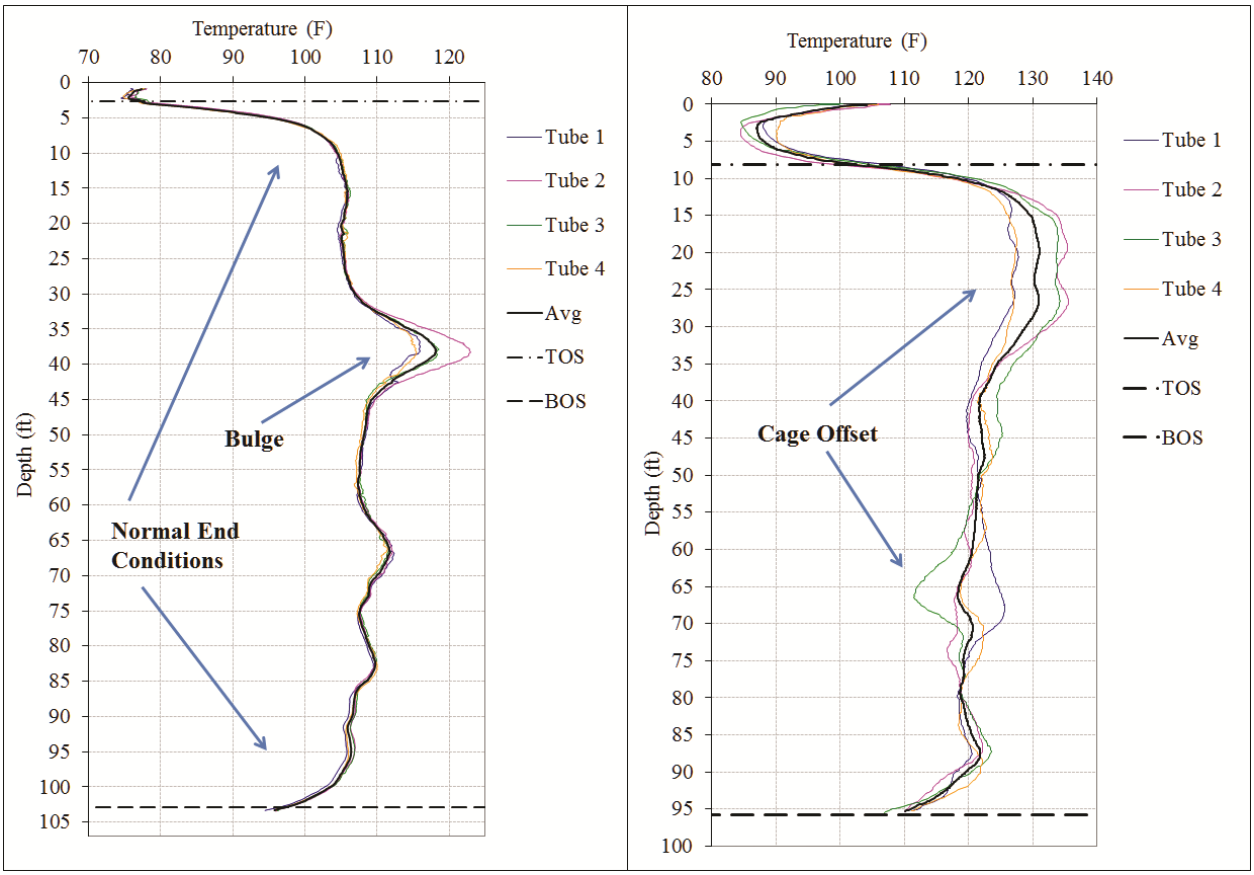

Figure 3.1 Example thermal profiles with anomalies.

Figure 3.2 shows the relationship between shaft radius, cage position, and measured temperature. The dashed lines represent cage position where measurements are taken, the bold lines represent the temperature distribution corresponding to the local shaft size, and the intersection of the lines reveals the temperature that would be measured. Note that the inflection point of each curve, where the slope is the steepest and most linear, is at the edge of shaft, near cage location. This makes temperature measurements at the cage highly sensitive to both shaft size and cage eccentricity. Distinction between the two can be made by comparison of cage temperatures on opposing sides of the bell curve. For a given radial position, the dashed lines in

Figure 3.2 reveal the unique correlation that exists between shaft size and temperature. This relationship is asymptotic towards soil temperature and the adiabatic concrete temperature, and has an inflection point where shaft radius equals the given measurement position. Note that measurements taken at cage radius will fall near the inflection point, where the relationship between shaft size and temperature is strongly linear. (Mullins, 2013)

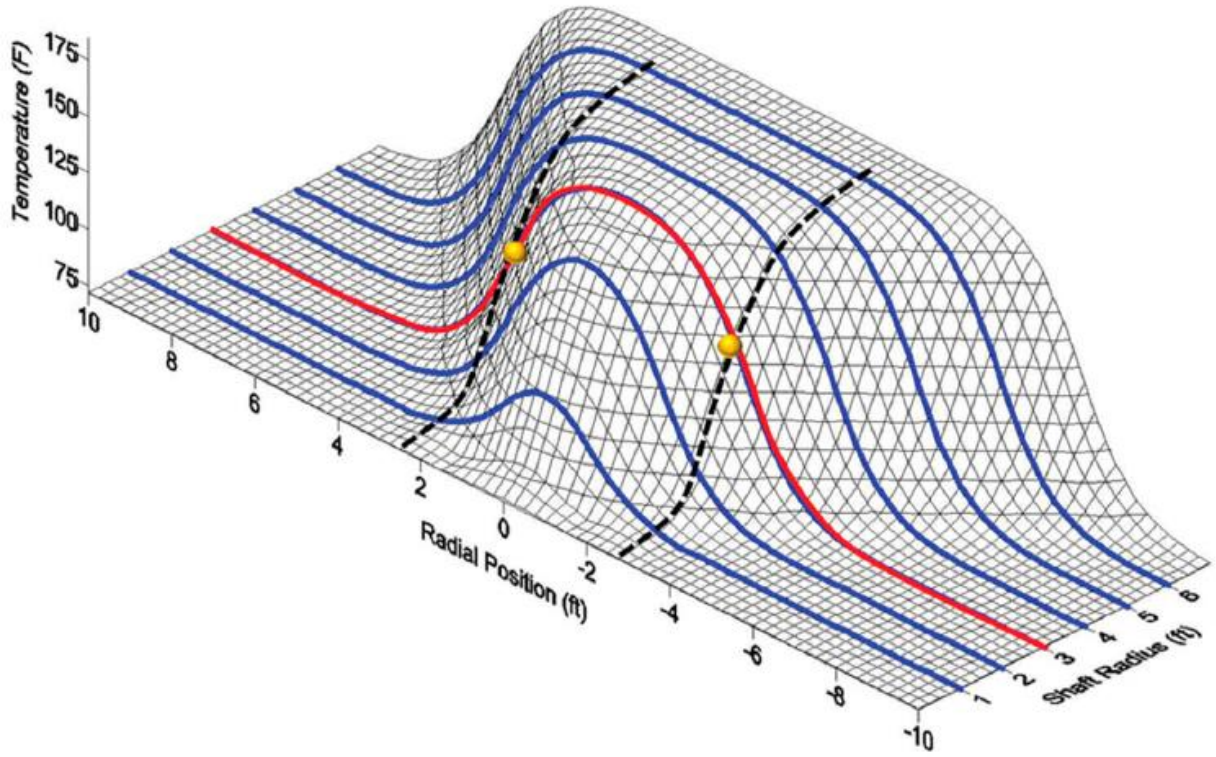

Figure 3.2 Relationship between cage position, shaft size, and temperature. (Mullins, 2013)

3.3 Concepts of TIP Analysis

Since the relationships illustrated in Figure 3.2 are specific to the nearly infinite combinations of variables like concrete mix, shaft surroundings, and regional climate, the relationship between temperature and radius for a given shaft is best determined by superimposing it with information provided by construction logs and concrete yield data. At the onset of the development of TIP technology, findings showed that the shape a thermal profile linearly corresponded with shaft dimensions as determined from concrete yield data (Figure 2.2). This led

to a method of analysis based on superimposing TIP data with concrete yield data to generate a temperature-radius (T-R) correlation which could be applied to an entire dataset. With this method, the average radius was computed from concrete volume placed (plus steel volume) over a given height and paired with the average measured temperature over the same height to provide a calibration point from which a T-R relationship was regressed. Although the true relationship is S-shaped (dashed lines in Figure 3.2), the assumption of linearity is valid for measurements taken at cage location. Variations in either direction from this point fall within the linear portion of the curve. A linear T-R relationship can be generated using the average radius and average temperature over the entire shaft derived from a single point solution; or, if concrete yield data is sufficiently resolved with multiple points, a best fit linear regression can be derived. Research suggests that a single point solution yields a close approximation to model results and is conservative against over-prediction of anomaly severity in most cases (Figure 3.3).

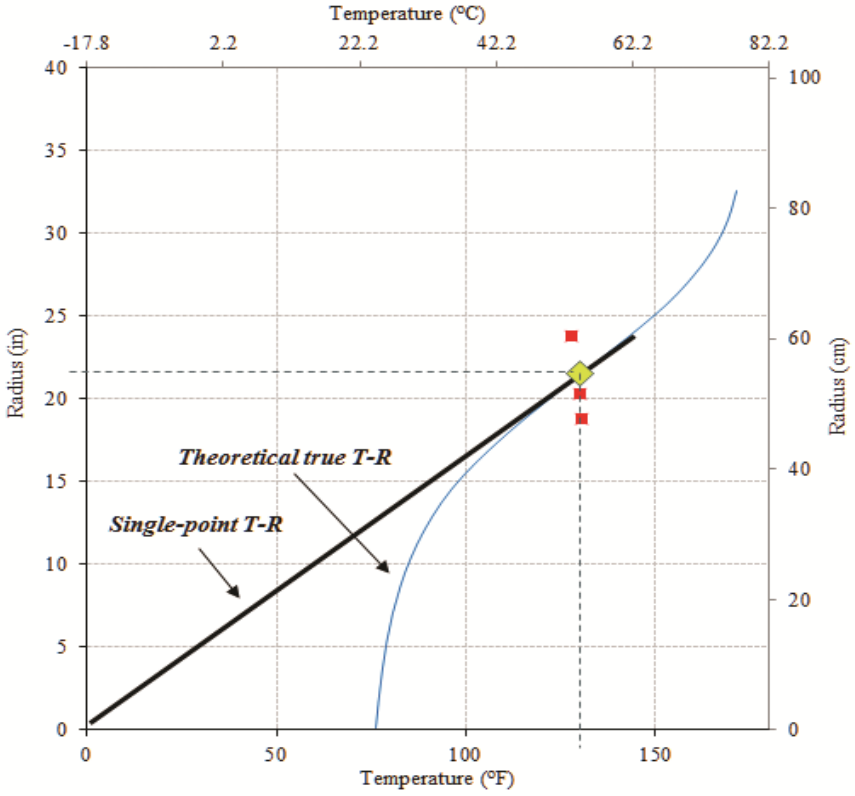

Figure 3.3 Single-point *T-R* curve compared to theoretical.

This type of calibration essentially eliminates the need to make assumptions about thermal properties that would be required for temperature prediction modeling. However, a single expression, whether it be linear or S-shaped, is limited to regions of uniform boundary conditions. Immediately apparent in any shaft is that the ends do not conform to this limitation due the additional heat loss boundary in the longitudinal directions. The temperature profiles exhibited at the top and bottom of a shaft do not follow a one-to-one correlation with radius, thus, without proper corrections, cannot be directly analyzed using a T-R relationship and should not be included in the development of such. Likewise, transitions between soil and water or air, or between drastically different soil strata, can produce similar thermal distributions which do not adhere to the limitations of a single T-R correlation. In fact, a boundary transition within the middle of a shaft will divide the thermal profile into regions that follow two different T-R relationships, thus a single expression for the shaft cannot be generated or applied until temperatures are corrected. As a result, algorithms have been developed to account for both end conditions and boundary transitions, and to normalize temperatures to remove fluctuations not caused by changes in cross section.

Modeling reveals that the theoretical heat dissipation at the ends of a perfectly cylindrical shaft closely mimic a hyperbolic tangent equation. This was first explained by Johnson (2014) where the normal temperature of the shaft close-to but not affected by end conditions was used to define one asymptote of the hyperbolic fit. The other asymptote was then defined by the soil temperature below the shaft or the air above. By comparing fitted to measured temperatures, the "roll-off" zone near the ends could then be adjusted/corrected to shaft temperatures away from the ends, and the radius predicted from the T-R relationship would then show the correct shape. The hyperbolic tangent formulation (Eqn. 3.1) and temperature correction algorithm (Eqn. 3.2) are

presented here, but slightly modified to be more interchangeable and universally applicable to both top and bottom roll-offs as well as mid-shaft transitions.

$$T_{fit} = \left(\frac{T_{below} - T_{above}}{2}\right) \tanh\left(\frac{z - z_0}{\alpha}\right) + T_0 \quad \{3.1\}$$

where,

$$T_{below} = Asymptotic\ temperature\ below\ inflection\ point$$

$$T_{above} = Asymptotic\ temperature\ above\ inflection\ point$$

$$T_0 = Temperature\ at\ inflection\ point = (T_{below} + T_{above})/2$$

$$z_0 = Depth\ of\ inflection\ point$$

$$\alpha = Time\ factor$$

$$T_{cor} = \left(T_{meas} - T_{fit}\right)\left(\frac{T_{norm}}{T_{fit}}\right) + T_{norm} \quad \{3.2\}$$

where,

$$T_{cor} = Corrected\ temperature$$

$$T_{meas} = Measured\ temperature$$

$$T_{norm} = Normalizing\ temperature$$

While the above hyperbolic tangent formula can be applied to almost any thermal transition zone, fits are rarely a 100% match, even with model data, and blind selection of parameters can lead to tedious levels of trial-and-error iterations and can even produce fits which are seemingly correct but with values that are physically impractical. To this end, the following analysis serves as an example of using hyperbolic corrections and provides insight into the proper selection of curve parameters.

3.4 Application of Hyperbolic Corrections

In order to evaluate the application of hyperbolic corrections, a set of thermal wire data was selected from a shaft containing clear top and bottom roll-offs as well a significant mid-shaft

thermal transition (discussed later). Before applying these analysis methods to the field collected data however, a model shaft was generated with similar conditions and was analyzed to assess any trends or patterns which may prove useful. Model data was generated, using the α-β-τ heat of hydration method as described by Schindler & Folliard (2005) and Poole (2007), for concrete curing times ranging up to 60hrs. The modeled profiles were then analyzed as if they were field collected data, using hyperbolic corrections and T-R conversions.

The profile in Figure 3.4 was generated from a model shaft with an upper cased portion of 69cm (27in) radius and a lower uncased portion of 61cm (24in) radius below the bottom of casing (BOC). Top of shaft (TOS) was located at ground surface and bottom of shaft (BOS) was located at a depth of 10.8m (35.4ft). Based on the input shaft dimensions, the concrete volume placed (CVP) was 14.7m^3 (19.25cy), which was used to calculate the average shaft radius for the T-R relationship. Also included was a drastic change in boundary layers (low diffusivity overlying high diffusivity) occurring at depth of about 3.6m (12ft). Ambient soil temperature was set to 15.6^{o}C (60^{o}F) and air temperature was set to have a diurnal fluctuation of 18.9-28.3^{o}C (66-83^{o}F). Once data was generated, peak temperatures were identified at 18hrs and the corresponding profile was selected for initial analysis.

The first step in applying temperature corrections is to properly identify regions of the profile where corrections are warranted. In almost all shafts, this includes the top and bottom, however any other suspected regions should be justified by strong evidence from site investigations (e.g. boring log, SPT, CPT). Also, for mid-shaft boundary changes, the boundary layer considered as normal should be identified. This is typically whichever layer is in soil (i.e. not water or air) and accounts for the majority of shaft length. In this case, everything in the low diffusivity layer was normalized to the underlying higher diffusivity layer.

Selection of hyperbolic parameters began by setting the inflection point depths based on the known depths of TOS, BOS, and the interface between differing boundary layers. Next, asymptotic and inflection point temperatures (T_{max}, T_{min}, T_0) were selected based on observed values within the profile as well as known environmental temperatures. At the interface between boundary layers, T_{min} and T_{max} was observed from the nearest regions of uniform temperature on either side of the transition zone, and T_0 was computed as the average between them. For the top and bottom roll-offs, the temperature of both the ambient air and soil are strong pieces of information which help to define each hyperbolic distribution. At the bottom, because the heat transfer characteristics of soil are similar to those of concrete, the temperature distribution in the soil is essentially a continuation of the same hyperbolic curve exhibited in the concrete. This results in a symmetrical curve with T_{min} equal to soil temperature, T_{max} equal to nearest uniform temperature in the shaft, and T_0 equal to the midpoint between them. Conversely, at the top of the shaft, the modes of heat transfer between concrete and air are drastically different. The much stronger convective cooling behavior of air results in little to no temperature distribution beyond the interface and dominates the temperature at the surface. Because of this effect, top roll-offs are best fit by setting the inflection point (T_0) to be ambient air temperature. Note that doing so results in a T_{min} value that has no physical significance.

After determining depth and temperature parameters for each curve, $\boldsymbol{\alpha}$ values were systematically selected to achieve the best fit. The parameter $\boldsymbol{\alpha}$ defines the distance to which the effects of a thermal transition extend away from the interface. It has units of distance and is defined by the intersection of the asymptote and the slope at the inflection point on a hyperbolic curve. Using this definition, a rough estimate can be made by visual inspection of the profile. Theoretically, $\boldsymbol{\alpha}$ ranges from zero at time zero, when no heat exchange has had time to occur, to

infinite once all heat exchange has occurred and equilibrium is reached. For the typical timeframe of testing, **α** generally ranges between 0.3-1.5m (1-5ft), increasing with time.

Table 3.1 gives the best fit hyperbolic parameter values for the model shaft at 18hrs. All depth and temperature parameters were kept in agreement with the shaft dimensions and boundary temperatures input into the model, and **α** values ranged from 0.38-0.43m (1.25-1.4ft). Figure 3.6 shows the applied hyperbolic fits and corrected temperatures along with the resulting effective radius profile.

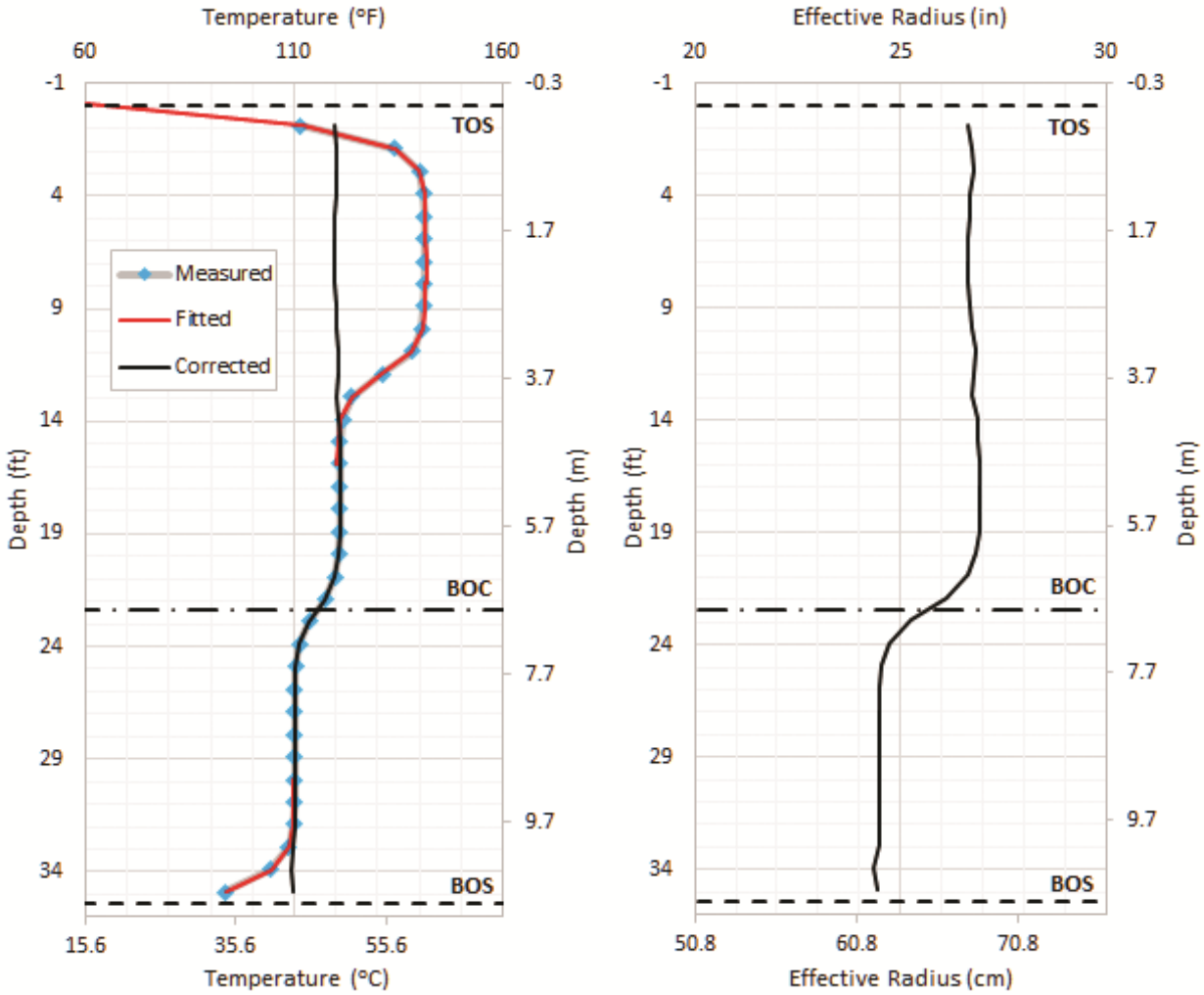

Figure 3.4 Results of model analysis at 18hrs.

Table 3.1 Hyperbolic equation parameters for model data at 18hrs.

	Z_0 m (ft)	T_{max} ^oC (^oF)	T_{min} ^oC (^oF)	T_0 ^oC (^oF)	α m (ft)
Top	0 (0)	60.9 (141.6)	…	19.1 (66.3)	0.39 (1.28)
Transition	3.6 (11.9)	60.9 (141.6)	49 (120.2)	…	0.38 (1.25)
Bottom	10.8 (35.4)	43.3 (110)	15.6 (60)	…	0.43 (1.4)

With the same model inputs, the same analysis procedure was performed for all times ranging from 9-60hrs in order to examine the effects of time. In each case, best fits were achieved with the same inflection point depths (z_0 = *top or bottom of concrete*) throughout, matching asymptotic temperatures within the shaft by visual inspection, and using soil temperature as the minimum for the bottom roll-off. The only parameters requiring trial and error iterations were the inflection point temperature (T_0) for the top roll-off and all three $\boldsymbol{\alpha}$ values, each of which revealed trends. Figure 3.5 shows the correlation that was exhibited between air temperatures and the inflection temperatures at the top roll-off. The pattern of inflection temperatures exhibits the same period as that of the diurnal air temperatures, but with a distinct lagging effect, suggesting that they are primarily influenced by the range of recent air temperatures experienced, rather than the current air temperature. Furthermore, the damping effect exhibited as time progressed suggests that inflection temperatures are less variable at later stages and could be more accurately estimated with the average of previous daily temperatures. Figure 3.6 shows the trends revealed by the best fit $\boldsymbol{\alpha}$ values from the model analysis. All three exhibit a strong linear relationship with the square root of time, and with similar slopes.

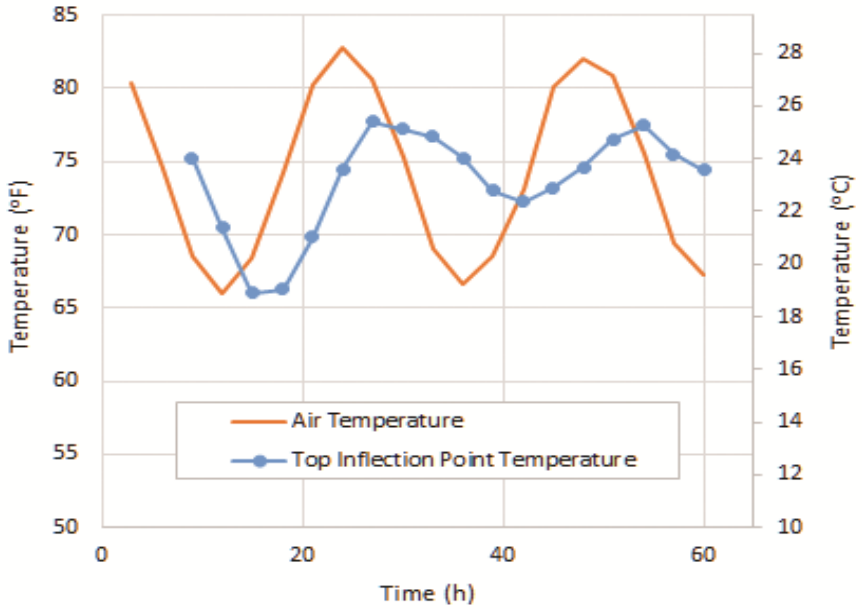

Figure 3.5 Variation of top roll-off inflection temperatures compared with air temperature.

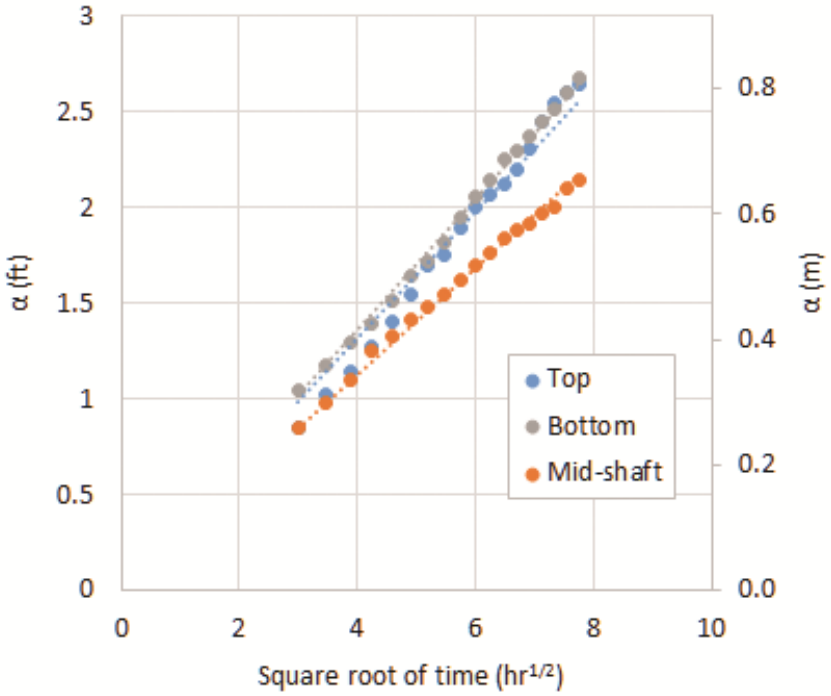

Figure 3.6 Variation of **α** with time resulting from analysis of model data.

3.5 Case Study

Using the insight gained from modeling, the same analysis was performed using data collected from a 10.7m (35ft) long, 1.2m (4ft) diameter shaft with partial length permanent casing.

Figure 3.7 shows the temperature profiles measured by five thermal wires fastened to the reinforcing cage. As the reinforcing cage is rarely perfectly concentric, the average of all profiles should be used for determining T-R relationships. As with the model data, peak temperatures were observed at 18hrs and this data was analyzed first (Figure 3.7). Hyperbolic parameters were selected using the same guidelines but were adjusted in order to obtain the best fits. Inflection point depths for the top and bottom roll-offs were adjusted from reported values up 0.3m (1ft) and down 0.1m (0.3ft), respectively. It is common for reported TOS and BOS elevations to vary slightly depending on factors like over-excavation of the bottom and the amount of over-pour (or under-pour) at the top. Thus, adjustment of inflection point depths up to about 0.3m (1ft) in either direction is reasonable. The inflection point for the mid-shaft transition was set at 3.5m (11.4ft) based on visual inspection of the data and then compared with the nearest boring log which indicated a water table depth of 3.4m (11ft) as well as an interface of clay overlying sand at the same depth. While soil type and saturation states can have an effect on soil conductivity, soil saturation does not typically vary significantly just above and below the water table (Johansen, 1977). However, in regions where the water table is relatively stable, this can occur. A more common cause of such a drastic temperature variation in this case is the presence of a small annular air gap that can form around the shaft due to predrilling of the clay layer to install the permanent casing. Soil temperature at depth was determined from the annual average air temperature of the region, which was 12.8^{o}C (55^{o}F), and was used for the bottom roll-off minimum temperature (T_{min}). Air temperature from the time of casting was conveniently available from the excess thermal wire sensors extending from the top of shaft, which recorded air temperatures ranging from 18.3^{o}C (65^{o}F) to 27.8^{o}C (82^{o}F). An inflection temperature of 25^{o}C (77^{o}F) provided the best fit for the top roll-off. All other temperature parameters were selected from observed values in the thermal

profile, and α was iterated by trial and error, using the general relationships in Figure 3.6 as an initial estimate. Table 3.2 gives the final parameter values.

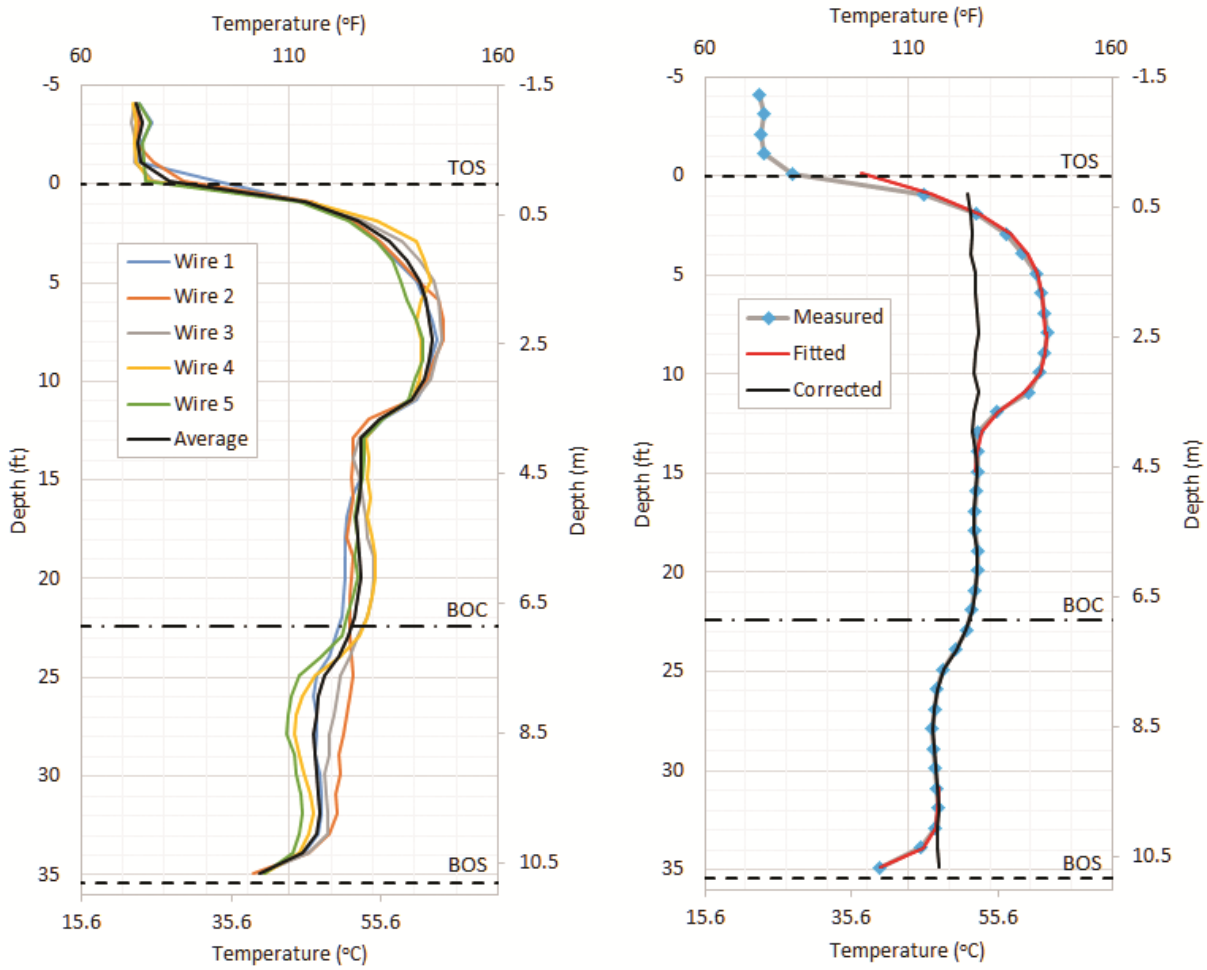

Figure 3.7 Measured field data (left) and applied temperature corrections (right).

Table 3.2 Hyperbolic equation parameters for field data at 18hrs.

	Z_0 m (ft)	T_{max} °C (°F)	T_{min} °C (°F)	T_0 °C (°F)	α m (ft)
Top	-0.3 (-1.0)	62.2 (144)	-	25 (77)	0.91 (3.0)
Transition	3.5 (11.4)	62.2 (144)	52.5 (126.5)	-	0.38 (1.25)
Bottom	10.9 (35.7)	47.5 (117.5)	12.8 (55)	-	0.41 (1.33)

Analysis of the entire time range that was collected (23hrs), yielded similar patterns to those revealed by the model analysis. Inflection point temperatures at the top were dominated by air temperature (Figure 3.8), and **α** values followed a linear increase with the square root of time (Figure 3.9). In fact, the **α** relationships for the bottom and middle fits adhered to a similar slope as found in modeling, however the top **α** values followed a pattern that increased at more than twice the rate of the others, possibly due to the strong effects of wind which can be difficult to accurately replicate in computer models.

Finally, with the corrected temperature profile, a T-R relationship was determined and applied to the data to produce an effective radius profile for each thermal wire (Figure 3.10, left). Because testing was performed via thermal wires, data was collected continuously for 23 hours after casting. To examine the effects of concrete age on analysis results, the same procedures were applied to the thermal profiles measured between 9hrs and 23hrs. In theory, analysis performed on the same shaft at different times during the dominant stages of concrete hydration will produce varied T-R relationships, but should ultimately compute the same effective radius. Figure 3.10 (right) shows a comparison of the average effective radius profiles determined from analyses of various times, revealing very little variation. Furthermore, construction log information revealed that the upper portion of the shaft was permanently cased and that the shaft took 0.76m^3 (1cy) more concrete than anticipated. This is strongly corroborated by the thermal results which indicate a close match to the casing radius in the upper part, and a slightly larger than intended radius in the lower uncased part, which was expected from the tool diameter.

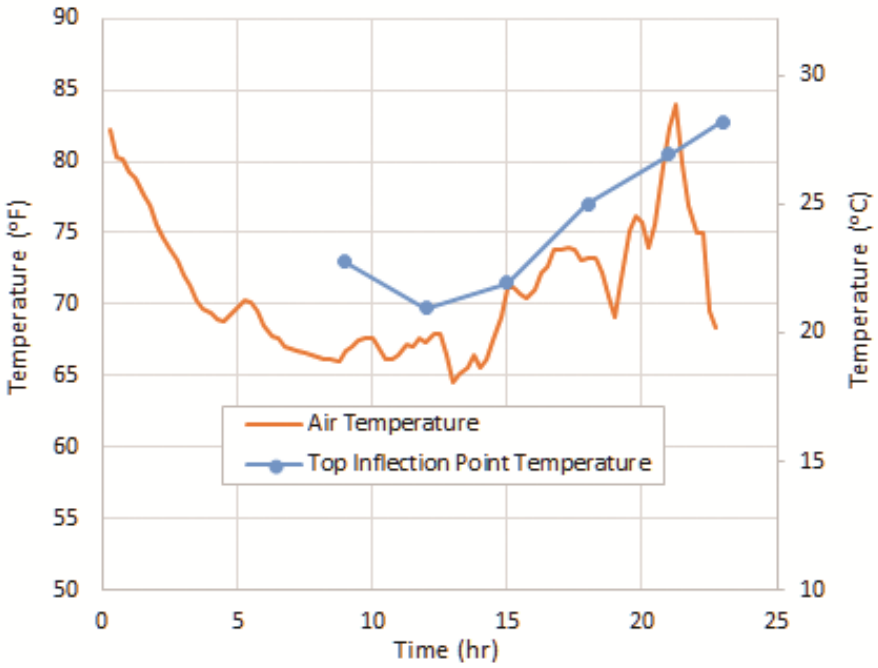

Figure 3.8 Top inflection point temperatures compared with measured air temperatures.

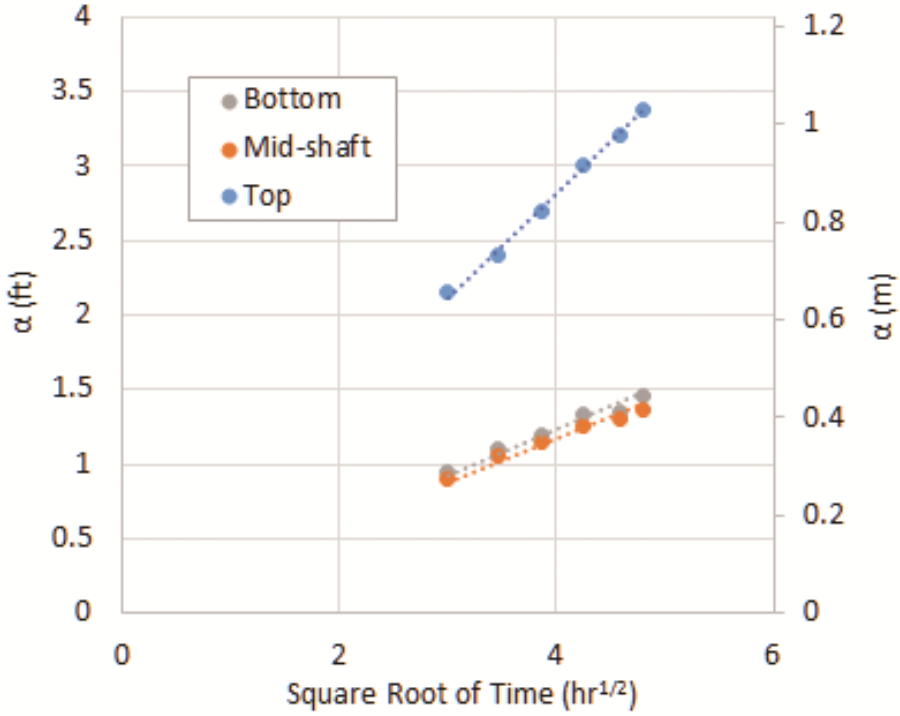

Figure 3.9 Correlation between **α** and time resulting from analysis of field data.

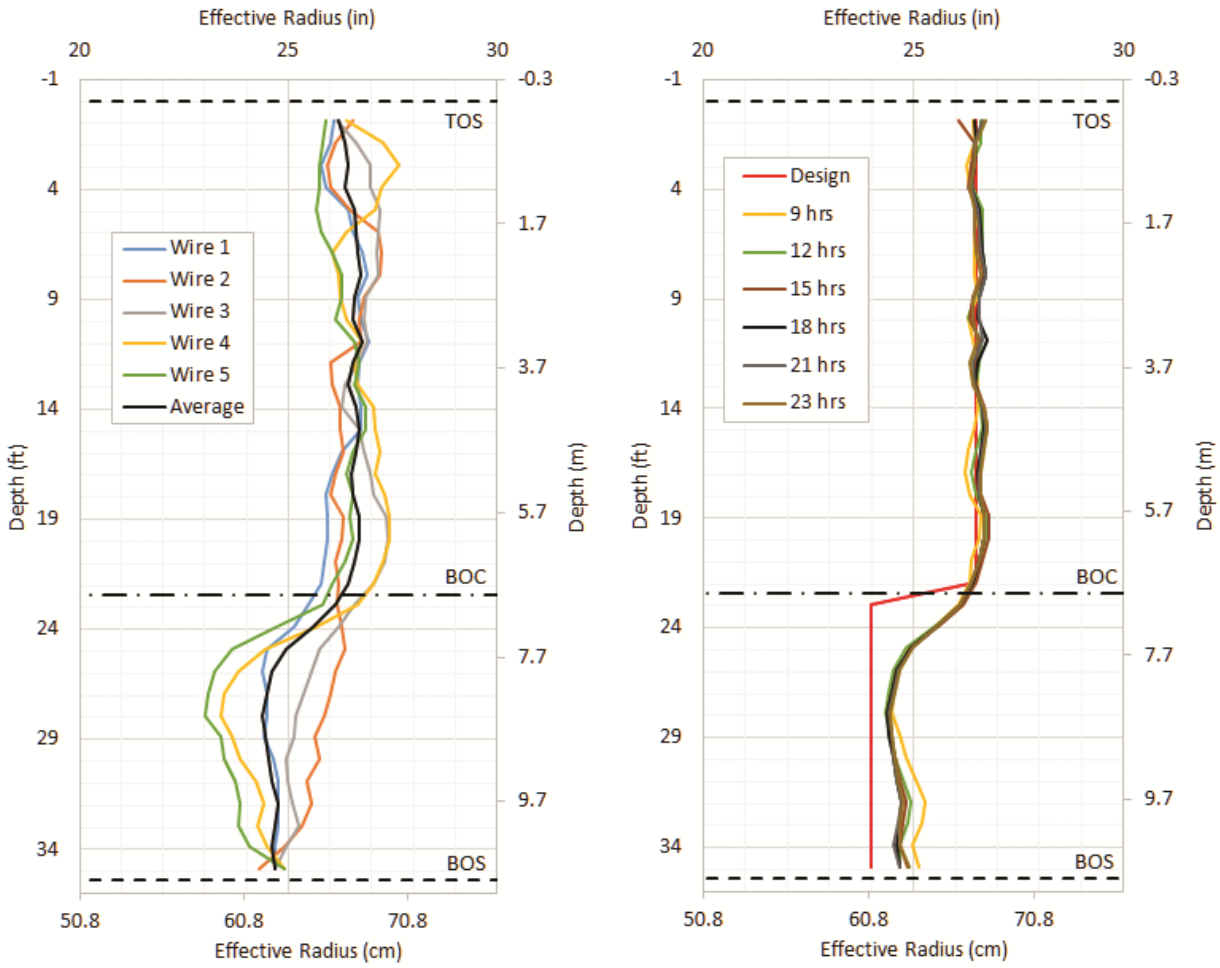

Figure 3.10 *T-R* results for analysis at 18hrs (left) and range of results for all times (right).

3.6 Chapter Summary

The temperature correction algorithm presented here provides a heightened level of traditional TIP analysis, allowing for previously problematic regions of a shaft to be analyzed using traditional T-R conversions. The results of the case study showed that analysis methods are largely insensitive to concrete age during the dominant stages of concrete hydration. Both model and field collected data show strong correlations with hyperbolic fitted curves in the top and bottom roll-off regions as well as in regions of mid-shaft thermal transitions due to changes in surrounding conditions. However, care must be taken to not abuse the application of mid-shaft transition corrections, as temperature variations due to actual radius changes can exhibit similar

patterns. These corrections should be justified with strong evidence that the occurrences are an effect of real boundary changes. The most common cases are overwater structures with shafts that transition from soil to water and/or to air.

Construction techniques can have significant effects on the quality of the interface/contact between the shaft and its surroundings and can have a distinctive temperature signature that may cause a mid-shaft transition. This manifested itself in this case study as a low diffusivity region most likely caused by the construction practice of predrilling before casing installation. Temporary, permanent, or isolation casing installation or extraction procedures can all be justification for mid-shaft transition corrections.

With the exception of the top of shaft $\boldsymbol{\alpha}$ factor, the modeled results presented agreed well with the field observed/fitted values. In all cases, $\boldsymbol{\alpha}$ should increase with time (as it did) and has been shown to be linearly proportional to the square root of curing time. Whether or not the fitted value is appropriate is best determined from site specific experience that may show increases in the upper shaft heat dissipation modes.

CHAPTER 4: STATISTICAL ANALYSIS OF FIELD DATA[3]

As with any signal matching approach, good matches can be found with physically impractical parameters. A strong sense of reasonable input values must be present when applying temperature corrections. To further investigate the selection of the most appropriate hyperbolic fitting parameters for TIP analyses, data from 232 field tested shafts were collectively examined to identify the trends exhibited by the best-fit hyperbolic parameters selected for each one. To do this, the data from each shaft were imported into a single spreadsheet and a curve-fitting algorithm was developed to find the best-fit solution for each top and bottom roll-offs by iterating through a range of values for each of the hyperbolic parameters (e.g., T_{max}, T_{min}, D_{inf}, T_{inf}, α, etc.). Once the best-fit hyperbolic solutions were found for every shaft, the resulting parameters were examined collectively and compared against contributing factors like concrete age and air temperature.

4.1 Selection of α Parameters

As noted previously, modeling shows the α factor to follow a strong increasing relationship with the square root of time, which was also corroborated by the case study in Chapter 3 (Figures 3.8 and 3.11). This relationship can be expressed by Equation 4.1, where α is in units of feet, *t* is units of hours, and the coefficient **c** is the subject of investigation (in units of ft·hr$^{-1/2}$).

$$\alpha = c\sqrt{t} \qquad \{4.1\}$$

Figure 4.1 shows the α values resulting from the best-fit top and bottom hyperbolic solutions versus the age of concrete at time of testing for the 232 shafts analyzed. Since testing on

[3] Portions of this chapter were published as part of a Florida Department of Transportation technical report. Permission is included in Appendix C.

this project was typically performed either one or two days after concreting, much of the data is clustered around the 24 and 48 hour timeframes, however some tests were performed as early as 12 hours and as late as 96 hours after concreting, providing a wide enough range of data to examine the time dependent trends.

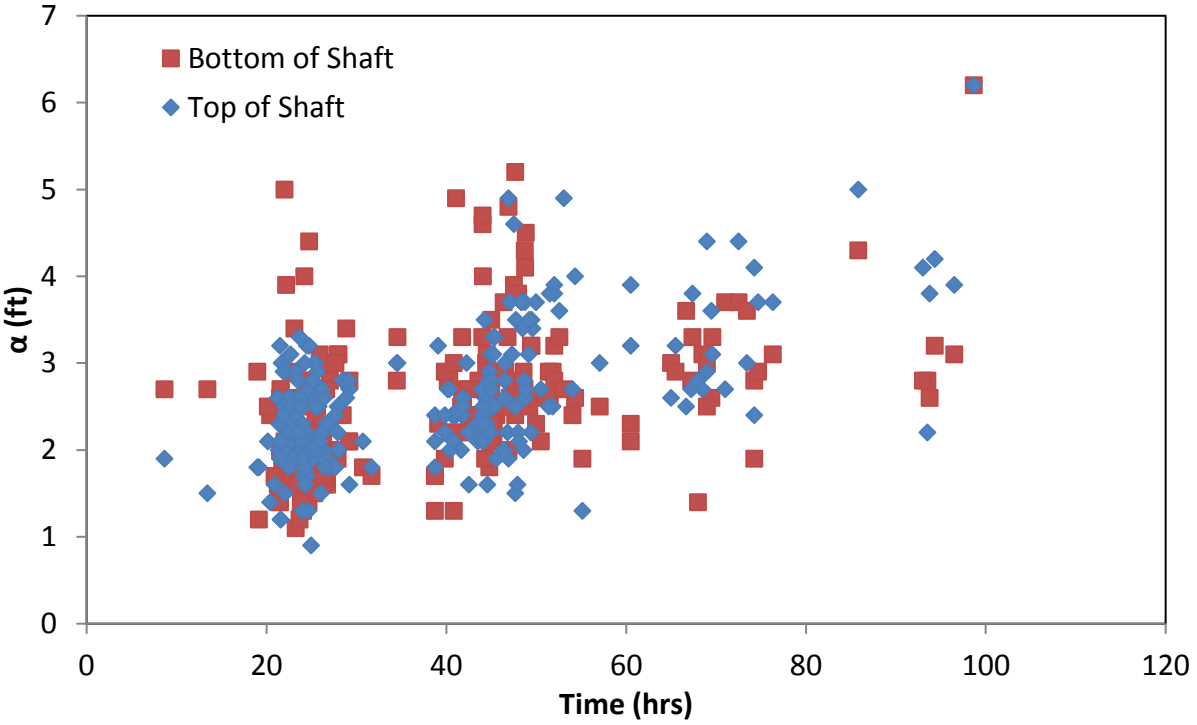

Figure 4.1 Best fit α values for both the top and bottom of shaft.

For each data point in Figure 4.1, the coefficient **c** was back calculated and rounded to nearest multiple of 0.025 for the purpose of creating the frequency distribution curve shown in Figure 4.2. The result is a positively skewed distribution, as opposed to a normal distribution, due to the hard boundary on the lower side imposed by the concept that **c** cannot equal zero. This is not uncommon for data with such a condition, but it results in a statistical average that is heavily weighted by the outliers on only one side of the distribution. Instead, the central tendency of the data is better represented by the median value, which in this case yielded a value of **c** = 0.4. The variability of the data is measured by the standard deviation (σ). Figure 4.3 shows the α vs. time relationship resulting from the statistical analyses.

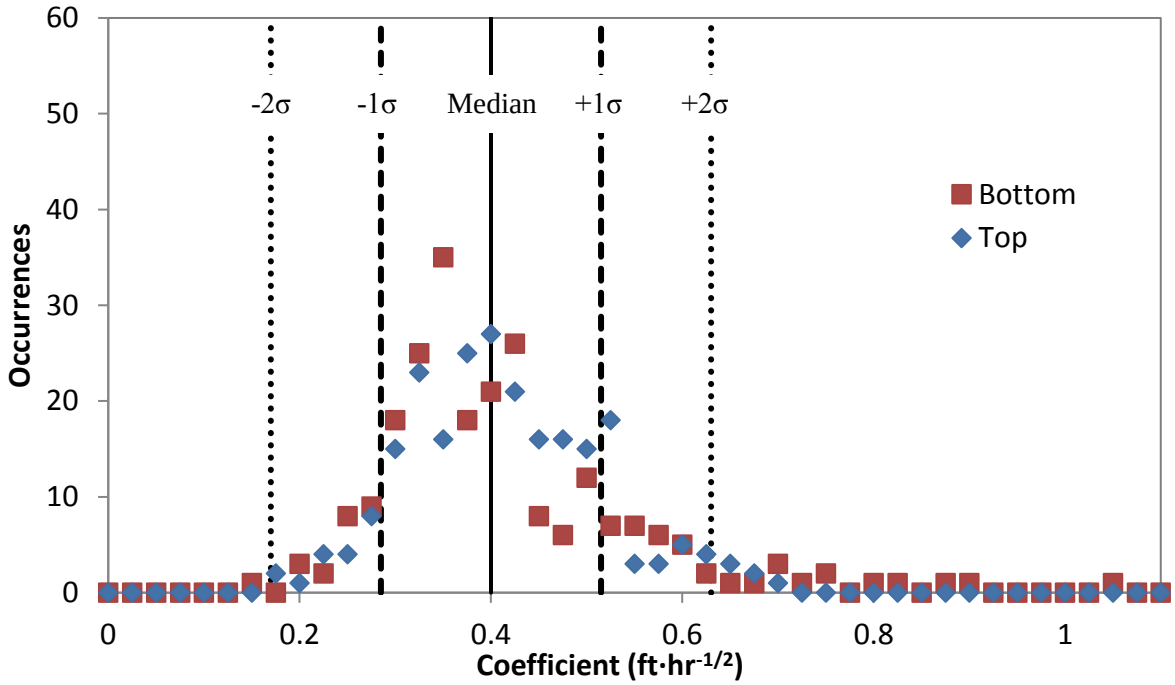

Figure 4.2 Probability density distribution for the coefficient c in the equation $\alpha = c\sqrt{t}$.

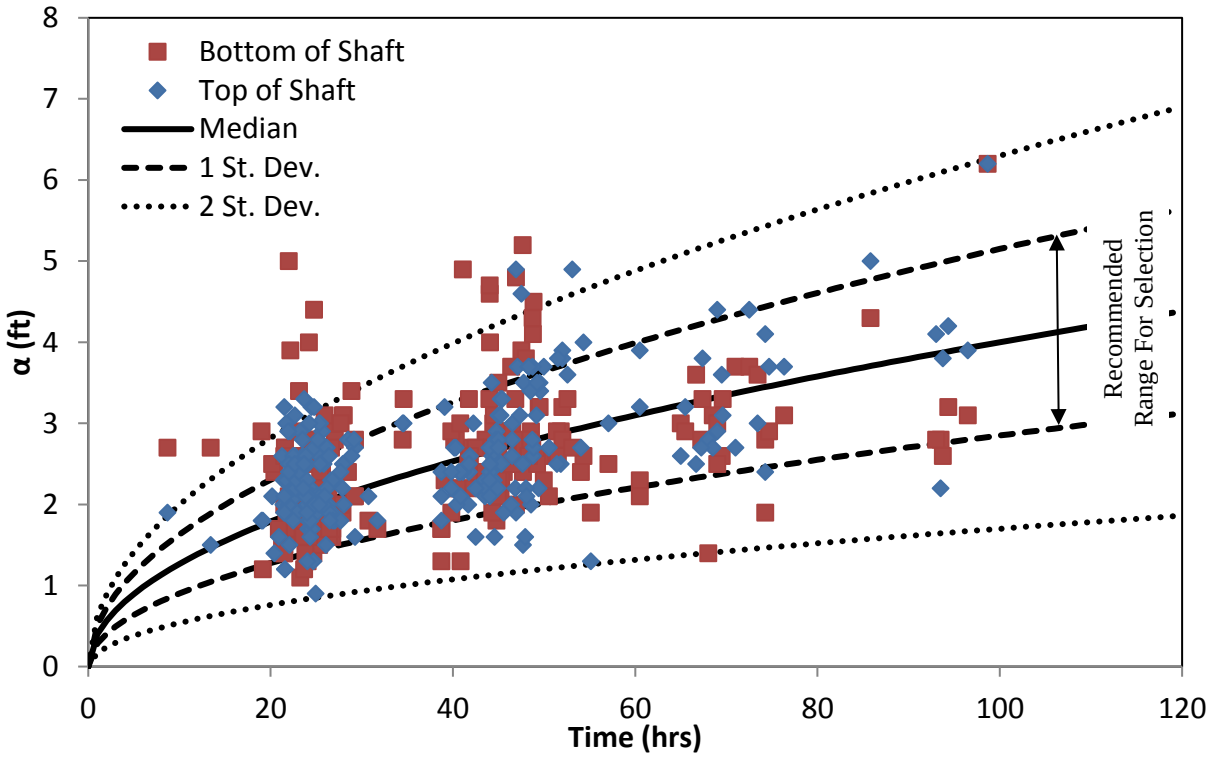

Figure 4.3 Statistically derived boundaries for α selection.

Note that the occurrence of α values less than one standard deviation below the median is less frequent than those more than one standard deviation above the median. This demonstrates

the effects of a positively skewed probability distribution where α values for bullet shaped shaft tips or misshaped tops are more likely than oversized tops or bell-shaped toes. A lower than expected α value only occurs in the presence of a significant belled shaft tip or bulge. At the surface this occurs when over pour concrete is left on the ground surface around the shaft top.

4.2 Top Inflection Point Temperatures

Further investigation of the fitted field data is aimed at proper selection of the inflection point temperature at the top of shaft. Because the convective cooling behavior of free air is much stronger the conductive heat transfer in soil, it directly influences the temperature at the top surface of a shaft. Figure 4.4 shows the best-fit top of shaft inflection point temperatures along with the daily high and low recorded air temperatures.

Note that the 232 shafts were all cast up to ground surface, but did not extend above. For shafts that are terminated well below ground (low cutoff elevation), there is less effect from air and those cases tend to be more aligned with bottom of shaft conditions.

One quick observation is that in warmer summer months, the inflection temperature more closely aligns with the lower daily air temperature and in winter months it aligns with the warmer daily air temperature. It should also be noted that the trend could also be affected by the regional deep soil temperature which was 73^{o}F for that site. Recall, the deep soil temperature is a constant that reflects the average annual air temperature for the geographical region. A further extension of this evaluation could be performed which would look more closely at the exact time of testing relative to the recent air temperature history (e.g., within the previous 4 to 24hrs, etc.).

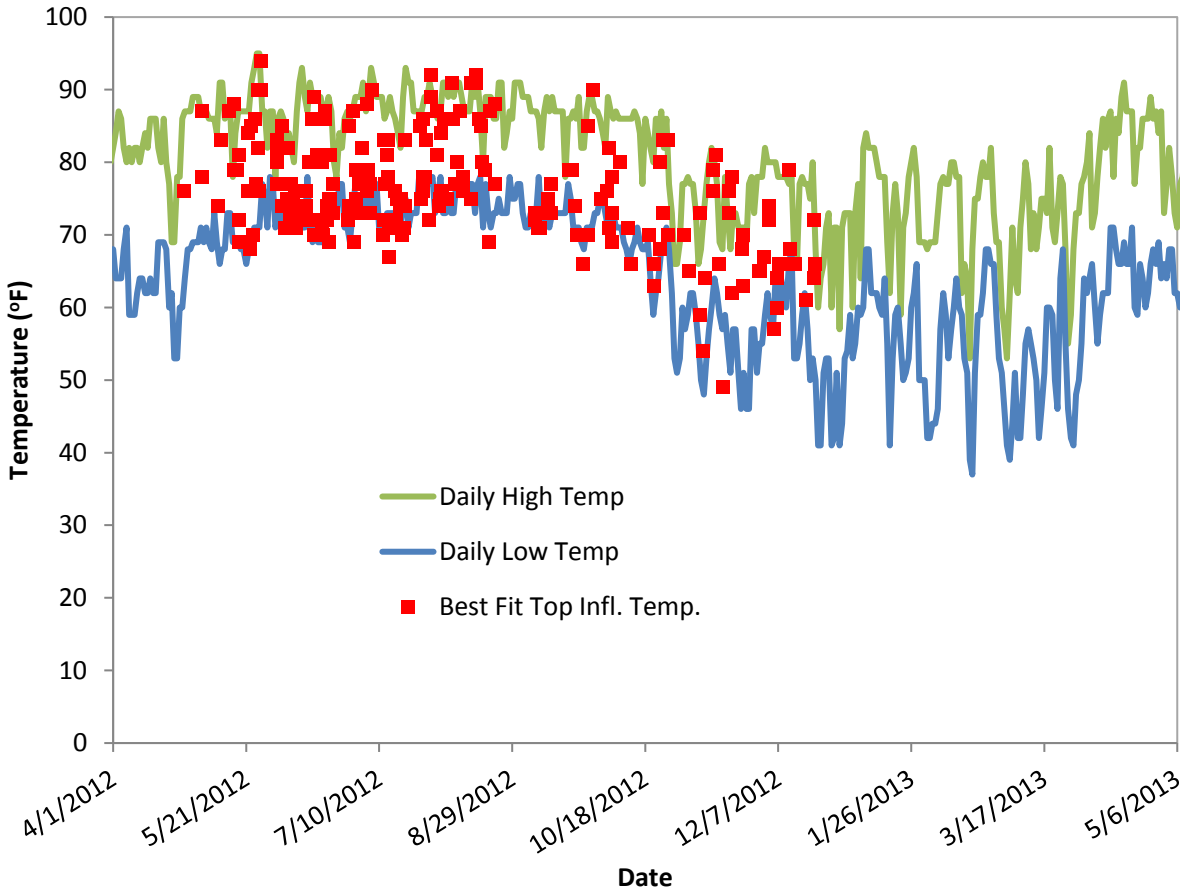

Figure 4.4 Top of shaft inflection temperature along with max. and min. daily air temperature.

4.3 Inflection Point Depth Offsets

The best fit algorithm also varied the inflection depth to account for known or unknown variations in construction details (e.g. where the excavation stopped or where the top of concrete truly concluded after the pour); bleed water can cause a slight reduction in the effective top of shaft elevation. Figure 4.5 shows that bottom of shaft inflection depths were virtually always within 1ft of the actual measured/reported shaft tip but rarely above. An inflection point above the reported tip indicates a problematic shaft that could only be "best fit" with a physically unreasonable condition. This can occur where the shaft is drastically bullet shaped for example. Only five of the 232 shafts exhibited this condition.

Similarly, the top of shaft inflection depth consistently showed the hyperbolically fitted solution to inflect above the shaft (negative refers to a depth less than top of shaft). Further evaluation showed that the TOS and BOS inflection points move slightly outside the shaft, increasing with time. This is a numerical curve fitting artifact that accounts for the difference in diffusivity between the concrete and air or concrete and soil, respectively.

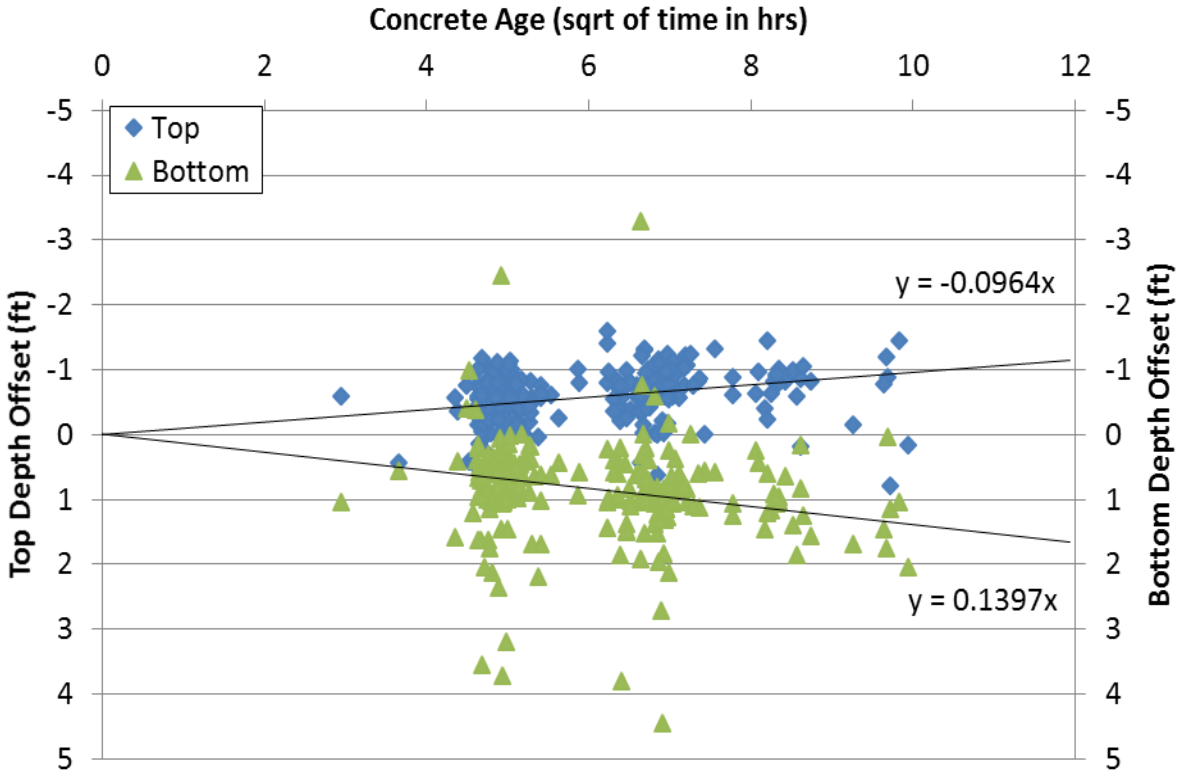

Figure 4.5 Hyperbolic inflection point offsets for top and bottom of shaft fits.

Figures 4.6 and 4.7 illustrate the effects of proper versus improper selection of the hyperbolic curve fitting parameters. The fitted curves in Figure 4.6 were produced by allowing the algorithm to blindly select the parameters necessary to produce best-fit solutions. For the top, the resulting parameters yielded a transition length (α) of 2.7ft and a depth offset (ΔD_{inf}) equal to -0.76ft. For the bottom, the resulting parameters were α = 2.8ft and ΔD_{inf} = -3.3ft. Shown in Figure

4.7 are the fitted curves resulting from parameter selections based on the trends exhibited in the above statistical analyses.

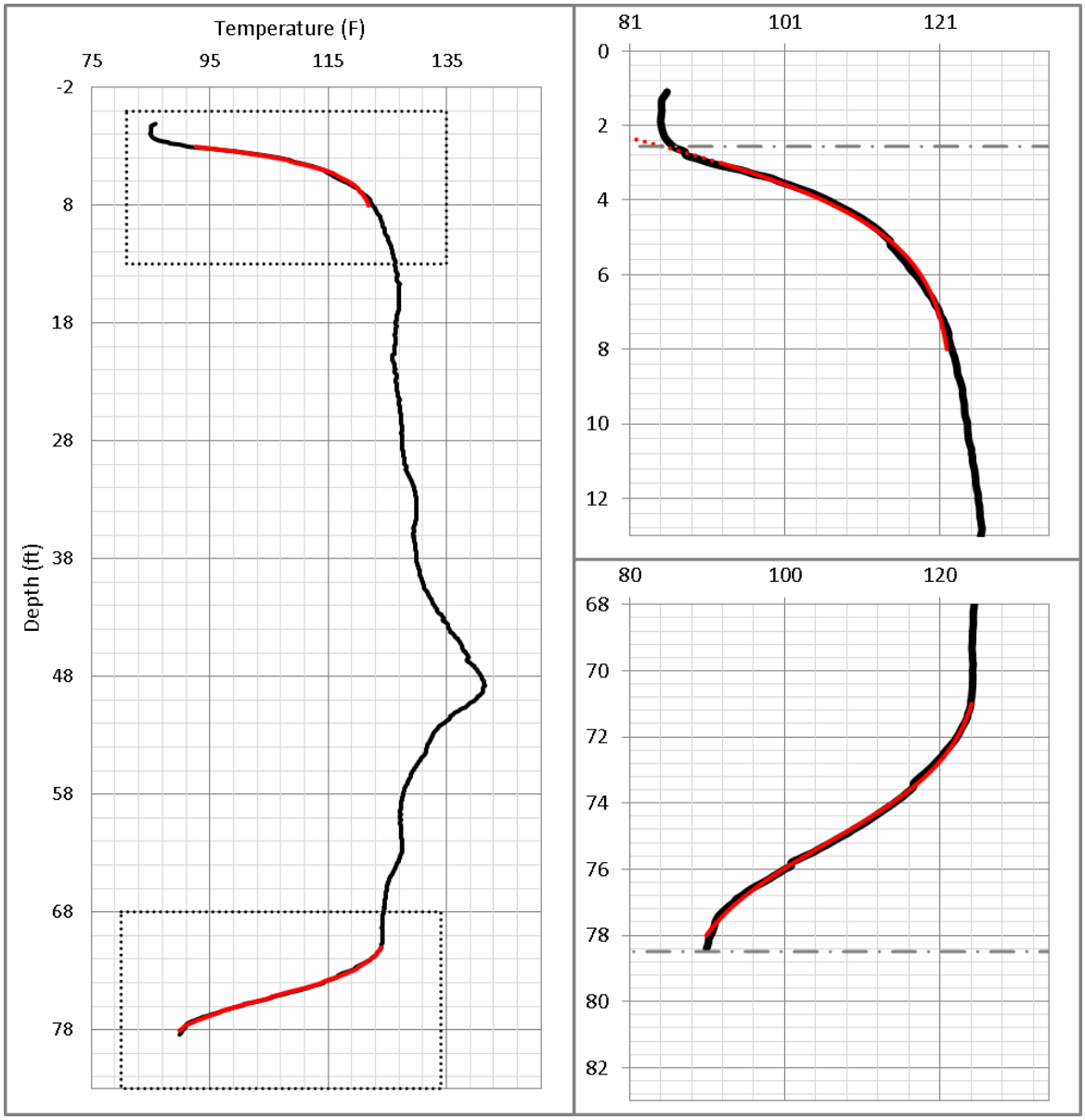

Figure 4.6 Example of toe fitted with best-fit solution, but with incorrectly selected parameters.

For a concrete age of 44hrs, as was the case for this profile, the relationships derived from Figure 4.5 yield ΔD_{inf} values of -0.64ft for the top and 0.93ft for the bottom. The relationship derived from Figure 4.3 yields α = 2.7ft (same for top and bottom). Compared to the blindly selected best-fit solutions above, the top shows good agreement with predicted parameters,

indicating normal conditions. At the bottom however, the disparity between predicted and best-fit ΔD_{inf} values (0.93ft vs. -3.3ft) indicates an anomalous toe condition. Essentially, the shaft is roughly 3 feet shorter than designed. Even upon direct observation of the thermal profile, this is visibly evident by the presence of the downward concavity temperature distribution below the inflection point, which indicates that measurements have extended beyond the heat producing medium (concrete) into the heat diffusing medium (soil).

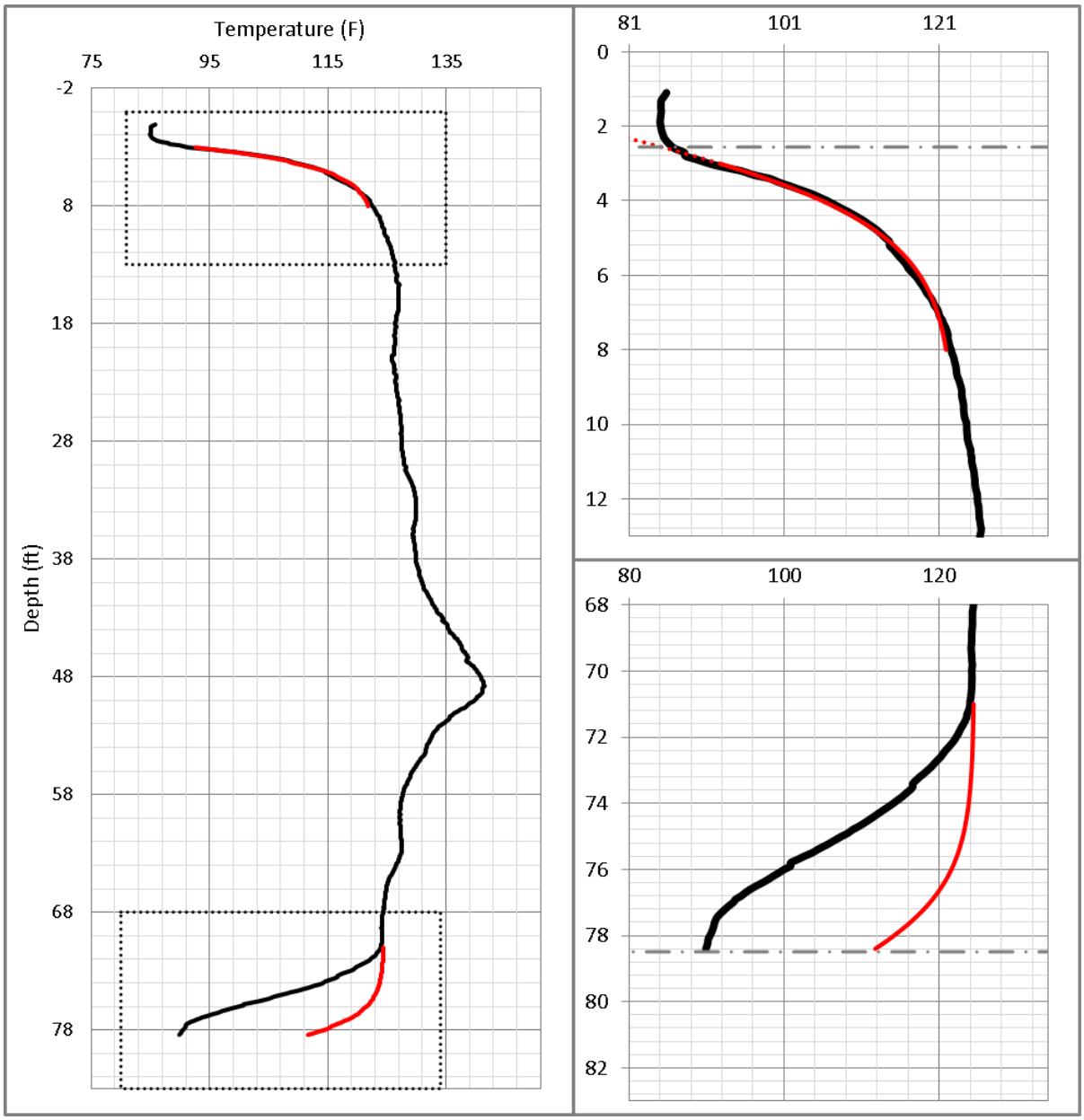

Figure 4.7 Same shaft with properly selected parameters, showing the correct shape of the toe.

4.4 Chapter Summary

Six input parameters are required when analyzing field data whereby the temperature profile can be converted to a radius profile. Therein, the shape of the top and bottom of the shaft can be predicted by adjusting the temperature profile to account for energy dissipation both radially and longitudinally where the rest of the shaft dissipates only radially. Proper selection of the parameters is vital; these include: top of shaft inflection temperature (T_{inf}), the top and bottom transition lengths (α), the top and bottom inflection depth/elevation (D_{inf}), and the local at-depth bottom soil temperature (T_{min}). It should also be noted that that the upper asymptotic temperature (T_{max}) is a required parameter, but is determined directly from the thermal profile itself and is not dependent on external information.

Statistical evaluation of 232 previously tested shafts showed that the selection of the most appropriate α value should vary between 0.3 and 0.5 times the square root of time in hours. This finding is in keeping with model findings and should serve as a limiting range in which future integrity evaluation is performed. Likewise, best-fit top of shaft inflection point temperatures were observed to fall within the range of recent daily air temperatures. Bottom and top of shaft depth offsets revealed a trend that consistently placed the inflection points slightly outside of the shaft, increasing with time when compared to empirically observed data sets and best fit hyperbolic tangent solutions. As opposed to previous thought, which suggested that depth offsets were reasonable in either direction due to discrepancies between planned and as-built elevations, these findings suggest that this is more likely a mathematical phenomenon due to the slight difference in thermal distributions between a shaft and surrounding boundaries. Therefore it should be considered normal for inflection point depths to be placed slightly outside of the shaft (i.e. negative ΔD_{inf} for the top, positive ΔD_{inf} for the bottom), and increase with time.

Near perfect fits of all shafts were achieved, but when the fit required unreasonable input parameters, the shaft had a flaw (deviation from normal). When hyperbolic parameters used to fit the top or bottom profile shape can be supported by statistically normal values, then the shaft can be considered normal. When the fitted values fall outside normal range, then the appropriate values should be assigned based on the criteria provided and the true shape of the shaft will be produced.

CHAPTER 5: CONCLUSIONS AND RECOMMENDATIONS

Analysis of TIP data for drilled shaft evaluation is still best performed using traditional methods, whereby the measured temperatures in a shaft are correlated to concrete yield data provided by construction logs to produce a temperature-radius relationship, which is then used to assess the effective radius, concrete cover, and cage alignment over the entire length of the shaft. However, objective and standardized procedures backed by scientific rationale are needed to ensure proper interpretation of data, which was the focus of this study. The general procedure for analysis of TIP data is outlined below and specific recommendations based on the findings of this study are presented herein:

1. Obtain and review all auxiliary information pertinent to the shaft, including construction logs, yield plots, borehole data, etc.
2. Determine concrete age at time of testing. If multiple times are available (e.g. wire data), select the time nearest peak temperatures.
3. Align data from all tubes/wires to same elevation.
4. Average the temperature profiles of all tubes/wires to produce an average profile.
5. Fit the top and bottom roll-off regions using the hyperbolic curve-fitting algorithm (Eq. 3.1) with properly selected parameters.
6. Apply temperature correction algorithm (Eq. 3.2) to properly fitted top and bottom roll-offs.
7. Repeat steps 5 and 6 for any mid-shaft transitions if warranted.

8. After corrections, determine the average temperature of the entire shaft.
9. Determine the volume and height of concrete placed in the excavation.
10. From volume and height of concrete, compute the average radius of the shaft, ensuring to account for additional volume from reinforcing steel, access tubes, O-cell, etc.
11. Compute linear T-R relationship.
12. Apply T-R conversion to each individual tube/wire thermal profile as well as the average profile to produce effective radius profiles.
13. Evaluate concrete cover and cage alignment from effective radius profile.
14. If needed, advanced numerical modeling can be used for comparison of results.

5.1 Use of Construction Logs in TIP Analysis

Analysis of any integrity test data should always make use of all available information. Hertlein (2015) highlighted the importance of incorporating all available "*collateral"* information stating failure to do so can lead to misinterpretation of the as-built foundation condition. This is particularly true when analyzing TIP data.

Paramount to a quantifiable analysis of TIP data is the determination of average shaft radius based on concrete yield data in order to generate a T-R relationship. In addition to records of concrete truck volume vs. change in concrete height, a truly accurate calculation must take into account all other factors. These include the volume of concrete to fill the tremie and/or lines, volume of concrete left in lines and/or hopper, volume used for quality control/assurance testing, volume of reinforcing steel, volume of other materials in excavation (e.g. O-cell, grouting tubes, cooling tubes, etc.), and changes in concrete height during casing removal.

Furthermore, the analysis should take into consideration the strength/reliability of the concrete volume values, and when possible, use known boundary conditions to adjust volume. Examples include known inspect-able dimensions such as the top of shaft or permanent casing diameter. However, permanent casing in itself does not imply a perfect section.

Additionally, information such as casing lengths, excavation depths, soil stratigraphy, construction procedures, and any noted abnormalities during construction (e.g. tremie breach, cage distortion during casing removal, etc.) can confirm observations or explain unexpected profile features. Sources of such information should include construction logs, borehole data, site investigations, and communication with the contractor.

The case study presented in Chapter 3 illustrated the usefulness of such information, wherein an otherwise inexplicable thermal transition in the middle of the shaft was found to coincide with an interface between dry clay overlying saturated sand, as well as the fact the clay layer had been pre-drilled for casing installation, likely resulting in a region of poor thermal contact between shaft and soil.

5.2 Hyperbolic Parameters for End Corrections

The hyperbolic temperature correction algorithm (Eq. 3.1) presented in this study requires several input parameters to account for increased diffusion near the ends of the shaft which should be selected on the basis of reasonable limits. These parameters include:

- Top and bottom of shaft transition lengths (α)
- Top of shaft inflection point temperature (T_{inf})
- Top and bottom of shaft inflections point depths (D_{inf})
- Bottom of shaft lower bound temperature (T_{min})
- Top and bottom of shaft upper bound temperatures (T_{max})

As with any signal matching algorithm, a strong match can be obtained for almost any profile, but the values selected may be unreasonable. Based on the findings of this study, the following guidelines for proper selection are recommended.

5.2.1 Transition Length (α)

The transition length (α) for the bottom and top of shaft follows a square root of time dependency where the most appropriate (average) value should be expressed as 0.4√time (time in hours). Based on the frequency distribution of all observations, reasonable values were shown to vary within one standard deviation, between 0.3 and 0.5√time (time in hours, Figure 4.3). Values that produce a good fit between the hyperbolic tangent function and the measured data that use transition lengths outside this range should be considered incorrect and indicate an abnormally shaped end (relative to a square ended cylindrical prism). In such cases, a value corresponding to 0.4√time should be applied to show the most probable shape.

5.2.2 Top of Shaft Inflection Point Temperature (T_{inf})

The top of shaft inflection temperature was found to be closely related to the average air temperature over the 12hr period prior to testing/time of evaluation (Figures 3.5 and 3.8). Furthermore, in winter months, the inflection temperature closely aligned with the highest daily temperature; in summer months aligned more closely with the lowest daily temperature; these values tended to be moderated by the local soil temperature (Figure 4.4). In general, the inflection temperature should not be outside the daily temperature extremes for the prior day.

5.2.3 Inflection Point Depths (D_{inf})

The top and bottom of shaft elevations (TOS and BOS) should align closely with the hyperbolic tangent inflection point location (D_{inf}) which indicates the interface between energy producer and energy dissipater. However, a single hyperbolic tangent function is used to represent

the two material types. As a result, the best fit inflection point locations were shown to slightly move outside the shaft progressing farther away with time (Figure 4.5). If the inflection point location is ever found to be best fit inside the shaft or is disparate from the recommended/shown range, that value should not be used. Again, in such cases, an inflection point location corresponding to Figure 4.5 should be used in conjunction with the most appropriate transition length note above.

5.2.4 Bottom of Shaft Lower Bound Temperature (T_{min})

With exception to those cases where geothermal heat sources are present, the average annual air temperature for a given geographical location (Figure 2.10) provides a direct indication of the at-depth constant temperature boundary condition used to fit the bottom of shaft hyperbolic tangent correction/adjustment. This value is perhaps the most trustworthy input parameter when analyzing field data and converting from temperature to radius profiles.

5.2.5 Upper Bound Temperatures (T_{max})

The upper bound temperatures (T_{max}) for top and bottom of shaft corrections are the only parameters that should not be estimated based external conditions or time. Rather, they should be matched to the measured temperature profile itself and estimated based on the nearest region of uniform temperature distribution. This can typically be found at a distance roughly equal to one diameter of the shaft away from the ends, but can depend on time of testing and whether or not the end condition is anomalous.

5.2.6 Normalizing Temperatures (T_{norm})

Once the top and bottom temperature distributions are fitted using properly selected parameters, the temperature correction algorithm (Eq. 3.2) should be applied and normalized

(T_{norm}) to T_{max} in order produce the temperature profile that would be expected had the additional heat loss boundary not been present.

5.3 Hyperbolic Parameters for Mid-Shaft Corrections

In cases where a shaft extends out of the ground (e.g., into water or air) or is known to have changed the external heat diffusing environment, the analysis should incorporate a mid-shaft correction. However, it should be noted that temperature distributions caused by actual changes in effective radius can exhibit similar patterns. Therefore, without a justifiable change in external environmental conditions within the length of a shaft, intermediate corrections should not be used and are not warranted.

When mid-shaft corrections are warranted however, the same hyperbolic temperature correction algorithms used for end effects should be applied, but with selection of parameters based on that which is appropriate for the given condition.

5.3.1 Transition Length (α)

The transition length (α) should adhere to same time dependent relationship as for end conditions, between 0.3 and 0.5√time (time in hours).

5.3.2 Inflection Point Depths (D_{inf})

The inflection point depth should be matched to the observed inflection point in the measured thermal profile, but corroborated by evidence from site investigation, borehole data, or construction logs. As opposed to the inflection point depth offsets observed in top and bottom corrections where mediums transfer to either soil or air, no offset should be expected in mid-shaft corrections as the medium never transfers out of concrete.

5.3.3 Upper and Lower Bound Temperatures (T_{max}, T_{min})

Both the upper and lower bound temperatures (T_{max}, T_{min}) for mid-shaft corrections should be matched to nearest regions of uniform temperature above and below the inflection point. Neither should be estimated based on external factors.

5.3.4 Normalizing Temperatures (T_{norm})

Once a mid-shaft transition has been fitted using properly selected parameters, the temperature correction algorithm (Eq. 3.2) should be applied in order produce the temperature profile that would be expected had the change in heat diffusion boundary not been present. However, unlike with top and bottom corrections, proper selection of the normalization temperature (T_{norm}) can vary between T_{min} and T_{max}. It is recommended that temperatures be normalized to whichever region of the shaft contains the most reliable conditions for analysis. Considerations for this should include the portion of the shaft that is in soil (as opposed to water or air), whether either portion constitutes a vast majority of the shaft length, or if either part of the shaft is permanently cased.

5.4 Temperature-Radius Relationship

Only after all appropriate hyperbolic temperature corrections have been applied, should the temperature-radius relationship for a shaft be determined and applied.

Mullins and Winters (2011) showed that the average temperature at a given depth can be linearly correlated to the local effective shaft radius for changes in radius generally less than 12in. Greater changes in radius tend to be under predicted though, as the true temperature-radius relationship becomes non-linear (e.g. a change in radius on the order of 16in might be reported as 14in). However, a shaft radius that is less than 6in of the design radius usually fails acceptance

criteria for multiple reasons (Piscsalko et al., 2016), making the linear approximation reasonable for virtually all cases of shaft integrity evaluation.

The model findings of this study have shown that the theoretical T-R relationship follows a non-linear S-shaped curve with lower and upper bounds of soil temperature and concrete adiabatic temperature, respectively. However, for measurements taken near the edge of shaft (e.g. cage location), data falls within the linear portion of the curve, thereby making a linearly approximated T-R relationship appropriate for analysis.

For very large shafts (e.g. 8ft diameter and larger), there is often a sufficient amount of yield plot data to determine a linear T-R relationship by multi-point regression (as demonstrated in Figure 2.3).

For most commonly constructed shafts however (e.g. less than 8ft diameter), where yield plot data is usually not sufficient for a multi-point regression, a single-point (or pole-point) solution, using the average temperature and average radius of the entire shaft, should be used. In this case, the linear T-R relationship is defined by the points (T_{avg},R_{avg}) and (*0*,*0*). Modeling has shown this type of solution to provide a close approximation to the linear portion of the theoretical T-R relationship and to also be conservative against false positives (i.e. over-prediction of anomalies) for shafts in the 3-8ft diameter range.

5.5 Effects of Concrete Age

The case study presented in Chapter 3 showed that time of testing has virtually no effect on the computed effective shaft radius. This finding, however, is limited to a reasonable timeframe that stays within the previously stated rule-of-thumb, whereby testing/evaluation time should be performed within a one day per foot of shaft diameter timeframe, corresponding to at or recently

after peak temperatures have occurred. This also requires that the effects of time are well understood as they pertain to the hyperbolic correction parameters.

Additionally, the start of hydration time should consider any delays caused by retarders added to the concrete. Top of shaft α values may be slightly higher to account for additional modes of heat transfer that include convection. This phenomenon is more pronounced in shafts that extend above ground via permanent casing or other similar means.

5.6 Use of Numerical Modeling in TIP Analysis

Modeling for exact temperature predictions should not be used as a means of direct analysis for thermal integrity data. The precision of such models is highly subjective to the estimation of many input parameters including cement mineralogy, concrete hydration behavior, subsurface stratigraphy, soil thermal properties, and the effects of air convection.

However, while numerical models are fraught with limitations associated with accurate estimation of input parameters, such models are a convenient mechanism to identify trends that occur regardless of actual field conditions. In such cases, all available information (as described in Section 5.1) should be considered and input appropriately into the model constraints. Appendix A provides the constitutive equations that define concrete hydration behavior based on Bogue calculations (commonly found in cement mill certificates), and Appendix B provides recommendations for the thermal properties of concrete and soil.

This study made use of numerical model data to confirm the applicability of temperature-radius relationships in drilled shafts, and to help define the non-uniform thermal distributions exhibited at the top and bottom of a shaft, as well as those that may be present within the middle of a shaft due to drastic changes in boundary conditions.

5.7 Future Work

With the rapid rise in TIP acceptance worldwide and the applications to which it is applied there will be continued need to develop analysis methods. Two areas can be noted in this regard: (1) analysis of non-cylindrical sections and (2) defining the non-linear temperature to radius relationship directly from field data. Designers and owners for projects involving cutoff walls, soldier pile walls or other rectangular concrete sections are now looking for ways to incorporate TIP capabilities to provide the same level of quality assurance. While direct observation of the data will follow in the same fashion as drilled shafts, effective radius will not be an appropriate indicator. Rather, a new set of acceptance criteria will be required.

The non-linear temperature to radius relationship defined herein via numerical modeling is not presently transferable to field collected data. It is conceivable that such a method could be developed with additional measurements or relationships derived from numerical models.

REFERENCES

Anderson, Byron (2011). "Thermal Integrity Profiling Instrumentation Development". Master's Thesis, University of South Florida. http://scholarcommons.usf.edu/etd/2987

ASTM Standard D7949-14, "Standard Test Methods for Thermal Integrity Profiling of Concrete Deep Foundations," ASTM International, West Conshohocken, PA

Bogue, Robert (1947). "The Chemistry of Portland Cement". Reinhold Publishing Corp.

Folliard, K.J., Juenger, M., Schindler, A., Riding, K., Poole, J., Kallivokas, L.F., Slatnick, S., Whigham, J., Meadows, J.L. (2008). *Prediction Model for Concrete Behavior* (Final Report). Austin, TX. Center for Transportation Research. The University of Austin at Texas. FHWA/TX-08/0-4563-1.

Ge, Zhing. (2005). "Predicting temperature and strength development of the field concrete". Doctoral Dissertation, Iowa State University. UMI No. 3200417.

Hertlein, B. H., (2015). "Analysis Collateral: Information Needed for Foundation Integrity Test Data Analysis, *Foundation Drilling*, ADSC, November/December.

Johansen, O. (1977). "Thermal Conductivity of Soils," U.S. Army Corps of Engineers Cold Regions Research and Engineering Laboratory. Hanover, NH

Johnson, Kevin R. (2014). "Temperature Prediction Modeling and Thermal Integrity Profiling of Drilled Shafts." ASCE Geo-Congress 2014 Technical Papers: pp. 1781-1794.

Johnson, Kevin R. (2016). "Analyzing thermal integrity profiling data for drilled shaft evaluation". DFI Journal – The Journal of the Deep Foundations Institute. Vol 10, No. 1, May 2016. pp. 25-33.

Kranc, S. and Mullins, G. (2007). *Inverse Method for the Detection of Voids in Drilled-Shaft Concrete Piles from Longitudinal Temperature Scans*. Inverse Problems, Design and Optimization Symposium. Miami, FL, U.S.A., April 16-18, 2007.

Mindess, S., Young, J.F., Darwin, D. (2003). "Concrete". Pearson Education, Inc., Upper Saddle River , NJ.

Mullins, Gray (2010). "Thermal Integrity Profiling of Drilled Shafts". DFI Journal – The Journal of the Deep Foundations Institute. Vol.4, No. 2 December 2010. pp. 54-64.

Mullins, Gray, and Winters, Danny (2011). *Infrared Thermal Integrity Testing: Quality Assurance Test Method to Detect Drilled Shaft Defects - Final Report*. Olympia, WA : Washington State Department of Transportation, Office of Research & Library Services. https://www.wsdot.wa.gov/Research/Reports/700/770.1.htm

Mullins, G., and Winters, D. (2012). "Thermal Integrity Profiling of Concrete Deep Foundations". Slideshow presented at the Association of Drilled Shaft Contractors Expo 2012, San Antonio, TX, March 14-17.

Mullins, Gray (2013). "Advancements in Drilled Shaft Construction, Design, and Quality Assurance: The Value of Research". Technical Paper. International Journal of Pavement Research and Technology. Vol. 6, No. 2, March 2013. pp 93-99. DOI: 106136/ijprt.org.tw/2013.6(2).93

Mullins, G., and Johnson, K. R. (2016). *Optimizing the Use of the Thermal Integrity System for Evaluating Auger-Cast Piles*. Final Report. Florida Department of Transportation, Tallahassee, FL. FDOT-BDV35-977-09.

Ozisik, M. Necati (1993). "Heat Conduction" Second Edition. Published by John Wiley & Sons, Inc., New York, NY. ISBN 0-471-53256-8.

Pauly, Nicole M. (2010). "Thermal Conductivity of Soils from the Analysis of Boring Logs." Master's Thesis, University of South Florida, Department of Civil and Environmental Engineering.

Piscsalko, G., Likins, G. and Mullins, G. (2016). "Drilled Shaft Acceptance Criteria Based upon Thermal Integrity Profiling," Deep Foundations Institute 41st Annual Conference on Deep Foundations, New York, NY.

Poole, Jonathan L. (2007). "Modeling Temperature Sensitivity and Heat Evolution of Concrete". Doctoral Dissertation, University of Texas at Austin. UMI No. 3285913.

Schindler, A.K. and Folliard, K.J. (2005). "Heat of Hydration Models for Cementitious Materials". Technical Paper, *ACI Materials Journal*, V. 102, No. 1, January-February 2005.

Schindler, A.K., Dossey, T., and McCullough, B.F. (2002). *Temperature Control During Construction to Improve the Long Term Performance of Portland Cement Concrete Pavements*. Austin, TX. Center for Transportation Research. The University of Austin at Texas. FHWA/TX-05/0-1700-2.

Taylor, H.F.W. (1997). "Cement Chemistry" Second Edition. Published by Thomas Telford Publishing, London. ISBN 0-7277-2592-0.

APPENDIX A: α-β-τ CONCRETE HYDRATION MODEL EQUATIONS

Below are the empirical equations and parameters, as described by Poole, 2007, used in defining the α-β-τ model for concrete hydration behavior.

$$H_{cem} = 500 \cdot p_{C_3S} + 260 \cdot p_{C_2S} + 866 \cdot p_{C_3A} + 420 \cdot p_{C_4AF} + 624 \cdot p_{SO_3} + 1186 \cdot p_{FreeCaO} + 850 \cdot p_{MgO} \quad \{A.1\}$$

$$H_u = H_{cem} \cdot p_{cem} + 461 \cdot p_{GGBFS-100} + 550 \cdot p_{GGBFS-120} + 1800 \cdot p_{FA-CaO} \cdot p_{FA} + 330 \cdot p_{SF} \quad \{A.2\}$$

$$E_a = 41{,}230 + 1{,}416{,}000 \cdot \left[\left(p_{C_3A} + p_{C_4AF}\right) \cdot p_{cem} \cdot p_{SO_3} \cdot p_{cem}\right] - 347{,}000 \cdot p_{Na_2O_{eq}} - 19.8 \cdot Blaine + 29{,}600 \cdot p_{FA} \cdot p_{FA-CaO} + 16{,}200 \cdot p_{GGBFS} - 51{,}600 \cdot p_{SF} - 3{,}090{,}000 \cdot WRRET - 345{,}000 \cdot ACCL \quad \{A.3\}$$

$$\alpha_u = \frac{1.031 \cdot w/cm}{0.194 + w/cm} + \exp\begin{pmatrix} -0.0885 - 13.7 \cdot p_{C_4AF} \cdot p_{cem} \\ -283 \cdot p_{Na_2O_{eq}} \cdot p_{cem} \\ -9.90 \cdot p_{FA} \cdot p_{FA-CaO} \\ -339 \cdot WRRET - 95.4 \cdot PCHRWR \end{pmatrix} \quad \{A.4\}$$

$$\beta = \exp\begin{pmatrix} -0.464 + 3.41 \cdot p_{C_3A} \cdot p_{cem} - 0.846 \cdot p_{GGBFS} \\ +107 \cdot WRRET + 33.8 \cdot LRWR + 15.7 \cdot MRWR \\ +38.3 \cdot PCHRWR + 8.97 \cdot NHRWR \end{pmatrix} \quad \{A.5\}$$

$$\tau = \exp\begin{pmatrix} 2.92 - 0.757 \cdot p_{C_3S} \cdot p_{cem} + 98.8 \cdot p_{Na_2O} \cdot p_{cem} + 1.44 \cdot p_{GGBFS} \\ +4.12 \cdot p_{FA} \cdot p_{FA-CaO} - 11.4 \cdot ACCL + 98.1 \cdot WRRET \end{pmatrix} \quad \{A.6\}$$

where,

$H_{cem} = Total\ heat\ of\ hydration\ of\ cement\ (kJ/kg)$

$H_u = Total\ heat\ of\ hydration\ of\ cementitious\ materials\ (kJ/kg)$

$E_a = Activation\ energy\ (J/mol)$

$\alpha_u = Ultimate\ degree\ of\ hydration$

$\beta = Hydration\ slope\ parameter$

$\tau = Hydration\ time\ parameter\ (hrs)$

$p_{cem} = Mass\ ratio\ of\ cement\ to\ all\ cementitious\ material$

$p_{FA} = Mass\ ratio\ of\ fly\ ash\ to\ all\ cementitious\ material$

$p_{GGBFS-100} = Mass\ ratio\ of\ grade\ 100\ slag\ to\ all\ cementitious\ material$

$p_{GGBFS-120} = Mass\ ratio\ of\ grade\ 120\ slag\ to\ all\ cementitious\ material$

$p_{SF} = Mass\ ratio\ of\ silica\ fume\ to\ all\ cementitious\ material$

$w/cm = Mass\ ratio\ of\ water\ to\ cementitious\ material$

$p_{C_3S} = Mass\ ratio\ of\ C_3S\ content\ in\ cement$

$p_{C_2S} = Mass\ ratio\ of\ C_2S\ content\ in\ cement$

$p_{C_3A} = Mass\ ratio\ of\ C_3A\ content\ in\ cement$

$p_{C_4AF} = Mass\ ratio\ of\ C_4AF\ content\ in\ cement$

$p_{SO_3} = Mass\ ratio\ of\ SO_3\ content\ in\ cement$

$p_{FreeCaO} = Mass\ ratio\ of\ free\ CaO\ (lime)\ content\ in\ cement$

$p_{MgO} = Mass\ ratio\ of\ MgO\ content\ in\ cement$

$p_{Na_2O} = Mass\ ratio\ of\ Na_2O\ content\ in\ cement$

$p_{Na_2O_{eq}} = Mass\ ratio\ of\ Na_2O\ equivalent\ alkalies\ in\ cement$

$$= p_{Na_2O} + 0.658 \cdot p_{K_2O}$$

$p_{K_2O} = Mass\ ratio\ of\ K_2O\ content\ in\ cement$

$Blaine = Blaine\ fineness\ of\ cement$

$p_{FA-CaO} = Mass\ ratio\ of\ CaO\ in\ fly\ ash$

$ACCL = Mass\ ratio\ of\ accelerator\ to\ cementitious\ material$

$WRRET = Mass\ ratio\ of\ water\ reducer/retarder\ (ASTM\ type\ B\&D)$ $to\ cementitious\ material$

$LRWR = Mass\ ratio\ of\ low\ range\ water\ reducer\ (ASTM\ type\ A)$ $to\ cementitious\ material$

$MRWR = Mass\ ratio\ of\ mid\ range\ water\ reducer\ to\ cementitious$ $material$

$NHRWR = Mass\ ratio\ of\ naphthalene\ or\ melamine\ based\ high\ range$ $water\ reducer\ (ASTM\ type\ F)\ to\ cementitious\ material$

$PCHRWR = Mass\ ratio\ of\ polycarboxylate\ based\ high\ range\ water$ $reducer\ (ASTM\ type\ F)\ to\ cementitious\ material$

APPENDIX B: CONCRETE AND SOIL THERMAL PROPERTIES

Table B.1 Thermal conductivity of mature concrete based on aggregate type. (Schindler et al., 2002)

Aggregate Type	Moist Density of Concrete		Thermal Conductivity	
	(kg/m^3)	(lbs/ft^3)	(W/m/°C)	(Btu/h/ft/°F)
Quartzite	2350-2440	147-152	4.1-3.1	2.33-1.75
Dolomite	2500	156	3.3	1.9
Limestone	2450-2440	153-151	3.2-2.2	1.83-1.25
Sandstone	2400-2130	150-133	2.9	1.7
Granite	2420	151	2.6	1.5
Basalt	2520-2350	158-157	2.0-1.9	1.17-1.08

Table B.2 Specific heat of concrete materials. (Schindler et al., 2002)

Material	Specific heat (J/kg/°C)	Reference
Cement	1140	Mindess and Young, 1981
Water	4187	Scanlon et al., 1994
Limestone / Dolomite	910	Trinhztfy et al., 1982
Sandstone	770	
Granite / Gneiss	780	
Siliceous River Gravel	770	
Basalt	900	

Table B.3 Conductive thermal properties of subsurface materials.

Material		Density, ρ (kg/m^3)	Thermal Conductivity, k (W/m/K)	Specific Heat, C_p (J/kg/K)	Diffusivity, $k/\rho C_p$ (mm^2/s)	Reference
Granite		2630	2.79	775	1.37	Incroperra & Dewitt (2007)
Limestone		2320	2.15	810	1.14	
Marble		2680	2.8	830	1.26	
Quartzite		2640	5.38	1105	1.84	
Sandstone		2150	2.9	745	1.81	
Sandy Soil - 40% pore space	Dry	1600	0.3	800	0.23	Arya (2001)
	Saturated	2000	2.2	1480	0.74	
Clay Soil - 40% pore space	Dry	1600	0.25	890	0.18	
	Saturated	2000	1.58	1550	0.51	
Peat Soil - 80% pore space	Dry	300	0.06	1920	0.10	
	Saturated	1100	0.5	3650	0.12	
Still Water (20^{o}C)		1000	0.57	4180	0.14	
Still Air (20^{o}C)		1.2	0.025	1010	20.63	

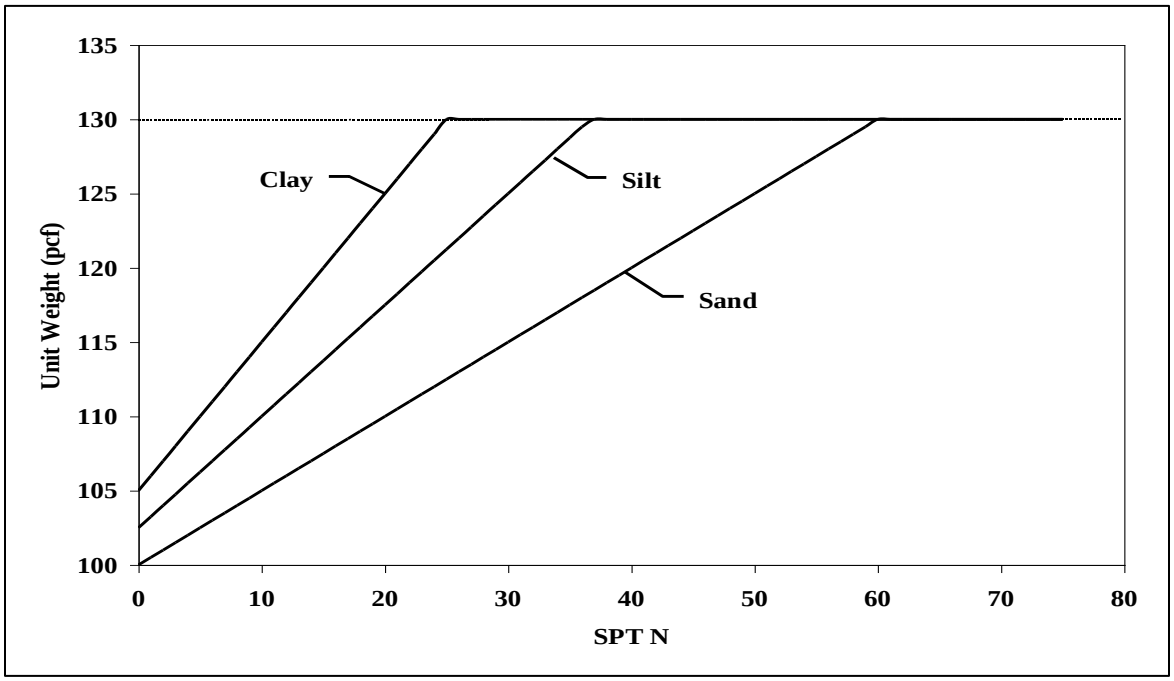

Figure B.1 Soil density as a function of uncorrected SPT blow count (N). (Pauly, 2010)

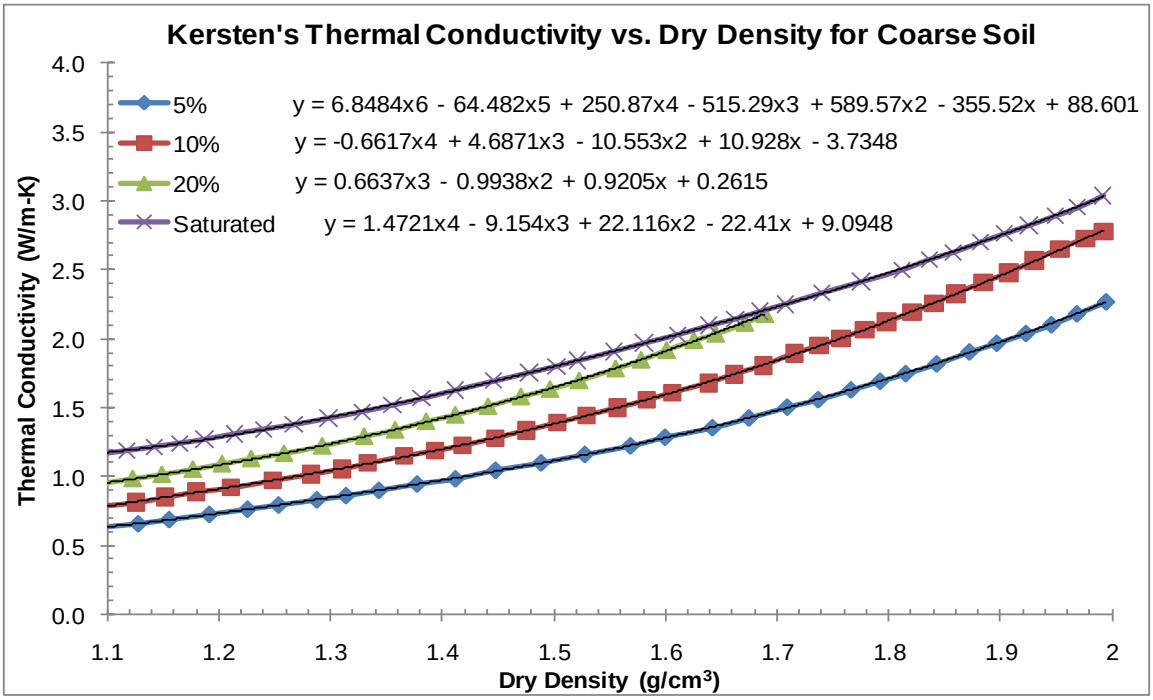

Figure B.2 Kersten's conductivity vs. density and moisture content for sandy soils. (Pauly, 2010)

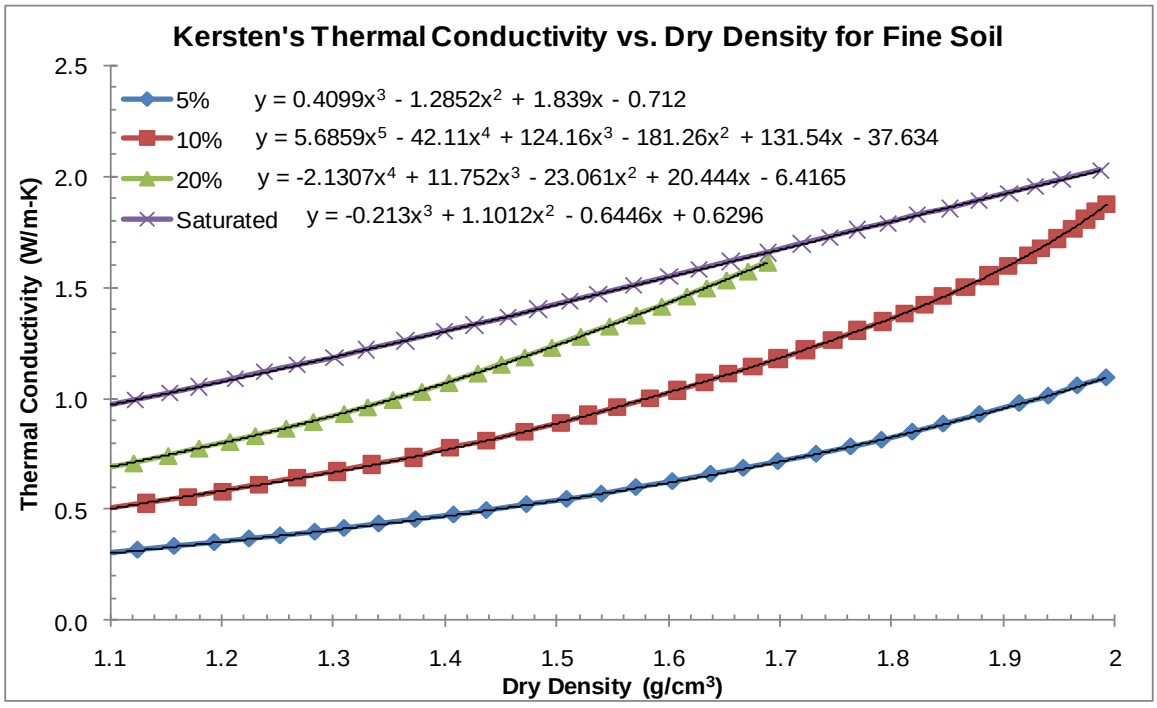

Figure B.3 Kersten's conductivity vs. density and moisture content for clayey soils. (Pauly, 2010)

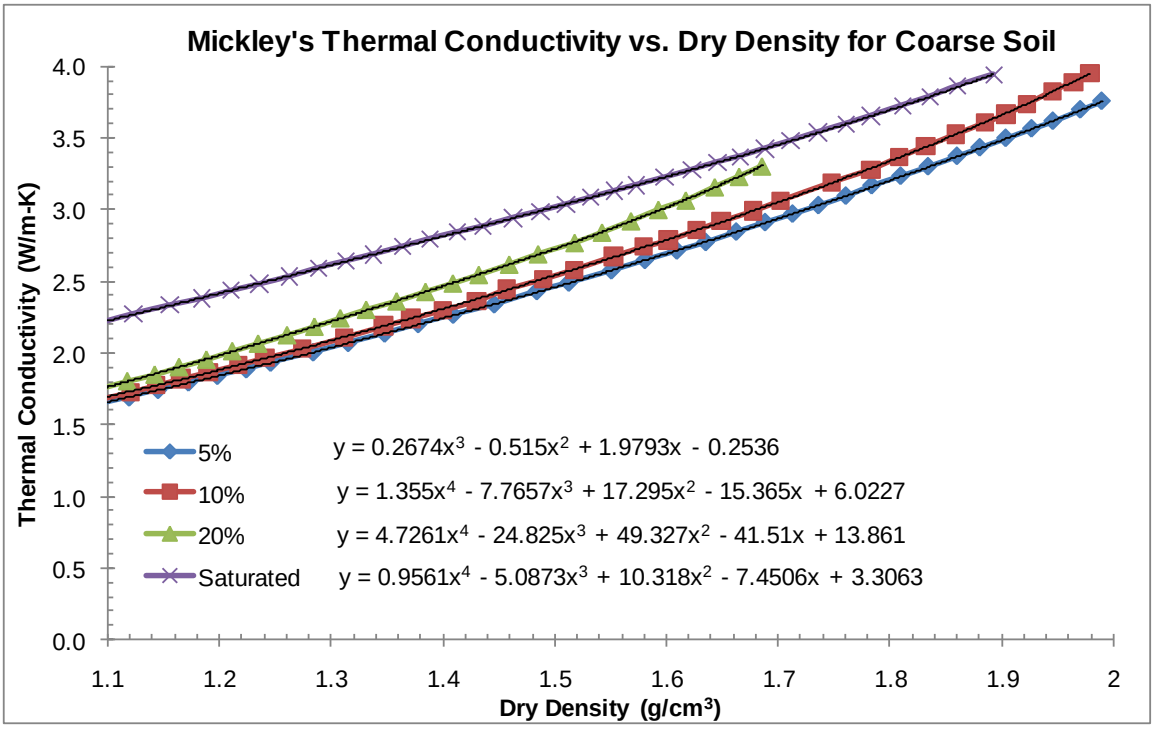

Figure B.4 Mickley's conductivity vs. density and moisture content for sandy soils. (Pauly, 2010)

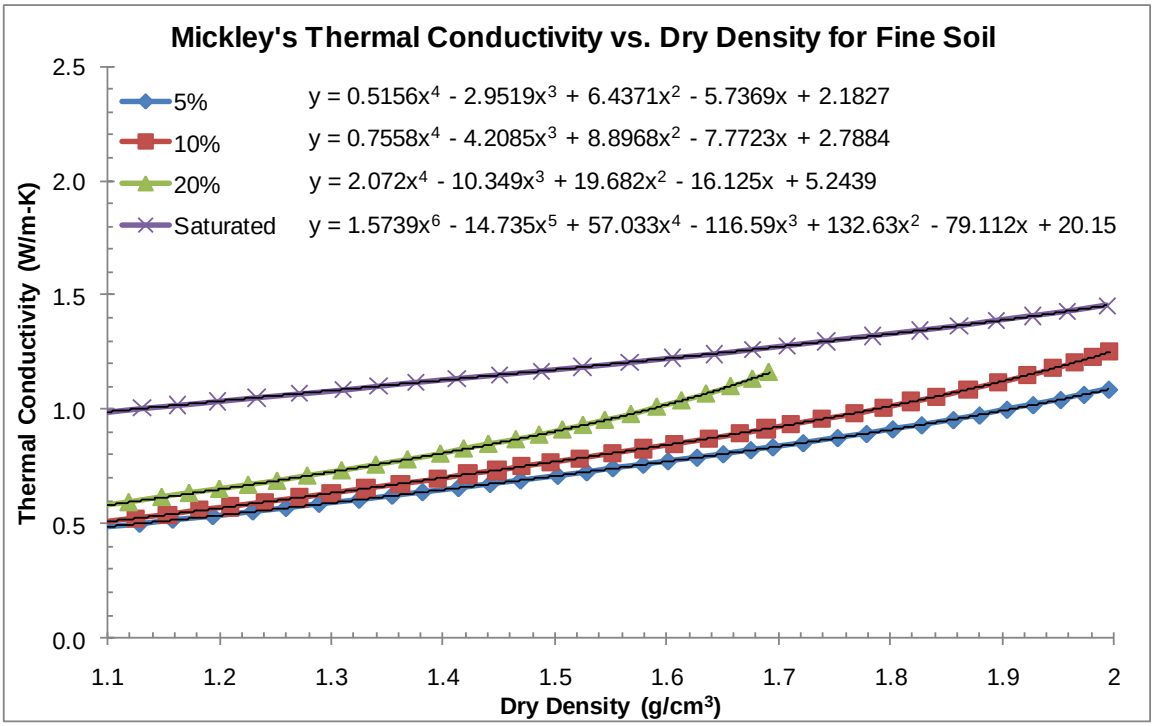

Figure B.5 Mickley's conductivity vs. density and moisture content for clayey soils. (Pauly, 2010)

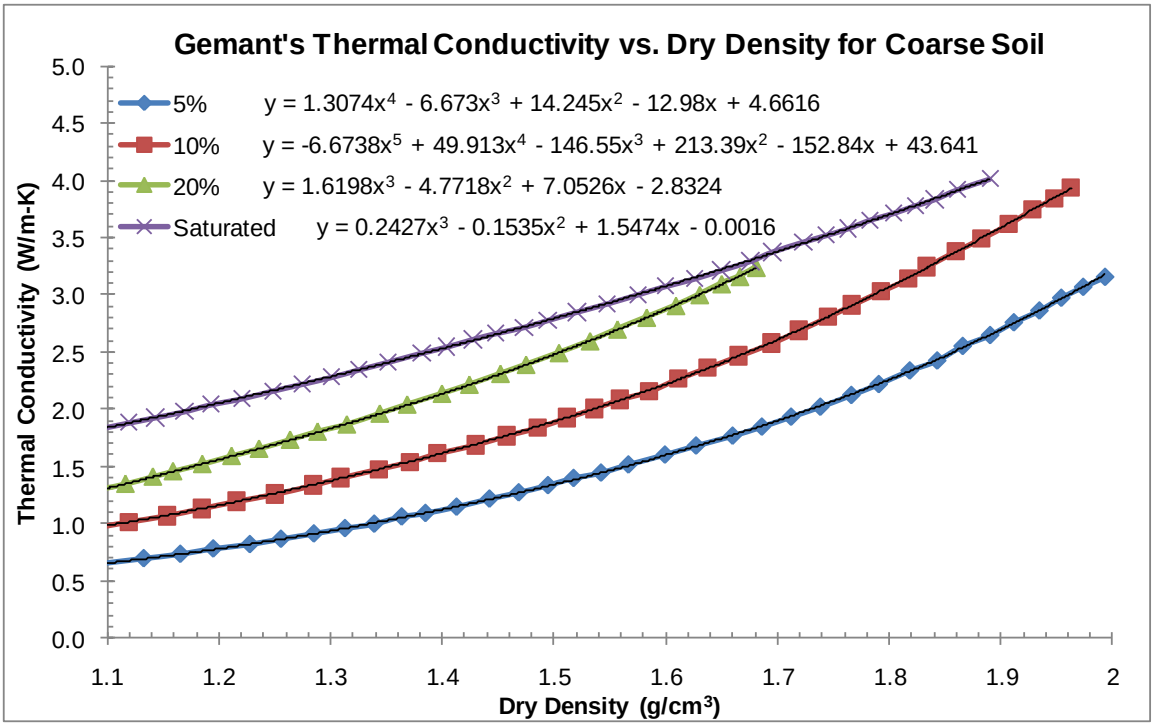

Figure B.6 Gemant's conductivity vs. density and moisture content for sandy soils. (Pauly, 2010)

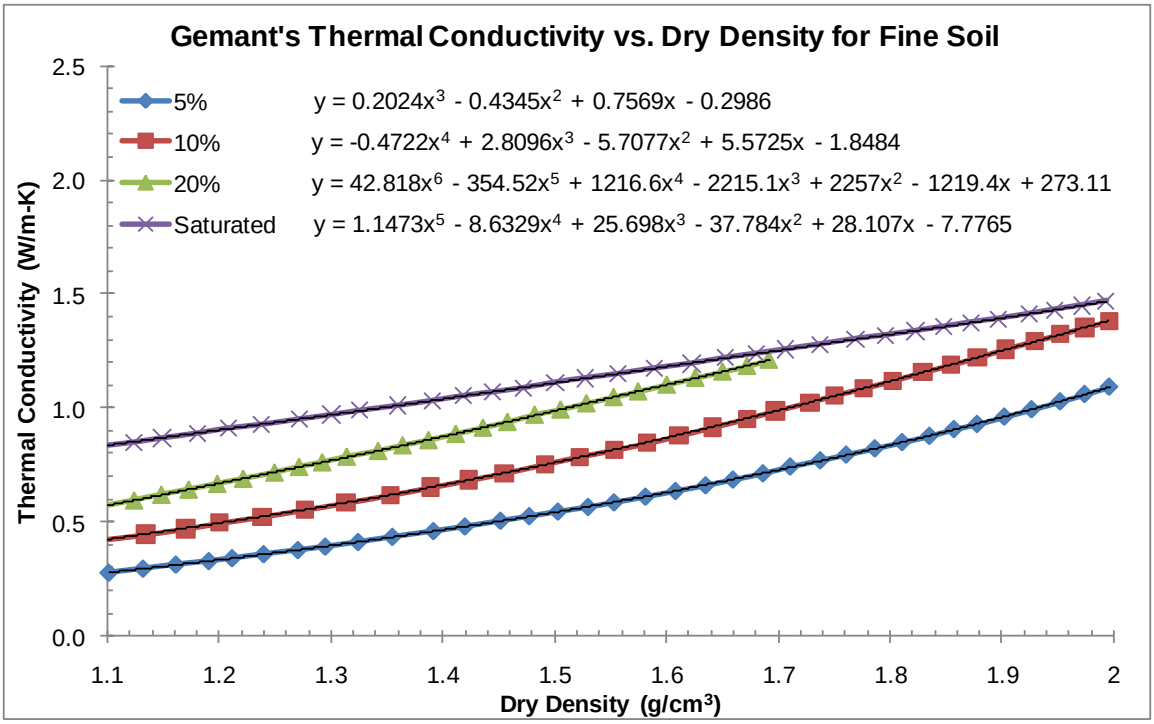

Figure B.7 Gemant's conductivity vs. density and moisture content for clayey soils. (Pauly, 2010)

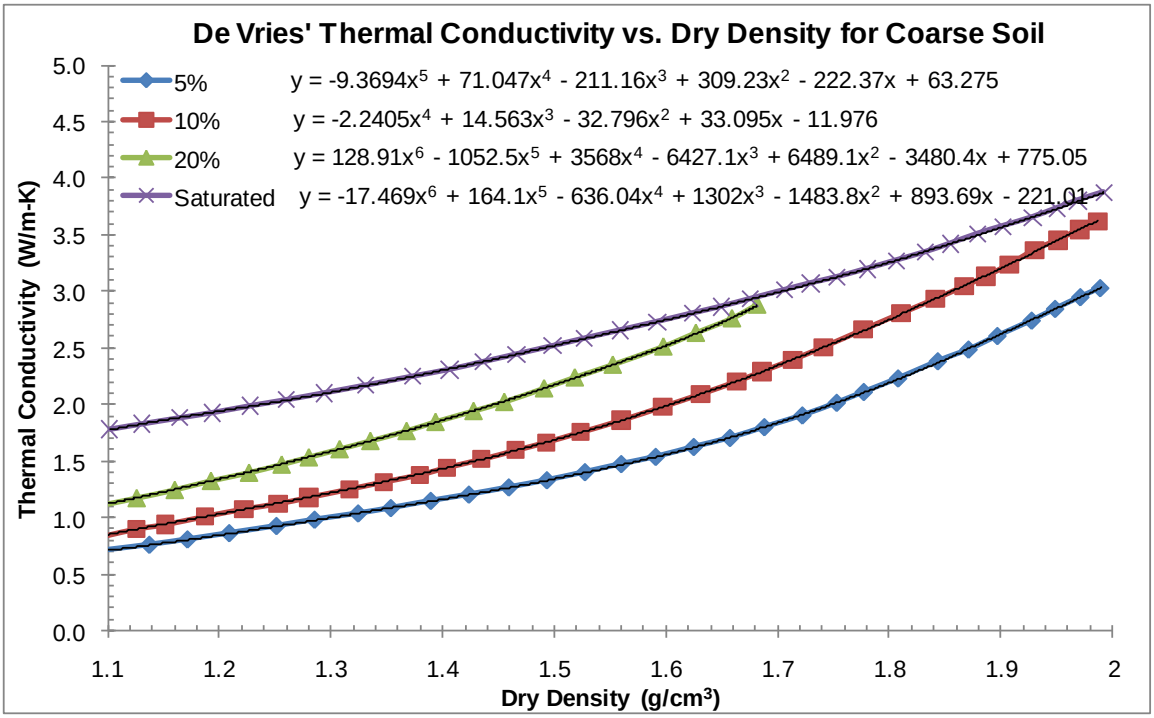

Figure B.8 De Vrie's conductivity vs. density and moisture content for sandy soils. (Pauly, 2010)

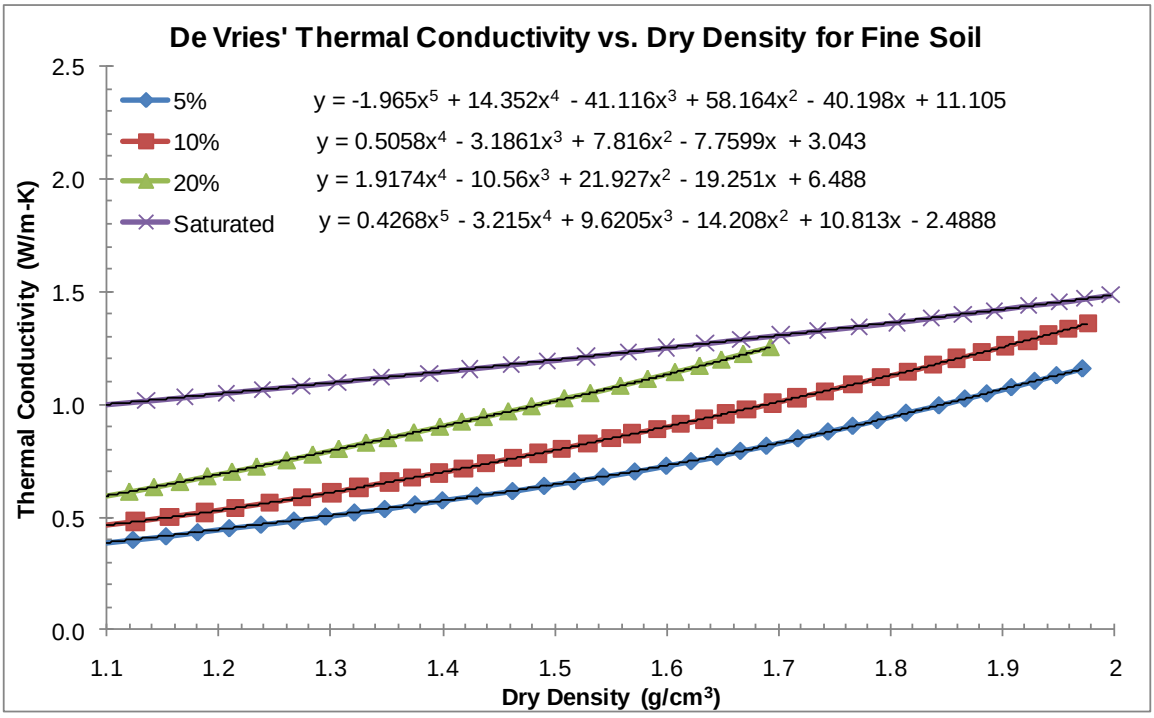

Figure B.9 De Vries's conductivity vs. density and moisture content for clayey soils. (Pauly, 2010)

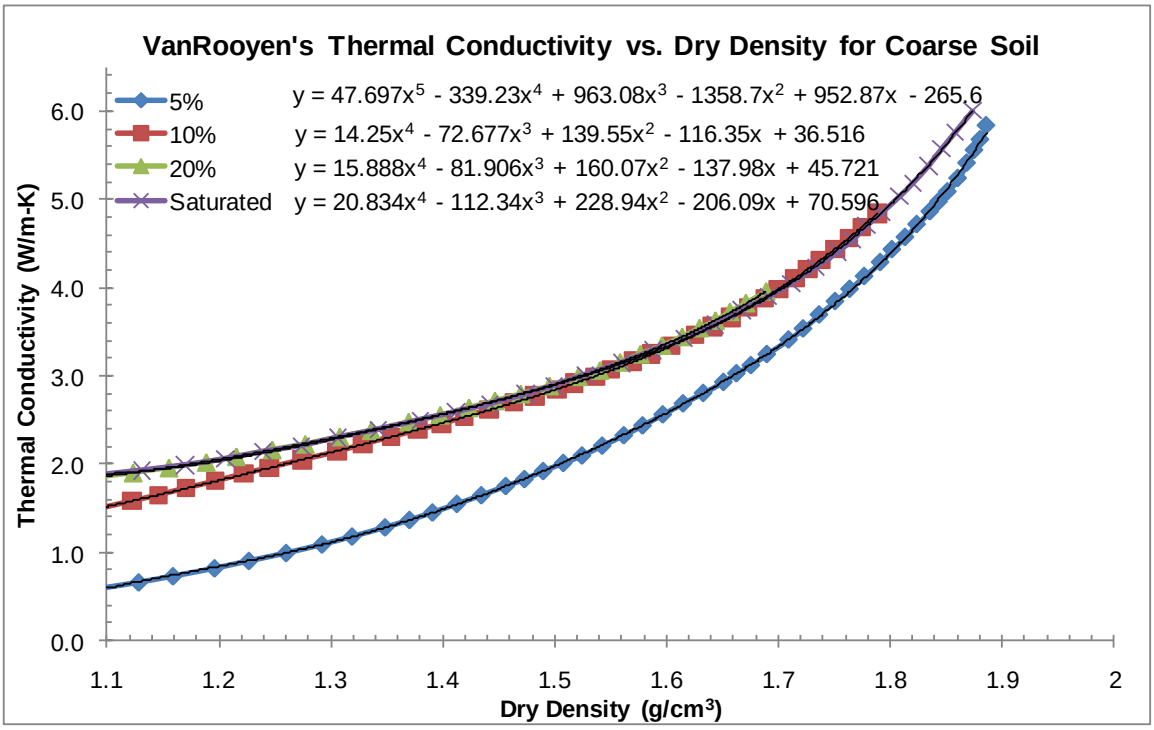

Figure B.10 VanRooyen's conductivity vs. density and moisture content for sandy soils. (Pauly, 2010)

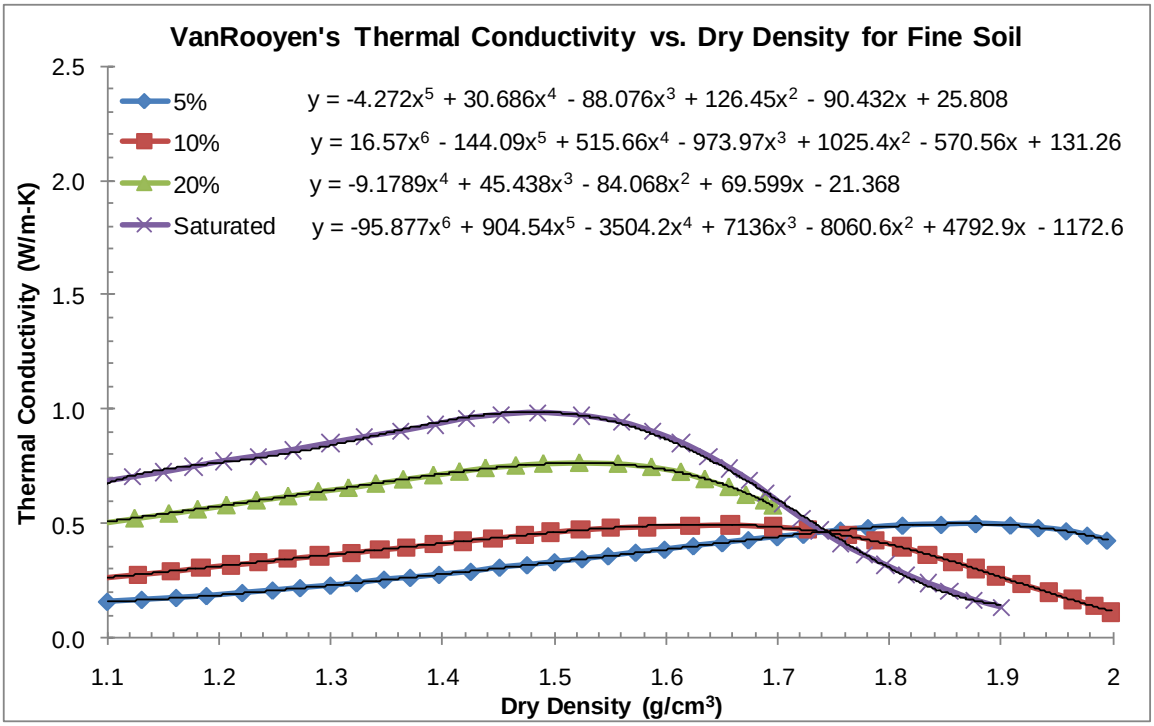

Figure B.11 VanRooyen's conductivity vs. density and moisture content for clayey soils. (Pauly, 2010)

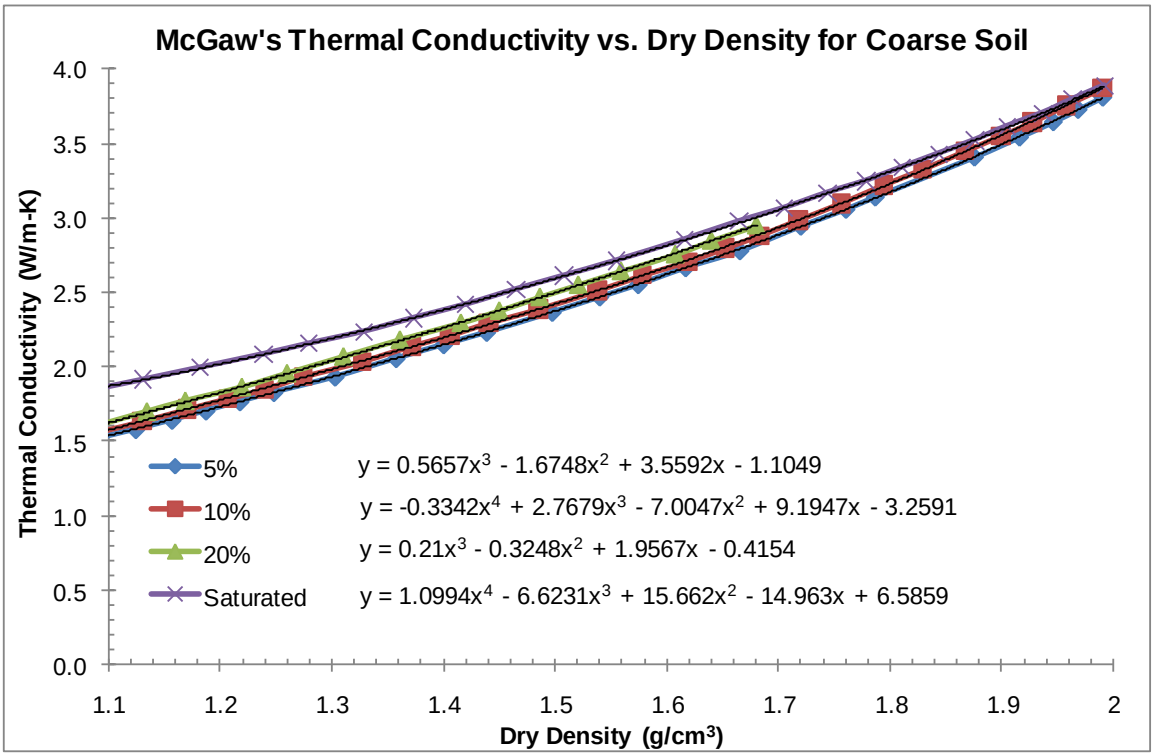

Figure B.12 McGaw's conductivity vs. density and moisture content for sandy soils. (Pauly, 2010)

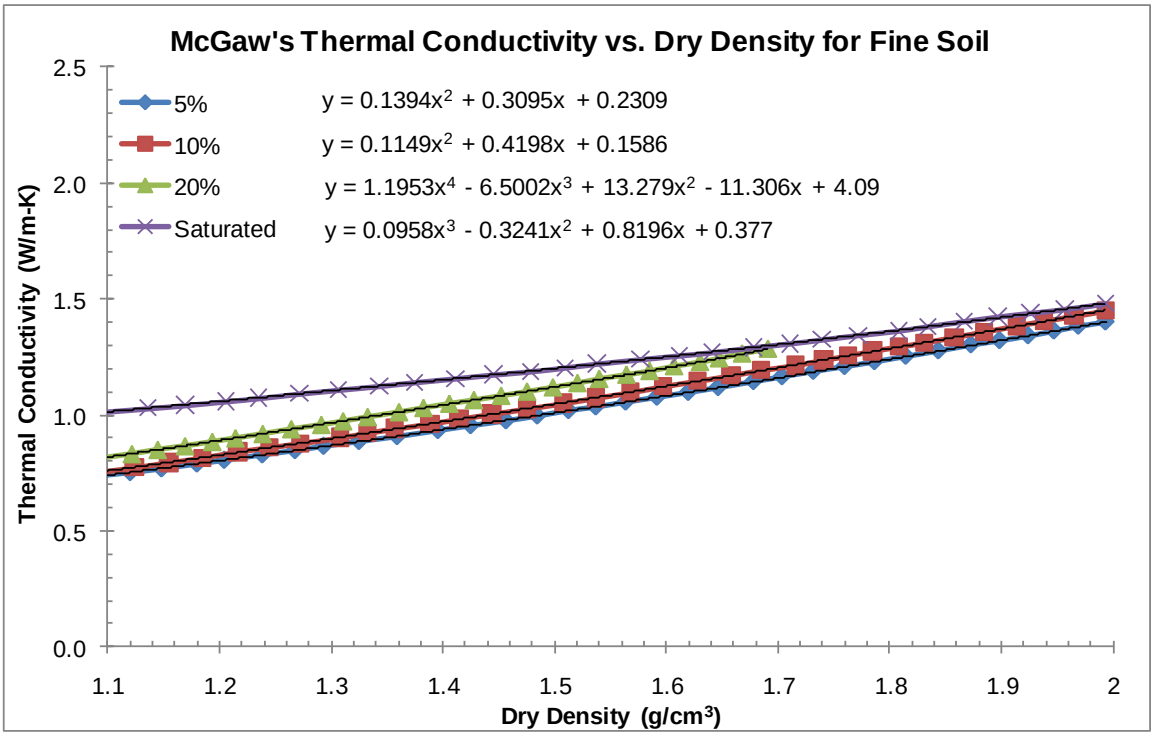

Figure B.13 McGaw's conductivity vs. density and moisture content for clayey soils. (Pauly, 2010)

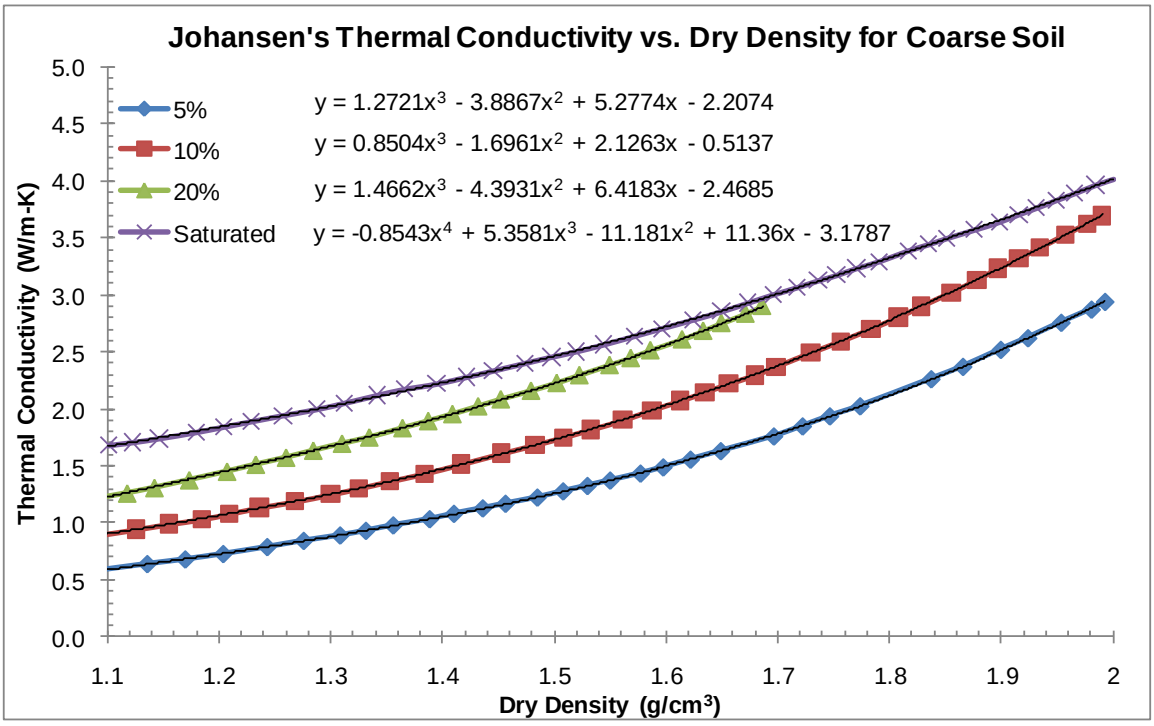

Figure B.14 Johansen's conductivity vs. density and moisture content for sandy soils. (Pauly, 2010)

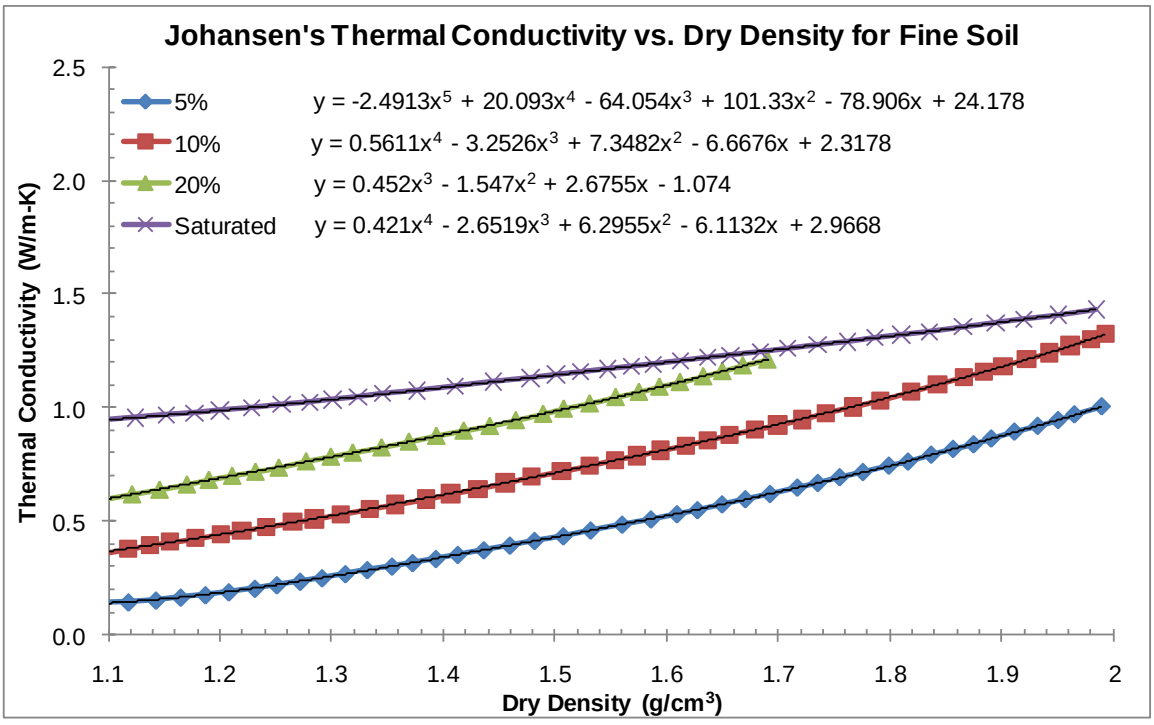

Figure B.15 Johansen's conductivity vs. density and moisture content for clayey soils. (Pauly, 2010)

APPENDIX C: COPYRIGHT PERMISSIONS

Below is permission for the use of material in Chapter 2.

9/19/2016 Rightslink® by Copyright Clearance Center

Copyright Clearance Center RightsLink®

Home | Create Account | Help | Live Chat

ASCE AMERICAN SOCIETY OF CIVIL ENGINEERS

Conference Proceeding:	Geo-Congress 2014 Technical Papers: Geo-Characterization and Modeling for Sustainability
Conference Proceeding Paper:	Temperature Prediction Modeling and Thermal Integrity Profiling of Drilled Shafts
Author:	Kevin R. Johnson
Publisher:	American Society of Civil Engineers
Date:	02/24/2014

Copyright © 2014, ASCE. All rights reserved.

LOGIN

If you're a copyright.com user, you can login to RightsLink using your copyright.com credentials. Already a RightsLink user or want to learn more?

Permissions Request

As an author of an ASCE journal article, you are permitted to reuse the accepted manuscript version of your article for your thesis or dissertation.

BACK CLOSE WINDOW

Copyright © 2016 Copyright Clearance Center, Inc. All Rights Reserved. Privacy statement. Terms and Conditions.
Comments? We would like to hear from you. E-mail us at customercare@copyright.com

Below is permission for the use of material in Chapter 3.

9/19/2016 Rightslink® by Copyright Clearance Center

Copyright Clearance Center RightsLink®

Home | Create Account | Help | Live Chat

Taylor & Francis
Taylor & Francis Group

Title: Analyzing thermal integrity profiling data for drilled shaft evaluation
Author: K. R. Johnson
Publication: DFI Journal - The Journal of the Deep Foundations Institute
Publisher: Taylor & Francis
Date: Jan 2, 2016
Copyright © 2016 Taylor & Francis

LOGIN
If you're a copyright.com user, you can login to RightsLink using your copyright.com credentials. Already a RightsLink user or want to learn more?

Thesis/Dissertation Reuse Request

Taylor & Francis is pleased to offer reuses of its content for a thesis or dissertation free of charge contingent on resubmission of permission request if work is published.

BACK CLOSE WINDOW

Copyright © 2016 Copyright Clearance Center, Inc. All Rights Reserved. Privacy statement. Terms and Conditions.
Comments? We would like to hear from you. E-mail us at customercare@copyright.com

Below is permission for the use of material in Chapter 4.

Hi LeEtta,

Yes, as long as USF owns the copyright and the students are using it for non-commercial, academic purposes. Please let me know if you need anything else.

Becky Alshefski
Licensing Manager
University of South Florida
Technology Transfer Office/Patents and Licensing
Tel: (813) 974-7409

From: Schmidt, Leetta
Sent: Tuesday, November 08, 2016 2:47 PM
To: Alshefski, Rebecca <alshefski@usf.edu>
Subject: RE: permissions to use images in a USF created FDOT report

Hi Becky,

Thank you so much for the response. Would this be the same for all FDOT reports prepared by USF investigators? I have received a similar question from another grad about

Optimizing the Use of the Thermal Integrity System for Evaluating Auger-Cast Piles: *http://www.fdot.gov/research/Completed_Proj/Summary_SMO/FDOT-BDV25-977-09-rpt.pdf*

Best,
LeEtta

LeEtta Schmidt
Resource Sharing and Copyright Librarian
4202 E Fowler Ave LIB107
Tampa, FL 33620
lmschmidt@usf.edu
813-974-1627 voice
813-974-3016 fax

Below is permission for the use of Figure 2.2.

Title: Thermal Integrity Profiling of Drilled Shafts
Author: Gray Mullins
Publication: DFI Journal - The Journal of the Deep Foundations Institute
Publisher: Taylor & Francis
Date: Dec 1, 2010

Thesis/Dissertation Reuse Request

Taylor & Francis is pleased to offer reuses of its content for a thesis or dissertation free of charge contingent on resubmission of permission request if work is published.

BACK CLOSE WINDOW

Below is permission for the use of Figure 2.4, Table B.1, and Table B.2.

Hi Kevin,

I am the copyright liaison at the Center, since the CTR Library acts as the official repository for approved and published TxDOT research. We don't have a copyright permission form, but I can authorize use of this report. Permission is authorized for this report. Please be sure the source in properly cited in the dissertation.

Please let me know if this statement is sufficient for your needs.

Thank you for your interest in our research,

Louise Rosenzweig

Louise Rosenzweig, Manager Library Services
Research Engineering/Scientist Associate IV
The University of Texas at Austin | Center for Transportation Research | 512 232 3138 |
1616 Guadalupe Street, Suite 4.202, Austin, Texas, 78701
louise.rosenzweig@engr.utexas.edu
ctrlib@austin.utexas.edu
http://ctr.utexas.edu/library

CENTER FOR TRANSPORTATION RESEARCH

Collaborate | Educate | Innovate

From: Kevin Johnson <krjohns8@mail.usf.edu>
Date: Tuesday, November 8, 2016 at 11:29 AM
To: "Rosenzweig, Louise A" <louise.rosenzweig@engr.utexas.edu>
Subject: Copyright Permissions Request

Ms. Rosenzweig,

I am interested in using figures from the following report in my dissertation:

Schindler, A.K., Dossey, T., and McCullough, B.F. (2002). *Temperature Control During Construction to Improve the Long Term Performance of Portland Cement Concrete Pavements*. Austin, TX. Center for Transportation Research. The University of Austin at Texas. FHWA/TX-05/0-1700-2.

Can you authorize permissions for this use?

Thank you

Kevin R. Johnson
University of South Florida
Civil Engineering Department

Below is permission for the use of Figures 2.5 – 2.7.

Dear LeEtta,

I am the copyright liaison at the Center, since the CTR Library acts as the official repository for approved and published TxDOT research. We don't have a copyright permission form, but I can authorize use of this report. Permission is authorized for this report. Please be sure the source in properly cited in the thesis/dissertation.

Please let me know if this statement is sufficient for your needs.

Thank you for your interest in our research,

Louise Rosenzweig

Louise Rosenzweig, Manager Library Services
Research Engineering/Scientist Associate IV
The University of Texas at Austin | Center for Transportation Research | 512 232 3138 |
1616 Guadalupe Street, Suite 4.202, Austin, Texas, 78701
louise.rosenzweig@engr.utexas.edu
ctrlib@austin.utexas.edu
http://ctr.utexas.edu/library

CTR Library
The University of Texas at Austin | Center for Transportation Research | o - 512.232.3126 | ctrlib@austin.utexas.edu

---

From: Schmidt, Leetta <lmschmidt@usf.edu>
Sent: Friday, October 21, 2016 8:44:32 AM
To: Ctr-Library
Subject: Request from CTR website

To Whom It May Concern,

I am working with a researcher who is interested in using figures from the following report in his thesis/dissertation:

[1] Folliard, K.J., Juenger, M., Schindler, A., Riding, K., Poole, J., Kallivokas, L.F., Slatnick, S., Whigham, J., Meadows, J.L. (2008). *Prediction Model for Concrete Behavior* (Final Report). Austin, TX. Center for Transportation Research. The University of Austin at Texas. FHWA/TX-08/0-4563-1.

Could you tell us the right way to request permissions for this use?

Sincerely,
LeEtta

LeEtta Schmidt
Resource Sharing and Copyright Librarian
4202 E Fowler Ave LIB107
Tampa, FL 33620
lmschmidt@usf.edu
813-974-1627 voice
813-974-3016 fax

Below is permission for the use of Figure 2.10 and Figures B.1 – B.15.

Yes, permission granted.

Thanks,

Nicole Pauly, PE
Moffatt & Nichol
1509 West Swann Avenue | Suite 225 | Tampa, Florida 33606 | **P** 813.258.8818 | **F** 813.258.8525

From: Kevin Johnson [mailto:krjohns8@mail.usf.edu]
Sent: Tuesday, November 08, 2016 8:00 PM
To: Pauly, Nicole <npauly@moffattnichol.com>
Subject: copyright permissions request

Nicole,

I am interested in using figures from the following thesis in my dissertation:

Pauly, Nicole M. (2010). "Thermal Conductivity of Soils from the Analysis of Boring Logs." Master's Thesis, University of South Florida, Department of Civil and Environmental Engineering.

Can you grant permission for this use?

Thank you

Kevin R. Johnson
University of South Florida
Civil Engineering Department

Below is permission for the use of Figure 2.3.

Hello again, LeEtta -- Upon obtaining approval from WSDOT's Research Director and the Research Manager in charge of the project which the report documents, this is to inform you that as publishers of the report in which the figure appears, WSDOT is granting permission for your university's researcher to use Figure 3-21 from:

Mullins G., and Winters, D. (2011). *Infrared Thermal Integrity Testing Quality Assurance Test Method to Detect Drilled Shaft Defects*. Final Report. Washington State Department of Transportation, Olympia, WA. Report No. WA-RD 770.1 (https://www.wsdot.wa.gov/Research/Reports/700/770.1.htm), with the following conditions:

In the thesis/dissertation to be published, the following credit line **should accompany the figure**:

Mullins, G., Winters, D. (2011), page 40.

In that publication's **references list**, please use the full citation:

Mullins, Gray, and Winters, Danny (2011). "Infrared Thermal Integrity Testing: Quality Assurance Test Methods to Detect Drilled Shaft Defects – Final Report." Olympia, WA : Washington State Department of Transportation, Office of Research & Library Services.
https://www.wsdot.wa.gov/Research/Reports/700/770.1.htm

If you have additional questions, please feel free to contact me.

Thank you for your interest in our research publication.

Kathy Szolomayer
WSDOT Librarian
Washington State Dept. of Transportation
PO Box 47425, Room SLC-15
Olympia WA 98504-7425
szolomk@wsdot.wa.gov | 360-705-7751
Library@wsdot.wa.gov

ABOUT THE AUTHOR

Kevin Russell Johnson, son of Gary Russell Johnson and Sherri Lynn Johnson, was born April 4, 1988 in Tampa, FL. In 2005, he began working for his father at Florida Masonry Construction Company, and continued working part-time after enrolling in the Civil Engineering program at the University of South Florida in 2006. Kevin received his Bachelor's and Master's degree in Civil and Environmental Engineering from USF in 2010 and 2011, respectively. Immediately following, he enrolled in the Doctoral program at USF and began working as a research and teaching assistant. He earned his Doctor of Philosophy degree in Civil Engineering in 2016. Kevin is currently engaged to Tori Empie, to whom he will be married on January 22, 2017.